NASA CONTRACTOR REPORT

NASA CR-2660

NASA CR-2660

EXPERIMENTAL AND THEORETICAL STUDIES OF SUBSONIC FAN NOISE

R. Mani and K. Bekofske

Prepared by
GENERAL ELECTRIC COMPANY
Schenectady, N. Y. 12301
for Lewis Research Center

NATIONAL AERONAUTICS AND SPACE ADMINISTRATION • WASHINGTON, D. C. • MARCH 1976

1. Report No.	2. Government Accession No.	3. Recipient's Cata
CR-2660		

4. Title and Subtitle	5. Report Date
EXPERIMENTAL AND THEORETICAL STUDIES OF SUBSONIC FAN NOISE	March 1976
	6. Performing Organization Code
7. Author(s)	8. Performing Organization Report No.
R. Mani and K. Bekofske	None
	10. Work Unit No.
9. Performing Organization Name and Address	
General Electric Company P.O. Box 43 Schenectady, New York 12301	11. Contract or Grant No. NAS3-17853
	13. Type of Report and Period Covered Contractor Report
12. Sponsoring Agency Name and Address	
National Aeronautics and Space Administration Washington, D.C. 20546	14. Sponsoring Agency Code

15. Supplementary Notes

Final Report. Project Manager, James H. Dittmar, V/STOL and Noise Division, NASA Lewis Research Center, Cleveland, Ohio

16. Abstract

An experimental and analytical study of the noise generated by inlet turbulence impinging on a subsonic axial flow fan as a function of tip speed, flow coefficient, and intensity and scale of turbulence was carried out. Both turbulence and far field acoustic measurements were made. The new elements introduced in the theoretical analysis were accounting for blade loading dependent noise mechanisms and consideration of anisotropic turbulence impinging on the rotor because of inlet flow contraction effects. Experimentally an unexplained increase of noise at about 1/2 and $1\frac{1}{2}$ times blade passing frequency was observed at low flow coefficients even though there was no evidence of compressor surge. In the final version the theory does a fair job of predicting variations of noise with blade loading and tip speed. Alteration of inlet turbulence length scales produced some but not very pronounced changes in the far field PWL spectra. Some degree of eddy contraction and resulting anisotropy were essential to explain the concentration of energy around the blade passing frequencies typically observed, though the degree of eddy anisotropy needed to reconcile far field PWL spectra was not as great as suggested by other investigators.

17. Key Words (Suggested by Author(s))	18. Distribution Statement
Airplane engine noise Inlet distortion Inlet turbulence	Unclassified - unlimited STAR Category 71 (rev.)

19. Security Classif. (of this report)	20. Security Classif. (of this page)	21. No. of Pages	22. Price*
Unclassified	Unclassified	72	$4.25

* For sale by the National Technical Information Service, Springfield, Virginia 22161

Contents

EXPERIMENTAL AND THEORETICAL STUDIES OF SUBSONIC FAN NOISE

Summary

The present report describes an experimental and theoretical study carried out to investigate mechanisms of inlet radiated noise from a subsonic, high performance, single stage aircraft engine fan. The fan is designed to operate at transonic speeds but only subsonic operation was studied. The fan has no inlet guide vanes and the outlet (stator) guide vanes are well separated (by 1.27 true rotor chords) from the rotor. The fan has 44 rotor blades and 86 outlet guide vanes. With this vane blade ratio and the use of large rotor-stator separation, it is believed that the study focused primarily on isolated, subsonic rotor noise mechanisms as far as inlet radiated noise was concerned.

The experiments involved varying the fan tip speed (three subsonic tip speeds were studied) and also at each tip speed varying the flow to the fan (two flows at each tip speed were studied). In addition at each tip speed/flow setting, we attempted to alter the character of the inlet turbulence impinging on the rotor by the use of three turbulence producing grids designed to create different ratios of length scale of inlet turbulence to rotor pitch.

Measurements included far field acoustics (in the GE anechoic chamber at Schenectady, N. Y.), mapping of the time averaged inlet total pressure pattern and radial mapping of the inlet turbulence in intensity and scale.

The anechoic chamber employed for these studies draws air from all its walls except the wall from which the inlet duct protrudes (it is designed to provide a "porous" box type inlet environment). No measurable stationary variation of total pressure was detected by us to an accuracy of 0.01 psi during the course of the study. Turbulence intensities (rms) of order 5 - 7% in the casing boundary layer and of order 1 to 2% mid-stream were measured with a clean inlet. Introduction of grids served to produce relatively more uniform intensity profiles. With a clean inlet (no grids) integral length scales vary (with radius) from about one to four times the rotor pitch. Again, grids produce much more uniform length scales (radially) with integral scales approximately half the grid mesh size. The clean inlet far field acoustic power level (PWL) spectra exhibit sharp peaks at the first, second and third harmonics of blade passing frequency at the larger flow coefficient for all tip speeds. The effect of the grids at the larger flow coefficient is to broaden the PWL spectra without significantly changing the tone levels.

An unexpected acoustic phenomenon was observed for all tip speeds at the reduced flow coefficient and with the clean inlet as well as with the grids. The fan operated in a stable fashion (no surge) but the far field PWL spectra were now dominated by the appearance of large amounts of relatively broad band energy at about one half and one and one-half times the blade passing frequency. In addition there was a general increase of acoustic energy in all frequency bands with decreased flow.

We carried out a theoretical analysis for the estimation of noise generated due to the interaction of inlet distortion or inlet turbulence with an isolated, subsonic rotor. Basically the procedure is a systematic second

order treatment of this problem wherein we account for the noise generated by quadrupole stress fields and also account for the diffraction or scattering of these source fields by the rotor blades. Comparisons with tone data previously obtained at NASA, Lewis suggested several refinements to the analysis which are described. Finally attempts to predict the complete PWL spectrum data obtained during the course of the study motivated a further extension to the theory involving its extension to anisotropic turbulence impinging on the rotor, the anisotropy being due to distortion of isotropic turbulence due to its ingestion into the fan inlet. The analysis in this final form does a fair job with one exception of predicting both our own data and the previously mentioned tone level data of NASA Lewis, as a function of fan tip speed and pressure ratio. No explanation emerges for the large increases in noise at ½ and 1½ times blade passing frequency observed in the study. Those increases appear to be related to some form of prestall phenomenon (the compressor flow itself was stable at this condition).

PART I: EXPERIMENTAL STUDIES

Introduction

Considerable interest exists in the aircraft noise area in the problem of noise mechanisms of an isolated, subsonic rotor. The motivation for the interest arises for two reasons. Firstly even though transonic fans are employed in current aircraft applications, approach operation of these fans generally occurs at about 60% of design speed at which condition the tip speeds are subsonic being of order 900 feet per second. Secondly, thanks to the studies of Tyler and Sofrin [1] and innumerable studies on effect of rotor-stator spacing, etc. on the fan noise (cf. e.g. Sofrin and McCann [2]), we now know several techniques of minimizing rotor-stator interaction noise. These include selection of vane/blade ratio, employment of large axial separation between the rotor and stator, elimination of inlet guide vanes, etc. Also as far as inlet radiated noise is concerned, one surmises that with the large axial separation causing rotor-stator interaction noise to be generated primarily at the outlet guide vanes (in conventional jargon, the "potential interaction" effect due to the outlet guide vanes on the rotor ought to be small), the highly staggered rotor blades carrying near sonic velocity flow relative to themselves ought to be quite effective in impeding the upward propagation of such noise into the forward quadrant. Putting these facts together, one is tempted to regard inlet radiated fan noise from such aircraft fans at subsonic tip speeds as primarily noise from an isolated rotor embedded in the engine duct.

The mechanisms by which such a rotor might generate noise were first given by Sharland [3] who classified them as due to vortex shedding, due to turbulent boundary layers on the blades and finally due to interaction of the rotor with upstream flow inhomogeneities such as inlet turbulence or distortion. Furthermore experiments by Sharland himself and order of magnitude estimates of these mechanisms suggests that the last of these three mechanisms is the dominant one for noise from well designed fans.

Accepting the interaction of an inflow inhomogeneity with an isolated rotor as a major contributor to subsonic fan noise, an important question arises as to how this noise mechanism varies with rotor tip speed and the loading on the rotor and also to what extent it can be affected by deliberately creating different types of inlet turbulence impinging on the rotor. The present program was undertaken with these objectives and also with the objective of carrying out sufficient aerodynamic measurements in front of the rotor for each configuration, tip speed and flow coefficient so that (in Part II) theoretical predictions could be attempted for purposes of comparison with data.

R. E. Sheer, Ralph Gunst, R. Otten, R. Warren, and Dr. James Wang provided valuable assistance during the course of the experimental study. Ivan H. Edelfelt helped considerably in programming the calculations.

Experimental Program

The primary objectives of the program were:

1) Assessment of the contribution of inlet turbulence or inlet distortion to isolated rotor noise by active control of the inlet conditions employing grid generated turbulence.

2) Influence of flow coefficient (pressure ratio) on isolated rotor noise at constant tip speed.

3) Acquisition of a sufficient amount of aerodynamic and acoustic data for each test to enable a detailed theory-data comparison in Part II.

An experimental study to investigate the noise generated by the interaction of inflow distortions and inlet turbulence with a fan rotor was performed to fulfill these objectives. Aerodynamic and acoustic data was taken for a fan rotor at three subsonic tip speeds and two different pressure ratios at each tip speed (Figure 1). At each speed and pressure ratio a radial mapping of the turbulence intensity and scale impinging on the rotor was carried out at one circumferential location. Circumferential mapping of the total pressure profile upstream of the rotor at three radial positions was performed to establish the degree of inlet distortion prevalent in the experiments. Forward radiated SPL and PWL noise spectra were measured at each tip speed and pressure ratio.

These aerodynamic and acoustic data were measured with and without inlet grids used to vary the intensity and scale of the incoming turbulence impinging on the rotor. The specifications of the grids were chosen so as to provide a significant variation in the predicted noise behavior of the rotor due to a variation in turbulence properties. The grid sizes were selected so that the integral scales of turbulence resulting therefrom were to be greater than, less than and approximately equal to the rotor pitch. It was therefore hoped that the resulting power spectra would correspondingly exhibit varying degrees of "peakiness" about the blade passing frequency.

The grid experiments as well as the mapping of the inlet distortion were basically designed to achieve objective (1) above. Thus the following criteria were employed in the selection of the grids:

a) The grids should provide widely varying length scales. However the turbulence intensities generated by the grids at the rotor face should be comparable. This necessitated using them at comparable values of the ratio, (distance from rotor/mesh size).

b) The ratio (distance of grid from rotor/grid mesh size) was chosen large enough to provide approximately isotropic turbulence impinging on the rotor.

c) The grids were placed sufficiently close to the rotor to ensure high enough mid-stream turbulence intensities impinging on the rotor.

Objective 2 was achieved by operating the aero-acoustic facility at its minimum and maximum resistance conditions. With the fan employed for these

tests whose map is shown in Figure 1, only a modest variation in pressure ratio at fixed wheel tip speed was possible. Above 70% tip speed, the fan was supersonic and exhibited substantial multiple pure tone noise in the forward arc. Thus this was a basic limitation imposed on this test program due to the type of compressor map that the fan and test facility possessed.

The program was conducted in the anechoic environment at the GE CR&D Aero-Acoustic Facility in Schenectady, New York.

An overall view of the facility is shown in Figure 2. It is comprised of:

1) A 2500 HP drive system for speeds up to 26,000 RPM.

2) An anechoic chamber approximately 35 ft. wide by 25 ft. long by 10 ft. high designed for less than ± 1 dB standing wave ratio at 200 Hz. All walls, floor, and ceiling are covered with an array of 28" polyurethane foam wedges.

3) Porous walls for minimum inflow distortion to the fan.

4) Far field noise measurement at 17 ft. radius from 0 to 110° to the inlet.

A 20 inch diameter fan supplies the airflow and sound source. The fan used in this program was a NASA Lewis model designated as Rotor #11 with a stator set and casing manufactured by GE. The overall fan system has the following design parameters:

- Inlet guide vanes = None
- Fan diameter = 19.84 inches
- Design stage pressure ratio = 1.57
- Design tip speed = 1394 ft/sec.
- Design weight flow = 65 lb/sec.
- Design RPM = 16,100
- Rotor blades = 44
- Stator vanes = 86
- Rotor/stator tip spacing = 1.27 true chords
- Hub/tip ratio = 0.5
- Design fan specific flow (W_2/frontal area) = 30 lb/sec/ft^2.
- Design fan specific flow (W_2/annulus area) = 39 lb/sec/ft^2.

The fan performance map is shown in Figure 1.

The inlet duct consisted of a 7.7" long and an 18.9" long cylindrical hardwall spool arranged in tandem. The 7.7" spool was nearer to the fan and the 18.9" spool nearer the inlet. All configurations were tested with a standard bellmouth designed to provide flight type velocity profiles at the fan rotor. The turbulence-producing grids were positioned at either the upstream or downstream flange of the 18.9" spool.

The following turbulence-producing grids were selected:

	Grid #1	Grid #2	Grid #3
Mesh size (inches)	2.25	0.50	1.677
Grid diameter or size (inches)	0.25	0.063	0.177
Distance from fan rotor (inches)	30.5	11.7	30.5
% open area	79.0	76.4	80.0

Grid #1 was constructed from rods with square cross section and grids #2 and 3 from wire with circular cross section. Figure 3 shows a photograph of the three grids.

Both acoustic and aerodynamic measurements were carried out. The former involved far field acoustic measurements in the anechoic chamber. The latter included sixteen three-probe Kiel total pressure rakes (see Figure 4), suitably arrayed wall statics, and a hot film traverse. Additional aerodynamic measurements were used to determine the fan performance.

Results

Aerodynamic

The total pressure probe array shown in Figure 4 provides a circumferential mapping of the inlet total pressure profile every 22½° at three radial stations. During the entire course of the program (for all the six settings of Figure 1 and with the clean inlet as well as with the three grids), no systematic circumferential variation of the time averaged inlet total pressure was detected at least to an accuracy of 0.01 psi. A dynamic head of 0.01 psi corresponds to a velocity of 35 fps with air at standard conditions and hence it is readily conceded that a mapping of the steady inlet velocity would have been a more sensitive measure of inlet distortion rather than that of the total pressure. Such a measurement (with either a multiple hot wire set up or a circumferentially traversing probe) was beyond the scope of our program.

The turbulence measurements were carried out 3.85" or 2.72 rotor pitch lengths ahead of the rotor or about 1.92 rotor chords (the true rotor chord length at the tip for rotor 11 is 2") ahead of the rotor. Both the mean and fluctuating parts of the velocity were measured. The hot film element itself was aligned with its axis parallel to an element of the duct circumference and hence the film was responsive to both the axial and radial velocity com-

ponents. Resolving the velocity into separate axial, radial and circumferential components was again beyond the scope of our effort.

In Figure 5 we show the results for the turbulence intensity normalized by the maximum value of steady velocity in the duct as a function of distance from the outer wall (normalized by the duct width H). These results were essentially independent of either fan tip speed or flow coefficient at given tip speed. The plots are actually an average for the six conditions shown in Figure 1. In Figure 6, we show the measured integral length scales for the inlet turbulence (obtained by identifying the (1/e) time delay point in the correlogram and setting $L = u_c \tau$ where u_c is the local mean velocity) with the clean inlet and with the various grids. These results were again relatively insensitive to variations of tip speed or flow coefficient. While grid generated turbulence has a relatively uniform distribution of length scale as a function of radius, the clean inlet exhibits mid-stream values of length scale nearly four times as great as the boundary layer length scale. Shown in Figure 6 is also an area averaged rotor pitch D defined by

$$\frac{2}{(r_t - r_h)} \int_{r_h}^{r_t} p(r) r \, dr$$

where r_h and r_t denote the hub and tip radii, p(r) the pitch at radius r ($= 2\pi r/N$ where N is the number of rotor blades). A similar area averaged length scale for the clean inlet turbulence (from Figure 6) works out to about 2.65" and with D = 1.11", one may estimate a ratio of integral length scale/rotor pitch of 2.39 for our clean inlet experiments. Another noteworthy feature of Figure 6 is that while the integral scale of the 2¼" mesh grid is greater than that of the 1-2/3" mesh grid which in turn is greater than that of the ½" grid, these scales are not quite in the ratio of 2¼:1-2/3:½. The 2¼" and 1-2/3" grids failed to generate as large a length scale as had been hoped. (Fortunately the clean inlet itself provided length scales substantially greater than the rotor pitch though, in retrospect, we ought to have mapping L in more detail in the transition region from y/H = .15 to y/H = 4 for the clean inlet.)

Since the hot film measurements were carried out 3.85" upstream of the rotor, a question arises as to whether it was inlet turbulence that was measured or actually the acoustic velocities associated with upstream noise. This issue is sometimes described as "acoustic contamination." There is no simple procedure of discriminating experimentally between turbulence and noise by means of fluctuating velocity measurements alone but several indirect observations may be offered here to support the inference that the hot film was measuring primarily turbulence rather than noise:

1) In a previous study of a similar nature in our Laboratory [4], an inlet of type similar to the present inlet was employed with a suction source (i.e. there was no rotor). Inlet turbulence data obtained on that program with a clean inlet correspond almost exactly with those shown in Figures 5, 6 (when nondimensionalized the same way).

2) The autocorrelation measurements show dominant turbulent energies from 1000 to 2500 Hz which are 1/6 to 1/3 the blade passing frequencies. There is also no obviously observable periodicity in the correlograms.

3) In-duct SPL's at this location are of order 140 dB corresponding to acoustic particle velocities of 2 - 3 fps where measured root mean square fluctuating velocities are at least 15 fps in the high intensity regions.

4) "Acoustic" contamination would not have been expected to lead to invariance of (u'/U) with tip speed and flow coefficient as observed. Acoustic contamination would have caused (u'/U) to increase with increased efficiency of noise generation and as the acoustic data will shortly reveal, this efficiency goes up markedly with increasing tip speed and decreasing flow coefficient (at given tip speed).

5) The general trend of variation of measured scales with introduction of grids with grid size suggests that we are measuring turbulence.

The only other aerodynamic data recorded was fan performance data (corrected weight flow and pressure ratio). For the clean inlet, these merely confirm that the six points shown in Figure 1 were where the acoustic data was obtained. In the aero-acoustic facility employed for these tests, the system resistance is varied by setting a discharge valve in the fan discharge flow path. Once the discharge valve had been set to correspond to the points in Figure 1, it was not adjusted further when the grids were employed. Since grids induce a slight pressure drop, it turned out that under comparable conditions the grid experiments were always at a slightly lesser flow and slightly higher pressure ratio (in terms of the fan map) than the clean inlet experiments. This effect was however fairly small (of order of 3 - 4% on the flow coefficient).

Acoustic

The primary measurement was the recording of SPL's on a 17 foot arc every 10° from 0° to 110°. As Figure 2 shows, the facility design is such that it is possible to separate the inlet and aft radiated noise in quite a clean fashion. The SPL's are integrated to derive PWL spectra which is all that we will present in what follows. (Full information on the third octave acoustic data obtained in this program is given in tabular form in Appendix 1.) No inlet probes employed for the aerodynamic measurements were left in stream during the acoustic measurements.

In Figures 7 - 10, we present all the PWL spectra obtained during the course of the study. These are 1/3 octave data re: 10^{-13} watts and are given from 790 Hz to 50 kHz which covers the fan noise spectrum from about one-tenth to about six times the blade passing frequency. It is clear from these figures that the 60% speed data is essentially intermediate between the 50% and 70% speed data and thus it suffices to discuss only the 50% and 70% speed data in terms of trends, etc.

Discussion of Results

Consider first the clean inlet data shown in Figure 11 for the 50 and 70% speeds. The low pressure ratio data is dominated by fairly concentrated energy in the first, second and third harmonics. This in itself needs some explanation because in the absence of any stationary inlet distortion, the interaction of isotropic turbulence with a rotor characterized by an L/D of 2.39 would not be expected to produce tones with almost a 10 dB fall off per third octave.

The low flow, high pressure ratio data exhibits unexpectedly large increases of broad band energy at about one-half and 1.5 times the blade passing frequency in addition to an overall increase in power levels in all octave bands. The explanation for the increases at half and 1½ times blade passing frequency is not clear. The fan operated in a stable fashion at these flow coefficients (no surge). As other data in Figures 7 - 10 show, this effect prevailed for all the low flow coefficient data (i.e. with all the grids). The phenomenon is not in any way a quirk of our experimental program for after completion of our program, we received Figure 12 from T. F. Gelder [5] of NASA, Lewis who reports a very similar experience with the same fan. Gelder has measured reverberant SPL in a hardwalled inlet plenum and his narrow band data are shown in Figure 12. Similar increases at ½ and 1½ times blade passing frequency are evident at 60% speed on changing the corrected weight flow from 37.7 lb/sec. to 31.3 lb/sec.

Figure 13 summarizes the effect of inlet grids at 50% speed at both the larger and lesser weight flows. At the high flow, grids broaden the PWL spectrum with relatively little effect on the tone levels. This was to be expected on the basis of Figure 6 which shows the turbulence length scales to be reduced (from the clean inlet) due to the introduction of grids although the ½" mesh data is puzzling inasmuch as it would have been expected to produce the most broad band signature of all.

The low flow data tends to be so dominated by the energies at ½ and 1½ times the blade passing frequency that it is difficult to distinguish any effect of the various grids.

The drawing of major conclusions of the study is postponed to Part II after a description of the analysis.

PART II: THEORETICAL STUDIES AND THEORY-DATA COMPARISONS

Introduction

The motivation for these theoretical studies (a preliminary version was given in Reference [6]) arose from the fact that the noise of subsonic tip speed rotors is often found to display a marked dependence on the loading on the rotor at constant wheel tip speed. A very good example of such data may be found in the work of Gelder and Soltis [7] who carried out studies of inlet noise radiation from isolated rotors. Figure 14 is a result taken from their study wherein we show the inlet acoustic power obtained in a 50 Hz bandwidth around the fundamental blade passing frequency for two different rotors. The two rotors are essentially the same except that one has 45 blades while the other has 90 blades. The measured data are shown for 50, 60, 70 and 80% of design speeds for these rotors. (Above these speeds, the noise of these fans tends to be dominated by multiple pure tones, characteristic of supersonic tip speed operation.) While the noise data are shown in the same manner that Gelder and Soltis showed it, i.e. as a function of relative Mach number at the tip for various fixed values of wheel speed, it is clear that decreasing values of M_{rel} (at fixed fan speed) also correspond to decreasing flow (or axial Mach number) and generally increasing pressure ratio. For example for fan 2, at 50% speed, the pressure ratio and axial Mach number change from 1.03 & .367, to 1.07 & .304, to 1.11 & .227, as the relative Mach number M_{rel} varies from .62 to .59 to .56. The feature of this data that needs explanation is that the noise often increases at fixed speed, when both the flow and M_{rel} are decreasing. In these studies of [7], the stators generally found aft of the rotor were deliberately eliminated so that we are, in fact, looking at pure, isolated rotor noise radiated in the inlet direction. Conventional dipole mechanisms would suggest a decrease of noise with decreasing relative Mach number to the blades.

Another feature of Figure 14 worth noting is that data from different experiments on effects of changing flow coefficient at constant wheel rpm are often not mutually consistent. We refer here to the different trends exhibited by the upper and lower halves of Figure 14. (After all, aerodynamically, rotors 1 and 2 are essentially identical.) Theoretically, doubling the number of blades should not have affected the relative variation of noise in a narrow band at the blade passing frequency with flow coefficient at constant wheel rpm.

In Reference [6], it was argued that a quadrupole interaction mechanism arising from an interaction of an inflow inhomogeneity such as inlet turbulence with the potential flow field of the rotor could conceivably explain such dependence on flow coefficient at constant wheel rpm. A first attempt to put some numbers into this argument in [6] showed however that estimates of the direct quadrupole induced acoustic field were too low to be able to explain the observed data. The purpose of the present study was to re-examine the theory used in [6] and carry out some major extensions of it in order to be better able to explain the data of [6] and our own work in Part I. A study similar in spirit to Reference [6] has also been published recently in Reference [18].

Theoretical Extensions

We start by giving a very brief summary of what was carried out in [6]. A form of the Lighthill equation for noise generation by quadrupole mechanisms for a medium characterized by a uniform velocity was first stated [8]. It was then pointed out that the relevant quadrupole mechanism involved one component of velocity due to an inflow inhomogeneity and another due to the potential flow generated by the steady rotor loading. The former can be readily calculated for simple inflow inhomogeneities such as stationary distortions of inlet total pressure and homogeneous, isotropic, inlet turbulence. The latter can be calculated if we employ methods of subsonic, linearized, cascade aerodynamics. The uniform flow quadrupole noise generation equation is then simply solved in the cascade plane as an inhomogeneous equation without regard to any boundary conditions imposed by the rotor blade surfaces. Preliminary attempts in [6] to carry out absolute theory-data comparisons with the data of [7] were not successful because of the prediction that in those situations (except possibly for the 80% speed data) the noise was dipole dominated and hence was predicted always to decrease with decreasing M_{rel} at fixed wheel rpm.

Before delving into the mathematical formulation, we wish to give a physical description of the new aspect of the "quadrupole" noise generation problem that we are trying to uncover in the present phase as opposed to what was accomplished in the previous phase [6]. We will draw heavily from remarks made by Professor J. E. Ffowcs Williams [9] in a recent lecture.

As pointed out in [9], as early as 1868, Stokes observed that the sound radiated from a tuning fork became much stronger when the blade of a large knife obstructed the motion local to the tine of the tuning fork. In fact it was this observation that motivated Sommerfield some fifty years later to carry out his classic studies of the diffraction of sound by semi-infinite plates. The explanation for what Stokes observed is as follows. Sources near a noncompact scattering surface induce an extensive distribution of linear surface terms acting as noncompact monopoles and dipoles. These usually account for far greater radiation than the source itself though they need provide none of the field's energy if they are stationary. For example, if we examine the effect of a rigid, stationary, semi-infinite plate on the acoustic output of a point dipole where λ is the wavelength of the sound emitted by the dipole and r_o is the separation between the dipole and the edge of the plate, one finds that the radiated energy (as compared to the energy emitted by the dipole in isolation) is increased by a factor (λ/r_o). In fact the higher the order of the original multipole singularity the greater the effect of the presence of nearby noncompact scattering surfaces. Such surfaces can destroy the delicate self-canceling interference leading to inefficiency of higher order singularities. It is precisely this mechanism by which the passive blade of a large knife placed near the tine of a tuning fork results in powerful amplification of the sound field generated by the fork which constitutes a quadrupole array. This specific example of the sound field generated by a point quadrupole in the presence of semi-infinite plate was worked out in detail by Ffowcs Williams and Hall [10]. They found that the resulting surface interaction contribution could be classified neither as a monopole or a dipole but something in between. The field scattered by the edge could be usefully thought of as originating in "one and half pole." Our purpose in citing this result is merely to point out that

whenever radiation from a multipole singularity distribution in the presence of noncompact scattering surfaces is involved, it may not be very profitable to classify the problem as of monopole, dipole or quadrupole type and draw inferences concerning tip speed dependence, relative importance of mechanisms, etc.

Let us now explain the application of these ideas to the current problem. The problem of the ducted, isolated rotor is characterized by three types of solid surfaces namely, the inner and outer duct surfaces and the blade surfaces themselves. The previous analysis [6] already implicitly albeit approximately accounts for the inner and outer duct surfaces by employing a two-dimensional or cascade plane formulation. (This approximation is obviously a high hub-tip ratio approximation.) However the presence of the rotor blade surfaces themselves in diffracting or scattering the sound was simply not accounted for. Now, in the cascade plane, one has an infinite number of blades and a good measure of the "density" of the blade surfaces is, of course, the solidity of the row. Thus the previous work [6] is in a sense a zero or low solidity approximation. (It does not seem characterizable in frequency terms as either a low or high frequency approximation.)

To incorporate this rotor blade scattering problem, we first note that it is mot sensible to first switch to a frame of reference in which the rotor row is stationary. (It is not very convenient to solve scattering problems in a frame of reference in which the scattering surfaces are moving.) This means now that the mean flow has both axial and tangential components but an advantage is gained in that the rotor potential field is a stationary one. Using the notation of [6] and in terms of Figure 15 we have to solve for a pressure field p' governed by:

$$\left[\frac{1}{c_o}\frac{\partial}{\partial t} + M_a\frac{\partial}{\partial x} + M_t\frac{\partial}{\partial y}\right]^2 p'$$

$$- \nabla^2 p' = 2\rho_o \frac{\partial^2}{\partial x_i\, \partial x_j}(u'_{ip}\, u'_{is}) \ldots \qquad (1)$$

where u'_{ip} (as mentioned earlier) is now stationary. The boundary conditions on (1) in addition to the usual outgoing wave conditions at $x = \pm\infty$ (neglecting duct termination effects) are as follows. Let a v'_i be associated with p' as under (see Equation (6) of [8]). Define $p'' = (p'/\rho_o c_o)$, operator $D_o/D\tau = \left(\frac{1}{c_o}\frac{\partial}{\partial t} + M_a\frac{\partial}{\partial x} + M_t\frac{\partial}{\partial y}\right)$, $T'_{ij} = [u'_{ip}\, u'_{js} + u'_{is}\, u'_{jp}]$. Then v'_i satisfies:

$$\frac{D_o p''}{D\tau} + \frac{\partial v'_j}{\partial x_j} = 0 \ldots \qquad (2)$$

$$\frac{D_o v'_i}{D\tau} + \frac{\partial p''}{\partial x_i} = -\frac{\partial T'_{ij}}{\partial x_j} \text{ (for } i = 1, 2) \ldots \qquad (3)$$

(Needless to say, (1) itself is just obtained from (2), (3) by elimination of v_i'.) Then we require that $\overline{v'} \cdot \bar{n} = 0$ on all blade surfaces where $\bar{n}$ is a unit normal to the blade surfaces.

To solve the problem posed by (1), (2), (3) (and subject to the radiation conditions) one has two options. The first would be to follow Ffowcs Williams and Hall [10] and more pertinently, Goldstein [8]. Goldstein (Equation (13) of [8]) has recently generalized the Lighthill-Curle theory of aerodynamic noise by allowing for a uniform motion of the medium as well as allowing for bounding surfaces to be in motion. (This latter generalization is not needed here since we use a frame of reference in which the rotor blades are fixed.) He shows (in Section III(B) of [8]) that if a Green's function solution to (1) is constructed such that $\partial G/\partial n$ vanished on all the blade surfaces, an integral representation of the solution to (1) can be readily written down. Essentially the same procedure was followed by Ffowcs Williams and Hall [10] except that they considered the no flow situation.

In the present study, a different procedure is followed. We first construct a particular solution to (1) and calculate the associated $v_i^{P'}$ from (2) and (3). We then seek a complementary function solution to the homogeneous form of (1) (and an associated $v_i^{C'}$ from the homogeneous forms of (2) and (3)) such that $[v^{P'} + v^{C'}] \cdot \bar{n}$ vanishes on the blade surfaces.

This procedure appears a little more direct (see Preface, Chapters I and II of [11] for general remarks on Green's function versus "direct" approaches for solution to diffraction and scattering problems) and also makes it possible to use effectively the analysis of [6] to derive the particular solution. It seems more suitable than the Green function method when dealing with extended source distributions. The Green's function method is more suitable when dealing with concentrated source distributions as in the case of the point quadrupole problem dealt with by Ffowcs Williams and Hall [5].

To illustrate the fix ideas, we start by considering the problem for inlet distortion noise. In terms of a coordinate system sketched in Figure 16, and with the notation of [6], the quadrupole noise generation problem may be written down as governed by:

$$\frac{\partial p}{\partial \tau} + M_a \frac{\partial p}{\partial x} + \frac{\partial v_1}{\partial x} + \frac{\partial v_2}{\partial y} = 0$$

$$\frac{\partial v_i}{\partial \tau} + M_a \frac{\partial v_i}{\partial x} + \frac{\partial p}{\partial x_i} = - \frac{\partial Q_{ij}}{\partial x_j} \qquad \text{(for } i = 1, 2\text{)}$$

where x_1, x_2 are sometimes used to denote x, y. (v_1, v_2 are velocity components normalized by W_r parallel to x, y, and p is the acoustic pressure normalized by $\rho W_r c_o$). In the above $Q_{11} = 2 u_p u_s$, $Q_{12} = Q_{21} = (u_p v_s + u_s v_p)$ and $Q_{22} = 2 v_p v_s$. For the distortion case with n an integer varying from 0 to ∞, typical expressions for Q_{11}, Q_{12}, Q_{22} would be:

$$Q_{11} = -(\pm 2A' + 2j B')C_i(\ldots)$$

$$Q_{12} = Q_{21} = \mp C'C_i(\ldots)$$

$$Q_{22} = 0$$

where (...) stands for

$$\exp[-\alpha_n|x|]\exp(j\,\delta_n\,x)\exp[j\,\beta_n(1 - \frac{iS}{nB})y]\exp(j\,\beta_n\,M_t\,\tau)$$

and for fixed n, "i" is an integer varying from $-\infty$ to $+\infty$. If n = 0, we must replace A', B', C' in the above by A, B and C. (A, B, C, A', B', C' are constants defined in Appendix 2.)

Since we are dealing with partial differential equations with constant coefficients, all the quantities p, v_1, v_2 must have a y-τ dependence of type given by the source term, i.e.

$$\exp[j\,\beta_n(1 - \frac{iS}{nB})y]\exp(j\,\beta_n\,M_t\,\tau).$$

We assume that this y-τ dependence has been "factored" out of the governing equations and we are thus left with a set of ordinary differential equations in x. These o.d.e. are again characterized by constant coefficients and thus we introduce axial Fourier transforms of all functions of x, say s(x) as $\tilde{s}$ by

$\tilde{s} = \int_{-\infty}^{\infty} s(x)\, e^{-jZx}\, dx$ with the inversion formula being $s(x) = \frac{1}{2\pi} \int_{-\infty}^{\infty} \tilde{s}(Z)\, e^{jZx}\, dZ.$

We thus have, with $k_o = \beta_n\, M_t$, $k_y = \beta_n(1 - \frac{iS}{nB})$, that:

$$(k_o + M_a Z)\tilde{p} + Z\tilde{v}_1 + k_y\,\tilde{v}_2 = 0$$

$$Z\tilde{p} + (k_o + M_a Z)\tilde{v}_1 = j[Z\,\tilde{Q}_{zz} + k_y\,\tilde{Q}_{12}] = \tilde{s}_1$$

$$k_y\,\tilde{p} + (k_o + M_a Z)\tilde{v}_2 = j[Z\,\tilde{Q}_{21} + k_y\,\tilde{Q}_{22}] = \tilde{s}_2$$

$\tilde{Q}_{11}$, $\tilde{Q}_{12}$, etc., denote axial Fourier transforms of the parts of Q_{11}, Q_{12}, etc., after factoring out of the part $\exp[j\,k_y\,y]\,\exp(j\,k_o\,\tau)$. Expressions for them are:

$$\tilde{Q}_{11} = \frac{2j[2(Z - \delta_n)A' - 2\,\alpha_n\,B']C_i}{(Z - Z_1)(Z - Z_2)}$$

where $Z_{1p} = \delta_n + j\,\alpha_n$ and $Z_{2p} = \delta_n - j\,\alpha_n$

$$\tilde{Q}_{12} = \frac{2j\,C'\,C_i(Z - \delta_n)}{(Z - Z_{1p})(Z - Z_{2p})}$$

and $\tilde{Q}_{22} = 0$.
Define $Z_v = (-k_o/M_a)$ and

$$Z_{1s} = \frac{k_o\,M_a - \{k_o^2 - k_y^2(1 - M_a^2)\}}{(1 - M_a^2)}$$

$$Z_{2s} = \frac{k_o\,M_a + \{k_o^2 - k_y^2(1 - M_a^2)\}}{(1 - M_a^2)}$$

Then if we define

$$D = M_a(1 - M_a^2)(Z - Z_v)(Z - Z_{1s})(Z - Z_{2s})$$

and

$$D_1 = (1 - M_a^2)(Z - Z_{1s})(Z - Z_{2s})$$

the solutions for $\tilde{v}_1$, $\tilde{v}_2$, $\tilde{p}$ are:

$$\tilde{v}_1 = \frac{(k_o + Z\,M_a)^2\,\tilde{s}_1 + k_y(Z\,\tilde{s}_2 - k_y\,\tilde{s}_1)}{D}$$

$$\tilde{v}_2 = \frac{(k_o + Z\,M_a)\tilde{s}_2 - Z(Z\,\tilde{s}_2 - k_y\,\tilde{s}_1)}{D}$$

$$\tilde{p} = \frac{-Z\,\tilde{s}_1 - k_y\,\tilde{s}_2}{D_1}$$

Upon inverting the expressions for $\tilde{v}_1$, $\tilde{v}_2$ and $\tilde{p}$, we note that wavelike contributions will appear at the poles of the expressions for $\tilde{v}_1$, $\tilde{v}_2$ and $\tilde{p}$. For $\tilde{v}_1$ and $\tilde{v}_2$ these are at Z_v, Z_{1s}, Z_{2s} and Z_{2p}. For $\tilde{p}$, they are Z_{1s}, Z_{2s}, Z_{1p} and Z_{2p}.

The physical interpretation of these results is as follows. In general, the quadrupole sources generate five types of waves. Firstly they generate (downstream of the location of the actuator disk) a rotational wave which is convected with the flow associated with the pole at Z_v. This wave is not involved in so far as the acoustic pressure p or $\tilde{p}$ is concerned obviously because no pressure fluctuations are associated with a rotational wave in a

uniformly flowing medium. Secondly the quadrupole sources generate two acoustic waves upstream and downstream associated with the poles at Z_{1s} and Z_{2s}. If $k_o > 0$, the pole at Z_{1s} is the downstream acoustic wave and that at Z_{2s} the upstream wave. If $k_o < 0$, the reverse is true. Now the previous study [6] in fact employed precisely these two pole contributions to deduce the noise generated by the quadrupole mechanism. Finally, two "potential" wave contributions appear due to the poles of Q_{11} and Q_{12} at Z_{1p} and Z_{2p} (downstream and upstream respectively). These two contributions represent decaying waves constituting the "particular" integral part of the solution to the governing equations and were of no interest previously because they represent decaying waves and hence have no acoustic energy associated with them.

Having developed the solutions for v_1, v_2 (or $\tilde{v}_1$ and $\tilde{v}_2$) we can now indicate what needs to be done to account for the scattering effect of the blade rows on these velocity fields. The problem with v_1 and v_2 as they stand is that after transforming them to a frame of reference fixed with the rotor (which step basically alters their frequency to [iS M_t c_o/a]) one finds in general that the combination [$v_1 \sin(\alpha_r) - v_2 \cos(\alpha_r)$] is not zero on the blade surfaces. This, of course, is a requirement that should be imposed to properly account for the scattering effect of the rotor blade row.

To carry out this requirement in all its generality is both not feasible and not even meaningful in view of the actuator disk model used to calculate the rotor associated velocity fields. An approximate method of handling this difficult problem has therefore been adopted as follows. We impose the requirement that [$v_1 \sin(\alpha_r) - v_2 \cos(\alpha_r)$] be zero on the three wave systems (associated with Z_v, Z_{1p} and Z_{1s} or Z_{2s} depending on whether $k_o \gtrless 0$) generated aft of the actuator disk plane. In other words, for estimation of forward radiated noise (which is all that we will compute in this program) we consider the effective actuator disk to be located in a plane coincident with the leading edge plane of the rotor. If one was calculating aft radiated noise, a more appropriate model might be one where the actuator disk plane was taken coincident with the trailing edge plane of the rotor.

With this model then, we retain the upstream noise calculated previously. In addition, we compute upstream generated acoustic waves when the condition that ($v_1 \sin(\alpha_r) - v_2 \cos(\alpha_r)$) vanish is imposed on the three aft radiated waves.

Even with these approximations, we have still to contend with a major physical aspect which renders the scattering problem complex. The velocity fields associated with v_1, v_2 are of the type $\exp[j k_y y]\exp[j k_o \tau]$ where $k_y = [(nB - iS)/a]$ and $k_o = nB M_t/a$ ($n \geq 0$ and $-\infty \leq l \leq \infty$) with "a" denoting the mean radius of analysis. The rotor blades can be written as having a y-τ dependence of $\exp(jmB \frac{y}{a})\exp[jmB M_t \frac{\tau}{a}]$ where m denotes any integer. This means that the scattering effect of the blade row on any field of type $\exp[j k_y y] \exp(j k_o \tau)$ is to alter the tangential or y dependence from $\exp(j k_y y)$ to $\exp\{j[k_y + (mB/a)]y\}$ and the frequency from $\exp(j k_o \tau)$ to $\exp[j(k_o + mB M_t)\tau]$. We may represent all of this diagrammatically as follows. Let us plot a normalized frequency $\omega_N = (k_o a/B M_t)$ versus a normalized lobe number $\ell = (a k_y/B)$ (Figure 17). The quadrupole source terms will plot as abscissa lines passing through $\omega_N = 0, 1, 2$, etc. The propagating acoustic regime of interest

on this plot clearly corresponds to $|\omega_N/\ell|^2 M_t^2 + M_a^2 > 1$ which is shown as the cross hatched region in the above plot. Finally we notice that the scattering effect of the rotor on the above plot manifests itself as a shift of both ω_N and ℓ by "m". We may represent this effect therefore on a $\omega_N - \ell$ plot by a line at 45° to the x or y axis.

The implication of the above is then as follows. If we are interested in say the noise corresponding to $\omega_N = 1$ (fundamental noise) we must account for all source terms that lie on the (Figure 18) line segments A_0B_0, A_1B_1, A_2B_2, etc., and C_0D_0, C_1D_1, etc. From each of these source regions, three v_n contributions corresponding to the rotational, sound and potential waves must be accounted for. One final simplification used is to consider all these contributions without regard to phase effects, i.e. they are added up in a mean square or power sense.

For a given harmonic, we first compute the three v_n contributions from the line segments A_0B_0, A_1B_1, etc., and C_0D_0, C_1D_1, etc. For each v_n, a gust load on each blade is computed according to assumptions to be explained in the following section. Using the assumption of compact forces one can then estimate the acoustic radiation upstream and downstream of the blade row though interest is only in the upstream radiated sound.

The above analysis has also been completed for the case of quadrupole noise generation by inlet turbulence. The details are similar to what has been sketched in Figure 18. u_s and v_s are now replaced by $d Z_u$ and $d Z_v$ [6] and there is now a need to directly construct an expression for the mean square pressure and employ the relations between $d Z_u$, $d Z_v$ and the spectrum of the turbulence.

Assumptions Used in Addition to Those Detailed Above and Also Mentioned in [6]

1) Both in the "primary" dipole analysis and in estimating gust loads due to the quadrupole induced v_n, Osborne's results [12] as expressed in closed form by Kemp [13] were used to compute the lift response. Osborne's work is a perturbation theory attempting to include compressibility effects in the Sears' type problem. It was found that the old Sears and Kemp-Sears type results lead to gross overestimation of noise at the high subsonic M_{rel} end.

2) The calculation of the rotor potential flow requires a knowledge of the lift coefficient produced by the rotor. In [6], this lift coefficient was deduced from the ideal work equation (sometimes called Euler turbine equation). It seems as though that when the rotor is operating substantially off design, e.g. when the flow incidence angle at the rotor exceeds 0.1 radian, the lift coefficient is better estimated by a relation of type $C_L = (2\pi)$ (incidence angle)(constant)$/\sqrt{1 - M_r^2}$ where the constant may be estimated from Weinig's work [14] as of order 0.8 for compressor rotor cascades. The factor $(1 - M_r^2)^{-\frac{1}{2}}$ accounts for the Prandtl-Glauert enhancement of C_L due to compressibility. Above $M_r \sim 0.85$ however such a formula was not used (since the steady aerodynamics of such high velocity cascade flows is not well understood) and only the work equation was used to deduce C_L.

Comparison with Data

In Figure 18, we show comparisons with the data of [7]. For rotor 1 (with

45 blades) comparisons are carried out by analyzing the interaction with a four lobed inlet distortion with 2% velocity defect and with the defect in the form of a triangular pulse of width equal to the width of the four struts employed ahead of the rotor in [6]. For rotor 2 (90 blades), comparisons are carried out with a model of homogeneous, isotropic turbulence impinging on the rotor. The turbulence parameters were deduced from our "clean inlet" measurements of Part I since no turbulence measurements were carried out in [6]. Firstly we note general agreement between the data and the predictions. Secondly we would like to reiterate a point made in the introduction that the theory would be expected to predict similar trends for the two rotors since they differ only in blade number but the data are not quite similar. With regard to rotor 2, the 60% speed data appear too high and the 80% speed data too low. Also agreement on the slope of the 60% speed data is found to be improved by subsequent use of an anisotropic turbulence model. If a turbulence model had been employed for both rotors the 90 bladed rotor (rotor 2) would be predicted to be about 3 - 4 dB quieter than the 45 bladed rotor. The variation with flow coefficient of the experimental data for rotor 2 looks peculiar. For future reference, we note that the theoretical curves shown here are fairly representative of what the theory predicts in general. The noise is predicted to be relatively independent of flow coefficient (or even decreasing with decreasing flow coefficient) at low relative Mach numbers (< .55), increasing monotonically with decreasing flow coefficient for relative Mach numbers from .55 to .85 and finally exhibiting a tendency to peak at a certain flow coefficient for relative Mach numbers > 0.85. We also wish to point out with regard to Figure 18 that whenever $M_{rel} > 0.85$, the "free" quadrupole contribution dominates as might be expected from dimensional reasoning. Since this involves the steady, rotor field which is estimated by linearized, subsonic, steady aerodynamics (Prandtl-Glauert) we may anticipate a tendency to overestimate the noise as M_{rel} approaches unity.

Figure 19 shows the first efforts to compare theory and data for our Part I experiments with regards to the PWL spectrum. The blade passing frequency levels are reasonably well predicted but the spectrum shape for the low loading case is not well predicted. (It is broader than the data.) The blade loading effect theory-data comparison it vitiated by the large increases about $f/f_b = \frac{1}{2}$ and $f/f_b = (3/2)$. In general the theory predicts a rather uniform change of order measured ΔOAPWL. Also we seem to have done a little better with the 70% speed data.

Motivated by the sharply peaked spectra at low loading, we tried to see if the theory-data comparison improved by trying to incorporate an anisotropic turbulence model. Motivation here is the suggestion by D. Hanson [15] that reasonably isotropic eddies from the ambient are stretched out streamwise in the process of being drawn through the contraction (Figure 20). A theory given in the early 50's by Batchelor, Ribner/Tucker [16, 17] on the distortion of the spectrum of homogeneous, isotropic turbulence due to convection through a sudden contraction is found useful in this regard. Theory considers deformation of vortex lines as shown in lower half of Figure 20. It's application to actual contractions is highly questionable as noted by Batchelor because the inequality for which it is valid is most unlikely to be met in the case of real contractions. Thus our use of it is only to employ the post contraction spectra as a sample of the kind of spectra we might associated with eddies stretched streamwise and contracted cross streamwise.

Implementation of the theory does lead to a considerably improved ability to predict the inlet PWL spectrum shape as shown in Figure 21. The contraction ratio of 2 was chosen on the basis that Hanson has reported (u_θ/u_a) values of about 3 and in our flow path the contraction ratio from the inlet to the rotor is 1-1/3. Of course for the static case, the concept of "contraction ratio" is somewhat meaningless since it is infinite. A contraction ratio of 4 leads to spectrum predictions even more peaked at f_b, $2f_b$, etc., and would be acceptable if one argued that sources other than isolated rotor-turbulence interaction were present. But a ratio of 2 yields best agreement with the spectrum shape if one argues that only rotor-turbulence interaction noise was present. The main message of Figure 21 is that even a modest extent of eddy anisotropy as represented by a sudden contraction ratio of 2 suffices to bring the predicted spectrum shape in line with the measured data.

Figure 22 summarizes the effects of grids at low loading. Three discrepancies are (a) failure to see predicted change at the blade passing frequency with the 1-2/3" and 2-1/4" grids, (b) higher than predicted change at low frequencies with the 1-2/3" and 2-1/4" grids and (c) lesser than predicted attenuation at high frequencies (> 10 kHz). With regards to (a) all we can say is that the predicted change was observed at both the third octave bands just adjacent to the blade passing frequency. (b) seems related to aeolian tones from the grids - a rough calculation assuming a Strouhal frequency peak at .2 gives a center frequency for these tones around 2 kHz. (c) is possibly explained by the fact that even with 10 kHz sound we are approaching wavelengths of order 1" so that perhaps the grids are attenuating some of the generated sound.

Conclusions

This study has introduced four new ideas over and above the ideas considered in [6] in order to explain the complicated nature of the experimentally obtained data on the influence of tip speed and flow coefficient on subsonic, inlet radiated fan noise. While the precise quantitative form employed for these ideas in this study (Part II) may be the subject of debate, it seems inescapable that a proper accounting of the data cannot be achieved without paying attention to each of these ideas. They are:

1) The "direct" quadrupole noise contribution alone cannot explain the flow coefficient/pressure ratio dependence. Especially for $M_{rel} < 0.85$, the scattering effect by the blade row of the direct quadrupole contribution has to be accounted for. The lower M_{rel} is the more true this remark is.

2) A major input needed to estimate the rotor locked potential flow field is the steady rotor lift coefficient (C_L). For near design incidence, C_L can be estimated from the ideal work equation (from the experimentally recorded pressure ratio) but when the blade row is operating way off-design (say at incidence angles greater than 0.1 radians) an incidence angle related estimation of C_L works better than a nominal pressure ratio related estimation of C_L. A more design oriented statement of this issue is as follows. Most of the subsonic fan noise data available in the aircraft engine noise area is actually part speed (say 50% to 80%) data of fans whose design (100% speed) M_{rel} is supersonic. In this part speed mode, such fans often exhibit very little nominal change in measured pressure ratio for substantial changes of flow coefficient/incidence angle. One also notes substantial changes in noise

at constant tip speed and trying to explain this on the basis of the ideas of [6] and Part II herein leads to the above mentioned conclusion concerning estimation of C_L.

3) Both in calculation of primary dipole noise and quadrupole induced dipole noise, it seems essential (in order to avoid gross overestimation of dipole noise) to incorporate compressibility effects in calculating blade induced unsteady forces in response to specified unsteady, upwash distributions. An approximate theory due to Osborne was used in the current study.

4) To get detailed agreement on the complete PWL spectrum it seems necessary to accommodate in some fashion the fact that the inlet contraction process leads to eddy asymmetry. An elementary theory for sudden contractions due to Batchelor, etc., was used in the present study.

A final formulation incorporating all these effects does succeed in explaining the data of [7] and the high flow data of Part I. As shown in Figure 22, the effect of grids is also predicted to some extent (see earlier discussion of Figure 22). So far as effect of changing flow coefficient in Part I goes, we are stuck with the uncertainty introduced by the pre-stall noise signature with peaks at ½ and 1½ times blade passing frequency. It is arguable that if we ignore increases around these bands, the theory shown in Figure 19 does do reasonably well in predicting the relative changes due to change of flow coefficient.

These types of theoretical studies involve at least four disciplines. Firstly steady state rotor aerodynamics is involved. Secondly unsteady rotor aerodynamics enters in. Third and fourth, we are also contending with acoustics of moving media and the area of stationary turbulence. In our view, in view of all the experimental problems and theoretical uncertainties in each of the four disciplines, it is somewhat questionable whether a more satisfactory "theory" can be developed. The two areas worthy of further study seem to be: (a) further theory-data comparison with other sources where data is available on effects on noise of varying pressure ratio at constant rmp (such an effort is currently underway using, e.g. data from the NASA Quiet Engine Program where data on fans A, B is available showing effects of employing small, nominal and large discharge nozzles); (b) further exploration of the nature/origin of the large increases of noise at low flows found in Part I. (Some assessment of this is currently underway by examining data obtained on other programs at GE on rotor 11 with flows intermediate between the two extremes studies in Part I.)

References

1. J. M. Tyler and T. G. Sofrin, 1962, SAE Trans., 70, 309. Axial Flow Compressor Noise Studies.

2. T. G. Sofrin and J. C. McCann, 1966, paper presented at the 72nd Meeting of the Acoustical Society of America. Pratt and Whitney Experience in Compressor Noise Reduction.

3. I. J. Sharland, 1964, J. Sound and Vibration, 1(3), 302. Sources of Noise in Axial Flow Fans.

4. J. A. Asher, M. Kurosaka and S. D. Savkar, 1972, SRD-72-079. Research on Noise Generation from Large Fan Engines.

5. T. F. Gelder, 1975, private communication.

6. R. Mani, NASA Contractor Report No. NASA CR-2479, October 1974. Isolated Rotor Noise Due to Inlet Distortion on Turbulence.

7. T. F. Gelder and R. F. Soltis, National Aeronautics and Space Administration TM X-2190, 1971. Inlet Plenum Chamber Noise Measurement Comparison and 20-Inch-Diameter Fan Rotors with Aspect Ratios 3.6 and 6.6.

8. M. Goldstein, J. Acoust. Soc. of America, 56, No. 2, August 1974, pp. 497-509. Unified Approach to Aerodynamic Sound Generation in the Presence of Solid Boundaries.

9. J. E. Ffowcs Williams, invited lecture at the Eighth International Congress on Acoustics, London, 1974. Sources of Sound.

10. J. E. Ffowcs Williams and L. H. Hall, J. Fluid Mechanics, 40, 1970, pp. 657-670. Aerodynamic Sound Generation by Turbulence Flow in the Vicinity of a Scattering Half Plane.

11. B. Noble, Pergammon Press, 1968. Methods Based on the Wiener-Hopf Procedure for the Solution of Partial Differential Equations.

12. C. Osborne, AIAA Journal, 11, 1973, p. 105. Unsteady Thin Airfoil Theory for Subsonic Flow.

13. N. H. Kemp, AIAA Journal, 11, 1973, p. 1359. Closed Form Lift and Moment for Osborne's Unsteady Thin-Airfoil Theory.

14. F. Weinig (Editor: W. R. Hawthorne) - Section B, 1964. Aerodynamics of Turbines and Compressors.

15. D. B. Hanson, AIAA paper presented at Aero-Acoustics Specialists' Conference at Langley, Virginia, 1975. Measurements of Static Inlet Turbulence.

16. G. K. Batchelor, Cambridge University Press, 1953. The Theory of Homogenous Turbulence.

17. H. S. Ribner and M. Tucker, NACA Report 1113, 1951. Spectrum of Turbulence in a Contracting Stream.

18. M. Goldstein, J. Dittmar and T. Gelder, NASA TN D-7676, 1974. A Combined Quadrupole-Dipole Model for Inlet Flow Distortion Noise from a Subsonic Fan.

APPENDIX I

Tabulation of One Third Octave SPL's, PWL's, OASPL and OAPWL Obtained During the Study of Part I

MODEL SOUND PRESSURE LEVELS (59. DEG. F, 70 PERCENT REL. HUM. DAY) - ANGLES FROM INLET

		0.	10.	20.	30.	40.	50.	60.	70.	80.	90.	100.	110.	PWL
	50													
	63													
RADIAL 17. FT.	80													
(5. M)	100	66.1	66.0	65.8	64.5	63.8	64.5	66.0	67.0	67.4	66.6	66.7	65.0	99.8
VEHICLE	125	71.1	70.5	69.3	67.0	67.6	67.5	69.0	69.5	70.4	68.8	70.4	69.8	103.0
	160	72.8	72.3	72.5	72.8	71.8	71.0	70.5	69.8	71.4	70.3	71.2	68.8	104.7
	200	77.3	78.5	78.0	77.3	76.8	77.0	74.5	72.8	71.2	69.1	72.2	70.8	108.1
NASA Rotor 11	250	82.3	82.3	81.5	80.3	79.1	78.0	76.7	74.8	73.7	73.1	72.4	69.8	110.3
	315	80.8	80.5	79.8	78.8	77.3	76.0	74.5	74.3	72.7	70.1	70.4	69.5	108.7
	400	79.0	79.3	78.8	77.7	77.1	75.5	73.2	71.5	70.4	68.6	68.4	66.8	107.5
BAR 29.7 HG	500	76.5	77.3	77.0	76.5	75.1	73.5	71.7	70.0	68.4	66.6	68.9	63.8	105.8
(00361. N/M2)	630	78.8	79.8	79.8	79.0	77.3	76.0	73.3	71.3	70.4	67.6	67.4	64.3	107.9
TAMB 82. DEG F	800	77.5	78.0	78.3	77.7	76.6	75.3	73.0	71.0	69.2	66.8	67.9	65.8	107.0
(301. DEG K)	1000	74.8	75.2	75.3	75.2	74.6	72.5	70.2	67.0	65.4	61.8	63.1	62.7	104.1
TWET 71. DEG F	1250	73.3	74.0	74.0	73.7	73.4	71.5	69.2	66.3	64.2	61.6	60.4	59.8	102.9
(295. DEG K)	1600	74.3	74.5	74.5	74.2	74.1	72.8	70.2	66.8	64.2	61.7	59.4	59.1	103.6
HACT15.74 GM/M3	2000	76.1	77.0	76.3	75.7	75.3	73.8	71.0	67.8	64.4	62.2	60.9	60.1	104.9
(.01574 KG/M3)	2500	78.0	77.5	78.0	77.6	77.8	76.0	73.7	70.5	66.7	65.2	63.1	62.1	107.1
NFA11510. RPM	3150	79.3	79.5	79.9	79.6	79.8	79.2	76.9	73.7	69.7	66.7	65.9	64.1	109.6
(1205. RAD/SEC)	4000	82.9	82.4	82.1	82.3	82.7	82.6	81.1	77.1	72.9	69.4	68.3	67.6	112.8
NFK11263. RPM	5000	83.9	83.6	84.8	83.7	83.9	83.3	81.8	78.1	74.1	70.1	69.7	69.0	114.0
(1179. RAD/SEC)	6300	83.7	85.7	87.3	86.6	86.9	86.0	83.8	79.3	75.1	72.5	71.4	70.5	116.5
NFD16100. RPM	8000	92.8	95.0	97.6	100.1	103.4	103.2	103.2	98.5	93.2	89.1	87.6	85.8	133.1
(1686. RAD/SEC)	10000	86.9	88.1	90.3	90.7	93.2	93.1	91.9	87.9	82.2	78.7	77.3	76.2	123.0
NO. OF BLADES 44	12500	86.3	87.9	88.8	88.4	88.6	87.9	86.8	80.8	75.3	71.9	71.5	71.5	118.8
	16000	96.9	94.4	93.6	94.1	95.9	95.3	93.9	87.5	80.7	78.1	77.2	77.2	125.8
Clean Inlet, 70% Speed, Discharge Valve Setting = 0	20000	87.7	88.1	89.6	88.5	89.1	88.6	86.3	80.2	73.3	70.3	68.9	69.8	119.9
	25000	86.1	87.5	91.5	90.2	92.2	91.5	89.0	81.6	74.8	69.0	69.4	68.9	122.9
	31500	82.6	84.0	87.0	86.1	87.5	86.5	84.9	76.5	68.4	63.2	63.0	65.4	119.3
	40000	78.5	79.2	82.9	81.0	83.5	82.2	79.9	70.5	64.1	58.5	60.8	67.0	116.2
	50000	77.2	76.5	78.0	77.2	80.3	81.3	76.8	66.3	63.8	57.6	62.5	68.1	115.3
	63000	75.5	72.6	72.6	72.6	77.1	77.7	7 .	1.	4.5	5 1	63.7	69.2	114.7
	80000	72.6	68.2	68.7	67.4	72.4	73.8	70.9	60.8	64.6	59.9	60.5	72.0	115.8
OVERALL MEASURED														
OVERALL CALCULATED		100.2	100.2	101.7	102.7	105.2	104.9	104.4	99.5	94.3	90.5	89.3	88.1	135.3

MODEL SOUND PRESSURE LEVELS (59. DEG. F, 70 PERCENT REL. HUM. DAY) - ANGLES FROM INLET

		0.	10.	20.	30.	40.	50.	60.	70.	80.	90.	100.	110.	PWL
	50													
	63													
RADIAL 17. FT.	80													
(5. M)	100	70.5	69.7	71.0	70.0	69.7	70.5	70.5	67.3	67.4	67.3	66.8	64.4	102.3
VEHICLE	125	72.2	72.2	72.7	71.0	71.7	71.5	71.2	70.5	70.9	69.8	70.8	69.6	104.6
	160	78.5	78.2	79.0	79.2	78.5	78.5	77.5	71.9	70.4	68.6	69.1	68.1	109.0
NASA Rotor 11	200	77.5	78.7	79.2	79.0	78.0	78.5	76.7	71.8	69.7	66.6	72.8	69.1	109.0
	250	81.2	80.7	80.0	78.7	77.7	77.0	76.5	73.0	72.2	71.3	69.8	67.1	108.9
	315	79.7	79.5	79.2	77.7	76.5	75.5	74.5	72.8	71.4	69.1	68.0	67.6	107.8
	400	77.7	78.2	77.7	77.0	76.2	75.5	73.7	72.0	68.7	67.1	66.0	63.8	106.7
BAR 29.7 HG	500	77.0	77.2	77.7	77.2	76.0	75.0	74.0	70.8	68.4	66.3	64.5	62.8	106.5
(00361. N/M2)	630	79.7	80.0	80.5	80.0	78.5	77.5	75.7	72.8	71.2	68.1	66.3	64.3	109.0
TAMB 82. DEG F	800	81.5	82.0	82.7	81.9	80.3	79.5	77.5	74.5	72.2	70.3	70.0	68.1	110.9
(301. DEG K)	1000	84.0	83.7	83.7	82.9	81.8	80.5	77.7	74.8	72.1	69.3	68.2	68.6	111.8
TWET 71. DEG F	1250	86.2	86.2	86.2	85.9	85.0	83.5	80.7	78.0	75.2	73.1	70.8	69.9	114.8
(295. DEG K)	1600	87.2	88.2	89.0	88.4	87.8	86.5	84.0	80.5	77.9	75.4	73.3	71.9	117.5
HACT15.74 GM/M3	2000	90.2	91.7	92.0	90.9	90.0	88.2	85.5	81.3	79.2	76.4	74.3	73.7	119.7
(.01574 KG/M3)	2500	95.5	95.5	94.2	93.4	92.2	91.2	87.9	84.0	80.9	79.2	76.5	75.2	122.3
NFA11507. RPM	3150	94.7	95.5	95.9	94.3	94.7	92.9	89.9	85.5	82.4	79.9	78.0	76.9	123.9
(1205. RAD/SEC)	4000	97.1	98.4	99.1	99.0	100.6	101.8	99.3	94.6	91.1	88.1	86.2	84.9	130.7
NFK11260. RPM	5000	101.3	106.1	106.0	102.9	102.3	101.3	97.5	93.1	89.8	87.8	86.6	85.6	132.6
(1179. RAD/SEC)	6300	98.2	100.9	101.5	100.6	100.3	99.0	96.3	93.8	87.4	85.0	83.8	82.9	129.9
NFD16100. RPM	8000	97.2	99.5	101.1	101.6	103.6	104.5	103.4	97.5	92.7	89.6	87.5	86.4	133.8
(1686. RAD/SEC)	10000	100.5	101.3	102.3	102.2	102.8	101.8	99.1	92.5	88.4	86.0	84.0	83.5	132.1
NO. OF BLADES 44	12500	100.0	101.8	104.1	106.6	106.1	104.9	103.8	96.1	91.3	88.6	87.1	86.9	135.7
	16000	99.1	99.2	100.6	100.1	100.3	99.8	97.6	89.2	84.2	82.3	81.0	82.3	130.5
Clean Inlet,	20000	95.9	97.6	99.5	100.7	101.5	99.8	98.0	89.2	82.6	80.3	78.0	77.9	131.3
70% Speed,	25000	94.3	95.9	98.2	97.5	98.6	97.0	94.5	85.6	79.3	75.3	74.5	73.0	129.0
Discharge Valve	31500	91.6	92.5	95.7	94.5	96.4	94.7	92.4	82.0	74.9	69.9	68.9	67.2	127.5
Setting = 1.45	40000	89.6	89.4	92.4	90.8	92.4	91.4	88.4	77.0	69.6	63.5	64.5	62.4	125.2
	50000	87.7	87.2	88.7	87.7	90.2	89.8	85.6	72.5	66.5	58.8	63.9	61.2	124.5
	63000	85.7	83.1	82.8	82.8	87.0	87.2	82.0	68.6	65.0	58.6	65.5	62.3	123.8
	80000	82.5	78.4	78.4	77.8	82.6	83.8	80.9	70.3	64.6	59.9	66.2	67.6	124.4
OVERALL MEASURED														
OVERALL CALCULATED		109.0	111.1	112.1	111.9	112.3	111.6	109.7	103.2	98.9	96.3	94.7	93.9	142.4

MODEL SOUND PRESSURE LEVELS (59. DEG. F, 70 PERCENT REL. HUM. DAY) - ANGLES FROM INLET

		0.	10.	20.	30.	40.	50.	60.	70.	80.	90.	100.	110.	PWL
	50													
	63													
RADIAL 17. FT.	80													
(5. M)	100	64.2	65.0	65.0	63.5	61.3	63.5	65.3	64.8	66.1	65.2	65.4	62.8	98.4
VEHICLE	125	70.7	70.3	68.8	66.8	66.6	67.0	67.8	69.5	69.8	69.7	69.4	69.0	102.6
	160	72.5	72.3	74.5	75.0	71.8	72.8	70.8	69.8	72.6	73.5	72.7	75.3	106.7
NASA Rotor 11	200	75.7	77.0	76.3	75.3	74.3	74.3	71.7	70.3	69.3	68.5	67.7	67.0	105.7
	250	82.0	81.8	80.8	79.5	78.8	77.5	76.2	74.3	73.6	73.0	71.6	69.0	109.8
	315	80.0	80.0	79.0	78.3	76.8	75.5	74.0	73.8	72.6	70.2	69.1	68.8	108.1
	400	76.7	76.8	76.5	75.2	74.1	73.0	71.0	69.0	67.8	66.5	65.9	64.3	104.9
BAR 29.7 HG	500	74.7	74.5	75.0	73.7	72.6	71.8	70.0	68.0	66.1	64.5	62.9	61.5	103.4
(100361. N/M2)	630	76.7	77.5	77.3	76.0	75.1	73.3	70.5	68.0	67.6	65.2	63.1	62.0	105.2
TAMB 82. DEG F	800	74.5	75.3	75.8	75.2	74.1	72.5	70.2	68.5	66.1	64.5	64.4	62.0	104.3
(301. DEG K)	1000	72.2	72.7	72.5	71.7	70.8	69.0	67.0	63.7	61.5	59.2	60.4	59.0	100.8
TWET 71. DEG F	1250	72.2	72.5	72.3	71.7	71.5	69.3	67.2	63.8	62.3	60.3	58.6	57.5	101.0
(295. DEG K)	1600	72.0	73.0	73.3	72.2	71.6	70.0	67.2	64.3	62.1	59.3	58.1	56.6	101.4
HACT15.74 GM/M3	2000	74.5	75.3	76.3	75.4	74.6	72.8	69.5	66.3	63.6	61.1	59.9	58.6	104.1
(.01574 KG/M3)	2500	77.2	77.0	77.2	77.1	76.6	75.5	72.7	69.0	66.1	63.6	62.9	61.1	106.2
NFA 9875. RPM	3150	79.7	80.2	79.2	79.4	80.5	79.2	75.7	71.5	68.1	66.6	64.4	63.4	109.3
(1034. RAD/SEC)	4000	81.9	82.2	81.6	81.0	81.7	81.6	78.8	74.4	70.8	68.5	66.0	65.6	111.4
NFK 9663. RPM	5000	84.1	84.1	84.8	84.7	83.9	84.1	82.0	77.3	73.5	71.2	68.7	68.3	114.3
(1012. RAD/SEC)	6300	88.1	90.7	92.0	92.6	93.9	93.0	91.8	85.8	82.0	79.6	78.4	77.0	123.2
NFD16100. RPM	8000	91.2	94.8	95.9	96.6	98.2	97.7	97.2	91.8	87.1	84.5	83.4	81.6	127.9
(1686. RAD/SEC)	10000	84.8	85.8	87.1	87.0	87.9	87.4	84.6	77.9	74.1	71.9	70.3	68.9	117.3
NO. OF BLADES 44	12500	88.8	89.1	90.1	89.2	89.6	89.4	88.8	81.3	76.5	73.5	73.0	72.3	120.1
	16000	91.1	92.7	91.4	91.8	92.1	92.6	92.6	85.5	79.9	77.5	75.4	75.2	123.5
Clean Inlet,	20000	84.1	84.9	87.8	90.7	90.8	88.6	87.8	79.2	72.5	69.1	67.6	66.8	120.6
60% Speed,	25000	81.8	82.2	85.7	85.7	87.2	86.0	85.2	76.1	69.7	65.7	65.2	62.9	117.9
Discharge Valve	31500	79.0	79.8	83.5	82.1	84.7	84.2	82.1	72.7	65.5	61.3	61.5	60.9	116.3
Setting = 0	40000	75.7	77.0	79.6	77.8	79.7	79.4	77.4	66.2	61.3	56.4	60.8	59.5	113.0
	50000	**74.4**	74.7	76.8	74.2	76.8	76.8	73.6	62.8	61.7	56.2	62.3	63.6	111.8
	63000	73.0	71.1	70.6	70.1	73.0	75.2	70.5	59.4	61.9	56.0	63.4	62.2	111.7
	80000	66.7	68.2	68.5	67.4	66.9	73.8	70.9	60.6	58.0	55.0	60.5	65.3	114.0
OVERALL MEASURED														
OVERALL CALCULATED		97.8	99.6	100.3	100.8	101.8	101.3	100.5	94.6	90.1	87.7	86.6	85.5	132.0

MODEL SOUND PRESSURE LEVELS (59. DEG. F, 70 PERCENT REL. HUM. DAY) - ANGLES FROM INLET

RADIAL 17. FT.
(5. M)
VEHICLE

NASA Rotor 11

BAR 29.7 HG
(00361. N/M2)
TAMB 81. DEG F
(300. DEG K)
TWET 71. DEG F
(295. DEG K)
HACT16.03 GM/M3
(.01603 KG/M3)
NFA 9875. RPM
(1034. RAD/SEC)
NFK 9672. RPM
(1013. RAD/SEC)
NFD16100. RPM
(1686. RAD/SEC)
NO. OF BLADES 44

Clean Inlet,
60% Speed,
Discharge Valve
Setting = 1.45

	0.	10.	20.	30.	40.	50.	60.	70.	80.	90.	100.	110.	PWL
50													
63													
80													
100	64.1	69.7	70.5	70.0	69.7	70.5	64.0	65.3	64.7	64.6	65.3	61.9	100.8
125	68.1	71.0	71.7	70.2	69.7	70.5	66.8	68.8	67.9	68.3	68.8	67.9	102.7
160	72.3	77.2	78.7	79.0	78.2	79.0	70.8	70.8	71.4	72.6	72.3	74.6	109.0
200	72.5	76.2	76.5	76.5	75.7	76.2	69.2	68.0	65.7	64.6	65.5	64.1	105.6
250	77.8	78.2	77.5	76.7	75.7	75.2	72.7	70.5	69.2	68.3	67.3	64.1	106.5
315	76.3	76.7	76.5	75.2	74.5	73.0	70.7	69.8	67.9	65.8	65.3	64.3	105.0
400	74.0	75.0	75.0	74.2	73.5	73.2	68.2	66.8	65.4	63.1	63.5	61.1	103.6
500	73.0	74.2	74.2	74.0	73.5	72.7	69.2	67.5	65.2	63.3	61.8	60.1	103.4
630	76.1	77.2	77.7	77.0	76.0	75.2	71.5	69.3	67.7	65.4	63.5	61.8	106.1
800	78.8	80.0	80.2	79.7	78.8	77.5	73.7	71.8	69.4	67.3	67.3	65.3	108.6
1000	81.0	81.2	81.0	80.4	79.5	77.7	75.2	71.8	69.1	66.6	65.5	64.8	109.2
1250	83.3	83.7	83.7	83.9	83.0	81.5	78.7	75.3	73.2	71.1	68.0	67.6	112.6
1600	85.8	86.0	86.7	86.4	86.3	84.5	82.0	78.5	76.2	73.4	71.3	70.2	115.6
2000	89.6	89.7	90.2	88.9	88.5	87.2	84.5	80.5	77.9	75.4	73.0	72.2	118.2
2500	93.5	93.5	91.9	91.6	91.0	89.5	85.7	82.5	79.7	77.2	75.0	74.2	120.5
3150	92.8	93.7	94.4	93.8	94.2	94.7	91.9	88.2	84.7	81.9	79.2	77.9	124.3
4000	100.2	103.4	105.8	105.2	103.6	104.1	100.6	95.6	92.9	90.4	88.7	88.1	134.1
5000	100.1	103.1	102.8	100.9	98.8	97.8	94.8	89.6	86.3	84.1	82.6	82.1	129.6
6300	96.0	96.6	98.5	98.1	98.6	97.7	95.6	90.3	86.6	84.2	82.5	81.4	128.0
8000	95.7	97.6	99.2	98.7	100.3	100.4	97.8	92.2	87.6	85.5	83.7	82.1	129.9
10000	97.1	99.0	102.8	103.9	106.6	104.8	102.1	95.7	90.7	88.2	87.2	85.7	134.8
12500	96.7	98.2	99.0	98.5	100.0	100.3	97.7	90.2	85.5	83.0	81.5	81.3	129.9
16000	95.1	97.1	98.7	97.6	98.2	97.7	96.3	87.4	82.4	80.2	79.2	79.2	128.5
20000	92.4	93.6	96.5	96.4	97.2	96.1	94.0	84.4	78.6	76.3	74.3	73.9	127.3
25000	90.3	91.7	94.2	93.5	94.6	94.0	92.0	82.1	75.5	71.5	70.8	68.8	125.5
31500	87.6	89.5	91.2	90.0	92.2	90.7	88.4	77.3	70.4	65.9	65.4	64.0	123.3
40000	84.5	85.9	88.1	86.5	88.1	87.4	84.2	72.0	65.4	60.5	62.7	59.6	121.0
50000	83.6	83.6	84.6	83.6	85.4	86.0	80.7	67.7	63.9	58.5	64.0	60.1	120.3
63000	80.4	80.0	79.4	78.7	83.1	83.8	76.1	66.0	63.9	58.2	65.9	62.7	119.9
80000	74.9	78.0	78.2	77.1	81.9	83.6	70.7	70.1	64.4	59.7	66.0	67.6	123.1
OVERALL MEASURED													
OVERALL CALCULATED	107.1	109.3	110.9	110.4	111.1	110.4	107.7	101.6	97.7	95.2	93.7	92.8	140.8

MODEL SOUND PRESSURE LEVELS (59. DEG. F, 70 PERCENT REL. HUM. DAY) - ANGLES FROM INLET

RADIAL 17. FT.
(5. M)
VEHICLE

NASA Rotor 11

BAR 29.7 HG
(00361. N/M2)
TAMB 82. DEG F
(301. DEG K)
TWET 71. DEG F
(295. DEG K)
HACT15.74 GM/M3
(.01574 KG/M3)
NFA 8216. RPM
(860. RAD/SEC)
NFK 8040. RPM
(842. RAD/SEC)
NFD16100. RPM
(1686. RAD/SEC)
NO. OF BLADES 44

Clean Inlet,
50% Speed,
Discharge Valve
Setting = 1.45

	0.	10.	20.	30.	40.	50.	60.	70.	80.	90.	100.	110.	PWL
50													
63													
80													
100	62.3	62.0	62.5	61.3	61.6	61.8	62.5	61.5	62.2	61.8	63.7	59.8	95.7
125	68.6	67.8	67.5	63.8	66.8	67.5	67.3	68.5	71.2	70.3	69.7	73.3	103.4
160	69.3	69.3	69.8	69.5	68.8	69.0	68.0	63.3	66.4	64.1	64.2	66.5	100.8
200	69.3	70.3	70.8	70.0	68.8	68.3	66.7	63.3	62.4	60.8	63.9	58.8	99.8
250	74.0	73.5	73.0	71.5	70.6	69.5	69.0	66.3	65.7	64.8	64.4	61.3	101.9
315	72.0	72.0	71.5	70.5	68.6	67.8	66.7	65.5	63.9	61.6	62.1	60.8	100.3
400	72.0	72.0	71.0	70.0	69.1	67.3	65.7	62.8	62.2	60.6	61.1	59.3	99.6
500	69.3	69.5	70.0	69.7	68.6	67.3	66.0	63.8	61.7	60.1	59.1	57.3	99.1
630	73.3	74.0	73.8	73.0	72.1	71.0	69.0	66.0	64.7	62.6	61.1	59.3	102.4
800	76.5	77.0	77.0	76.7	75.6	74.0	72.0	69.0	67.4	65.6	65.1	63.5	105.7
1000	77.8	78.7	78.5	77.9	76.8	75.3	73.0	70.0	67.1	64.3	63.6	63.2	106.8
1250	80.8	81.3	82.0	81.9	81.4	80.0	77.0	74.3	71.7	69.1	66.9	66.5	110.9
1600	84.3	85.0	85.0	85.7	85.4	83.8	80.7	77.8	74.7	72.9	70.6	69.8	114.6
2000	88.1	88.5	88.5	87.9	87.3	85.5	83.2	79.8	75.9	73.7	72.4	71.3	116.9
2500	89.5	90.0	89.7	89.6	89.6	88.0	85.0	81.5	77.9	76.2	74.6	73.1	118.8
3150	93.0	94.7	96.2	96.9	97.8	97.0	94.4	90.2	87.2	83.7	83.9	81.6	126.9
4000	97.4	99.4	98.4	97.8	96.2	94.6	90.8	86.1	82.6	80.9	79.8	79.3	126.1
5000	94.6	95.4	95.0	94.0	93.9	92.8	89.8	84.8	81.6	78.3	78.2	77.5	123.5
6300	94.5	96.2	97.0	96.1	95.9	95.0	92.6	87.8	84.1	81.2	80.7	79.8	125.7
8000	94.3	96.3	98.4	100.4	100.9	101.2	96.7	90.3	86.7	85.1	83.9	82.6	130.1
10000	93.1	94.6	96.1	97.5	101.4	101.6	97.1	89.9	86.4	84.2	82.8	81.2	130.0
12500	94.3	96.6	97.1	96.2	96.6	96.2	93.3	85.3	80.8	78.9	78.7	77.8	126.5
16000	90.7	93.2	94.9	93.1	94.1	93.1	90.6	82.0	77.0	75.3	74.7	75.7	124.0
20000	87.9	90.1	92.3	91.7	92.3	91.6	88.3	78.9	73.6	71.5	69.9	70.5	122.6
25000	86.1	88.2	89.5	88.7	89.4	89.0	86.0	75.6	70.5	66.3	66.9	65.2	120.4
31500	83.1	84.5	87.0	85.1	86.5	85.7	82.1	71.0	65.9	60.9	62.2	60.4	118.1
40000	80.3	81.5	83.4	80.5	82.7	82.2	77.4	65.5	62.1	57.5	60.8	58.3	115.6
50000	79.2	78.7	79.5	77.5	79.6	79.3	74.3	61.0	63.0	57.6	62.3	59.8	114.3
63000	77.3	74.1	73.6	71.8	76.6	76.2	71.0	58.1	64.5	57.8	63.4	61.7	113.5
80000	72.6	68.5	68.7	67.6	72.4	73.8	70.9	60.6	64.6	59.9	60.3	66.3	115.0
OVERALL MEASURED													
OVERALL CALCULATED	104.0	105.8	106.4	106.5	107.4	107.1	103.4	97.3	93.8	91.5	90.7	89.5	136.9

MODEL SOUND PRESSURE LEVELS (59. DEG. F, 70 PERCENT REL. HUM. DAY) - ANGLES FROM INLET

		0.	10.	20.	30.	40.	50.	60.	70.	80.	90.	100.	110.	PWL
	50													
	63													
RADIAL 17. FT.	80													
(5. M)	100	63.0	63.0	62.6	61.2	59.6	60.9	62.4	63.5	64.3	64.5	64.4	61.8	96.8
VEHICLE	125	69.2	69.0	68.6	64.2	66.6	67.6	66.4	69.5	71.6	71.2	70.2	72.8	103.7
	160	69.5	68.5	69.3	69.0	68.1	66.4	64.7	65.8	67.3	65.2	65.2	67.0	100.5
NASA Rotor 11	200	73.2	74.3	73.6	72.4	71.5	71.4	68.4	67.5	66.6	65.2	65.9	63.0	102.8
	250	79.7	79.8	79.1	77.2	76.5	74.9	73.9	72.3	71.6	71.0	69.4	67.0	107.7
	315	77.2	77.0	76.3	74.9	74.0	72.4	71.1	71.3	69.6	67.2	65.9	65.5	105.2
	400	73.2	73.5	73.3	71.4	70.8	68.9	67.2	65.0	64.3	62.2	62.4	60.5	101.3
BAR 29.7 HG	500	70.5	70.8	71.3	69.7	69.1	67.9	65.9	64.3	62.1	60.7	59.4	57.8	99.6
(00361. N/M2)	630	72.2	72.8	72.8	71.4	70.6	68.6	66.4	64.3	63.1	60.7	59.1	57.8	100.7
TAMB 82. DEG F	800	70.2	71.3	71.8	70.6	69.6	67.6	65.4	63.8	62.3	60.2	60.6	58.3	99.9
(301. DEG K)	1000	69.2	69.7	69.3	68.4	67.8	66.3	63.6	61.2	58.8	56.2	58.6	55.5	97.8
TWET 71. DEG F	1250	69.2	70.0	70.6	69.9	69.1	66.9	63.9	60.8	59.3	57.5	56.4	55.0	98.6
(295. DEG K)	1600	69.5	71.3	71.3	70.4	69.8	68.1	64.9	62.0	59.8	58.0	56.9	55.1	99.5
HACT15.74 GM/M3	2000	72.2	74.0	73.8	73.1	73.1	71.3	68.6	64.8	62.3	60.1	58.6	57.6	102.4
(.01574 KG/M3)	2500	76.0	76.8	76.3	76.3	76.1	75.1	72.4	68.0	65.3	63.1	61.9	59.4	105.6
NFA 8225. RPM	3150	77.4	78.5	78.2	76.8	78.0	77.6	75.1	71.2	67.8	65.1	63.9	61.4	107.6
(861. RAD/SEC)	4000	80.4	80.7	81.7	80.5	81.0	80.0	76.0	72.1	69.5	67.0	65.3	63.8	110.3
NFK 8048. RPM	5000	84.3	85.4	86.6	85.6	85.1	83.2	80.4	75.8	72.7	70.5	69.0	68.0	114.5
(843. RAD/SEC)	6300	92.1	94.4	95.8	95.8	93.4	93.4	91.0	86.0	83.5	80.1	79.2	78.5	124.2
NFD16100. RPM	8000	82.4	84.0	84.4	84.5	85.4	84.1	79.3	74.3	71.4	70.0	68.1	67.3	114.1
(1685. RAD/SEC)	10000	84.3	85.5	86.1	85.6	87.4	85.7	82.8	75.9	71.6	70.1	68.6	67.9	116.1
NO. OF BLADES 44	12500	92.5	92.9	92.6	89.4	91.1	89.5	87.5	80.8	76.2	73.8	72.7	72.0	120.8
	16000	82.1	84.9	85.7	84.8	86.1	84.2	82.3	74.2	69.4	67.5	66.9	67.7	115.5
Clean Inlet,	20000	81.1	82.9	85.6	84.9	87.8	84.9	82.9	74.7	68.7	66.6	65.4	64.8	116.7
50% Speed,	25000	78.5	80.2	83.0	81.9	83.7	82.1	81.1	71.9	66.7	62.2	62.7	59.9	114.3
Discharge Valve	31500	75.0	76.3	79.8	78.0	80.2	78.6	75.0	65.5	60.8	57.3	60.5	57.9	111.2
Setting = 0	40000	71.7	73.2	76.4	73.7	75.2	74.5	70.6	60.5	59.5	55.1	60.3	56.8	108.4
	50000	**70.4**	70.5	72.1	70.1	72.6	71.9	**67.5**	**58.0**	61.2	55.9	62.3	59.6	107.4
	63000	69.2	66.3	66.4	65.0	69.8	69.0	63.4	57.6	61.9	56.0	63.2	63.5	107.4
	80000	64.2	60.7	60.5	59.3	64.4	64.4	61.1	60.6	58.5	55.3	60.5	65.3	108.4
OVERALL MEASURED														
OVERALL CALCULATED		97.0	98.4	99.2	98.4	98.1	97.1	94.6	89.0	86.2	83.6	82.7	82.2	128.3

MODEL SOUND PRESSURE LEVELS (59. DEG. F, 70 PERCENT REL. HUM. DAY) - ANGLES FROM INLET

		0.	10.	20.	30.	40.	50.	60.	70.	80.	90.	100.	110.	PWL
	50													
	63													
RADIAL 17. FT.	80													
(5. M)	100	65.1	65.3	64.8	63.8	63.1	63.8	65.0	66.0	65.9	64.8	69.2	62.9	99.3
VEHICLE	125	70.3	70.3	68.8	67.0	67.1	67.5	68.8	70.0	69.9	68.6	69.9	67.4	102.5
	160	73.8	72.5	73.0	73.3	72.3	71.5	70.8	71.8	70.9	69.6	71.2	68.1	104.9
	200	77.5	79.0	78.0	77.3	77.1	77.3	74.5	73.3	71.4	69.3	72.9	69.8	108.3
NASA Rotor 11	250	82.3	82.5	81.3	80.5	78.8	77.8	76.5	75.3	73.7	73.1	72.1	68.8	110.2
	315	82.3	82.5	81.3	80.3	79.1	77.8	76.5	75.5	73.9	71.8	71.9	70.1	110.2
	400	81.0	81.8	81.0	80.5	79.6	78.5	76.2	74.3	73.2	71.6	70.6	68.8	110.1
BAR 29.7 HG	500	83.0	83.3	83.3	82.5	81.3	80.0	78.5	76.5	74.4	72.6	70.9	68.3	111.9
(00361. N/M2)	630	86.8	87.3	87.8	86.5	85.6	84.0	82.0	80.0	78.9	76.1	74.4	72.1	115.9
TAMB 76. DEG F	800	88.3	89.0	89.3	89.2	88.6	86.5	84.7	82.3	80.7	79.1	78.9	76.3	118.4
(298. DEG K)	1000	89.5	89.7	89.0	88.9	88.3	86.8	84.5	81.0	78.9	76.6	76.6	75.8	118.0
TWET 69. DEG F	1250	90.5	90.5	89.5	88.7	88.9	88.3	85.7	83.0	80.7	77.9	76.4	74.6	118.9
(294. DEG K)	1600	90.6	90.5	91.3	90.7	90.1	89.0	86.7	83.3	80.7	78.2	76.4	74.4	119.9
HACT15.74 GM/M3	2000	92.8	94.0	94.3	94.9	94.1	94.3	92.2	89.3	86.2	83.2	82.4	79.2	124.5
(.01574 KG/M3)	2500	95.8	96.5	95.5	97.4	95.6	97.5	96.7	94.0	90.7	87.4	85.6	84.2	127.7
NFA11447. RPM	3150	92.5	92.7	92.4	91.4	90.3	89.0	86.9	82.7	79.4	76.9	74.9	73.4	120.4
(1199. RAD/SEC)	4000	92.9	94.2	93.1	91.5	91.0	89.6	87.1	82.9	79.4	76.6	75.5	74.6	121.0
NFK11264. RPM	5000	94.1	94.4	94.0	92.7	91.9	91.1	88.3	83.8	80.3	77.6	76.7	75.4	122.0
(1179. RAD/SEC)	6300	96.2	96.7	96.3	96.1	96.4	95.0	93.1	88.8	84.6	81.7	80.4	79.1	125.8
NFD16100. RPM	8000	100.4	100.2	101.8	100.3	102.1	102.9	100.3	94.9	90.9	87.8	86.0	85.3	132.2
(1686. RAD/SEC)	10000	99.1	99.3	99.8	98.7	99.2	98.6	97.1	91.7	86.9	84.0	83.1	81.2	129.2
NO. OF BLADES 44	12500	97.2	97.5	97.2	96.1	96.3	94.6	92.7	86.2	81.5	78.8	78.1	77.0	126.1
	16000	97.3	97.3	97.8	96.0	96.5	95.2	92.8	86.1	80.4	78.2	77.8	78.2	126.7
Grid #1,	20000	94.4	95.1	95.3	93.5	93.6	92.8	89.8	83.2	76.1	73.5	72.1	71.9	124.4
70% Speed,	25000	93.2	94.4	93.9	91.9	92.1	91.2	88.1	81.8	74.2	69.2	69.6	67.7	123.6
Discharge Valve	31500	90.3	90.4	91.4	88.0	88.7	87.1	84.0	76.7	69.3	63.8	64.1	62.1	120.9
Setting = 0	40000	86.2	85.9	86.5	82.9	83.6	83.1	79.6	72.1	64.8	58.9	61.0	59.5	117.5
	50000	83.7	82.2	81.5	78.9	80.8	80.5	77.0	68.7	64.7	59.5	64.2	63.6	116.1
	63000	79.7	76.3	74.5	73.0	77.0	77.1	72.4	67.1	65.0	59.3	64.1	66.7	114.5
	80000	74.6	69.2	68.7	67.4	71.9	73.3	70.4	69.8	64.1	59.4	60.3	66.6	115.2
OVERALL MEASURED														
OVERALL CALCULATED		107.6	107.9	108.2	107.2	107.6	107.4	105.3	100.6	96.9	94.0	92.7	91.3	137.9

MODEL SOUND PRESSURE LEVELS (59. DEG. F, 70 PERCENT REL. HUM. DAY) - ANGLES FROM INLET

		0.	10.	20.	30.	40.	50.	60.	70.	80.	90.	100.	110.	PWL
	50													
	63													
RADIAL 17. FT.	80													
(5. M)	100	70.2	69.7	70.2	70.0	70.0	70.5	70.7	65.8	66.7	64.8	67.8	62.6	102.0
VEHICLE	125	72.0	72.0	72.2	72.0	70.5	72.0	72.2	68.8	70.4	68.8	69.6	68.1	104.2
	160	79.5	78.7	79.5	79.7	78.7	79.2	78.5	71.3	71.4	69.1	70.8	68.6	109.6
	200	79.0	80.0	80.2	79.7	79.2	79.2	78.0	72.8	71.7	69.1	74.5	69.1	110.0
NASA Rotor 11	250	82.0	81.7	81.0	79.5	79.0	77.7	77.5	74.0	73.2	72.3	71.3	68.3	109.9
	315	81.7	81.2	81.0	79.7	78.7	77.0	76.5	74.5	73.4	70.8	70.3	69.1	109.6
	400	81.2	81.7	82.0	80.0	79.7	78.5	77.5	73.0	72.9	70.6	69.5	67.6	110.1
BAR 29.7 HG	500	81.2	81.2	81.5	81.0	80.5	79.0	80.0	75.3	72.9	71.1	69.0	67.6	111.0
(00361. N/M2)	630	84.2	84.7	85.5	85.0	84.0	83.0	80.5	78.5	77.4	74.4	72.0	69.8	114.2
TAMB 76. DEG F	800	86.0	86.7	87.0	87.2	86.3	85.0	83.7	80.5	78.4	76.8	76.5	74.6	116.5
(298. DEG K)	1000	87.2	87.0	87.0	86.9	86.3	85.2	83.2	79.8	77.4	75.1	73.7	73.8	116.2
TWET 69. DEG F	1250	88.5	89.5	89.0	88.9	88.8	87.7	85.7	82.8	81.2	77.9	75.5	75.1	118.6
(294. DEG K)	1600	92.7	92.5	93.2	92.9	92.0	91.7	89.5	86.8	83.9	81.4	78.8	77.4	122.3
HACT15.74 GM/M3	2000	93.5	95.0	95.0	94.9	93.5	93.0	91.5	87.5	85.4	82.2	80.0	78.4	124.0
(.01574 KG/M3)	2500	97.2	97.5	95.7	95.1	94.2	92.5	89.7	85.7	82.9	80.7	78.5	77.2	124.0
NFA11454. RPM	3150	96.5	97.2	97.2	96.3	96.0	94.2	90.9	86.7	83.2	81.2	79.2	77.4	125.3
(1199. RAD/SEC)	4000	99.4	100.9	101.3	101.5	101.9	102.1	98.8	94.4	91.1	88.4	86.7	85.6	131.6
NFK11271. RPM	5000	103.3	107.1	107.5	104.4	103.3	102.0	98.3	93.1	90.1	88.3	86.6	86.4	133.7
(1180. RAD/SEC)	6300	100.2	101.9	102.0	101.3	101.1	100.0	97.3	92.3	88.9	86.5	84.8	84.1	130.7
NFD16100. RPM	8000	101.1	101.9	102.2	102.7	103.8	104.1	101.8	96.7	91.4	88.3	87.2	85.1	133.6
(1686. RAD/SEC)	10000	103.5	104.3	103.8	103.2	103.6	102.6	100.4	94.0	88.9	86.7	85.5	84.5	133.2
NO. OF BLADES 44	12500	104.2	104.7	105.2	105.8	105.5	104.8	102.5	95.5	90.2	88.0	87.0	86.0	135.4
	16000	100.8	101.1	101.2	100.0	100.2	99.0	96.2	88.4	84.1	82.0	80.9	81.7	130.3
Grid #1,	20000	100.1	100.4	101.3	100.4	100.5	99.1	96.3	87.9	82.1	79.3	77.8	77.9	130.8
70% Speed,	25000	98.4	98.8	99.3	97.1	97.5	96.6	93.6	85.3	78.9	74.4	73.7	72.7	128.8
Discharge Valve	31500	95.7	96.6	96.8	93.7	94.6	93.8	90.5	81.2	73.3	68.6	68.0	67.4	126.9
Setting = 1.45	40000	92.6	92.3	93.5	89.9	91.0	89.5	86.3	76.1	68.5	62.4	63.6	62.5	124.3
	50000	90.6	89.6	89.4	86.6	88.2	88.0	83.8	72.2	66.2	59.5	64.1	61.1	123.4
	63000	92.2	84.5	83.2	81.5	85.2	85.4	80.9	68.8	65.0	58.3	66.0	63.0	122.4
	80000	94.0	78.4	78.4	77.1	81.8	83.3	80.4	69.8	64.1	59.4	65.7	70.1	123.9
OVERALL MEASURED														
OVERALL CALCULATED		112.0	113.2	113.4	112.5	112.5	111.8	109.2	103.4	99.2	96.7	95.3	94.3	142.7

MODEL SOUND PRESSURE LEVELS (59. DEG. F, 70 PERCENT REL. HUM. DAY) - ANGLES FROM INLET

		0.	10.	20.	30.	40.	50.	60.	70.	80.	90.	100.	110.	PWL
	50													
	63													
RADIAL 17. FT.	80													
(5. M)	100	66.6	64.8	64.5	62.8	64.3	63.3	65.5	64.5	64.8	63.6	63.4	61.5	97.7
VEHICLE	125	70.1	69.3	68.5	66.5	66.8	66.3	68.0	69.3	68.8	67.8	67.7	68.3	101.7
	160	73.6	73.3	75.0	74.8	73.3	72.5	71.0	70.8	73.6	72.3	76.2	75.8	107.5
NASA Rotor 11	200	76.8	77.3	77.0	75.5	75.1	74.8	72.5	70.8	69.6	67.8	69.2	67.3	106.2
	250	81.8	81.3	80.5	79.5	78.8	77.0	76.2	74.3	73.3	72.1	71.4	68.5	109.6
	315	81.8	81.3	80.8	79.5	79.1	76.5	75.7	74.8	73.1	70.3	70.4	69.5	109.3
	400	80.0	80.5	80.0	79.0	78.6	77.3	75.5	73.8	72.3	70.3	68.9	68.0	109.0
BAR 29.7 HG	500	80.8	81.5	81.5	80.7	80.1	78.3	76.7	74.8	72.8	70.6	68.9	67.0	110.2
(00361. N/M2)	630	84.3	84.8	85.0	84.5	83.6	82.0	79.8	77.8	76.8	73.4	72.1	70.0	113.7
TAMB 76. DEG F	800	85.8	86.3	87.0	86.5	86.3	84.0	82.2	80.0	78.3	76.1	76.4	74.8	115.9
(298. DEG K)	1000	86.3	85.5	86.0	85.4	85.6	83.5	81.2	78.2	76.3	73.1	73.1	73.2	114.9
TWET 69. DEG F	1250	86.8	87.3	86.3	86.2	86.1	84.8	82.7	79.8	77.6	74.9	72.9	72.5	115.8
(294. DEG K)	1600	87.8	87.3	88.3	87.7	86.6	86.3	84.0	80.5	78.1	75.2	73.4	72.8	117.0
HACT15.74 GM/M3	2000	88.1	90.8	90.5	90.7	90.3	89.8	88.2	84.8	82.3	78.2	76.9	76.1	120.4
(.01574 KG/M3)	2500	88.0	89.3	88.5	87.9	86.8	85.5	83.0	79.2	76.8	73.4	72.1	70.9	116.7
NFA 9819. RPM	3150	87.8	88.5	88.7	87.6	87.3	85.7	82.9	79.0	75.8	73.7	71.6	71.1	116.8
(1028. RAD/SEC)	4000	90.4	90.7	89.6	88.9	89.0	89.1	86.6	82.4	79.0	75.4	73.5	73.6	119.0
NFK 9662. RPM	5000	91.9	92.4	92.0	91.5	90.9	91.1	88.8	85.3	80.7	78.8	76.2	75.8	121.4
(1012. RAD/SEC)	6300	96.2	96.2	97.3	95.6	95.9	96.5	94.6	91.5	87.5	83.5	81.7	80.3	126.5
NFD16100. RPM	8000	96.9	97.4	97.8	97.5	97.6	98.4	96.8	92.4	89.5	85.3	83.0	81.5	128.4
(1686. RAD/SEC)	10000	94.6	95.1	94.8	93.7	94.2	92.9	90.9	85.4	80.6	77.5	76.8	75.7	123.9
NO. OF BLADES 44	12500	94.5	94.8	94.7	93.3	93.8	92.8	90.2	84.0	78.6	76.0	76.1	75.4	123.7
	16000	93.6	94.6	94.3	92.2	92.8	92.2	90.0	82.6	77.3	75.0	74.6	75.1	123.3
Grid #1,	20000	91.2	91.9	92.3	91.2	91.3	89.8	87.0	78.9	73.7	70.8	69.4	69.5	121.7
60% Speed,	25000	89.2	88.9	89.4	87.1	87.8	87.2	84.9	76.3	70.3	65.9	66.1	64.6	119.3
Discharge Valve	31500	86.0	85.7	86.4	84.0	84.7	83.9	80.3	71.9	65.2	60.6	62.1	60.3	116.8
Setting = 0	40000	82.4	81.6	82.5	79.4	79.6	78.8	75.3	66.9	61.9	57.6	60.7	60.7	113.5
	50000	85.7	78.7	78.2	75.2	77.3	77.0	73.0	63.5	62.1	58.8	63.2	62.3	112.6
	63000	91.7	73.3	75.3	70.0	74.3	75.1	71.2	60.6	62.1	58.3	62.9	64.4	112.5
	80000	91.8	67.7	69.2	66.9	71.7	73.3	70.4	60.3	58.2	59.9	60.0	64.3	114.2
OVERALL MEASURED														
OVERALL CALCULATED		104.8	104.8	105.0	103.9	104.1	103.8	101.8	97.3	94.1	90.7	89.3	88.3	134.6

MODEL SOUND PRESSURE LEVELS (59. DEG. F, 70 PERCENT REL. HUM. DAY) - ANGLES FROM INLET

		0.	10.	20.	30.	40.	50.	60.	70.	80.	90.	100.	110.	PWL
	50													
	63													
RADIAL 17. FT.	80													
(5. M)	100	70.2	69.2	70.7	70.0	69.7	77.5	72.7	66.3	63.4	62.6	62.3	60.4	104.0
VEHICLE	125	71.5	70.5	71.2	70.7	69.7	79.5	73.5	69.8	67.2	66.6	67.8	66.9	105.9
	160	78.2	78.0	79.5	79.2	78.2	83.5	79.0	73.0	72.4	71.3	75.3	74.6	111.4
NASA Rotor 11	200	77.5	77.7	78.2	77.0	76.5	82.5	75.7	71.3	67.7	66.1	67.8	64.8	109.2
	250	79.2	78.5	78.5	77.0	76.0	79.5	76.7	72.0	69.9	69.3	68.3	65.3	108.4
	315	80.0	79.5	80.5	78.0	76.7	78.0	75.7	72.5	70.4	68.6	68.0	67.1	108.4
	400	79.5	79.7	80.0	78.5	77.0	79.2	74.7	72.0	69.9	68.1	66.8	65.3	108.5
BAR 29.7 HG	500	78.7	78.7	80.0	78.7	78.0	79.7	76.7	76.0	70.7	69.1	66.8	65.1	109.4
(00361. N/M2)	630	81.2	82.2	83.2	82.2	81.8	87.5	79.2	77.5	74.2	71.1	69.5	67.1	114.1
TAMB 76. DEG F	800	83.2	84.2	85.0	84.4	83.5	89.5	84.0	78.3	75.4	74.1	72.8	71.1	116.4
(298. DEG K)	1000	84.2	84.5	85.0	84.2	83.8	92.5	84.0	78.0	74.9	71.8	70.5	70.8	118.0
TWET 69. DEG F	1250	87.2	87.7	88.5	87.9	87.5	95.0	88.2	82.0	79.2	77.1	74.5	73.6	121.0
(294. DEG K)	1600	93.0	91.0	91.2	90.7	89.8	91.5	90.7	83.8	81.2	79.2	76.8	75.2	121.2
HACT15.74 GM/M3	2000	91.5	92.2	92.5	91.1	90.3	89.2	89.2	81.5	78.7	75.9	74.8	73.7	120.6
(.01574 KG/M3)	2500	95.2	95.5	94.4	93.6	92.5	91.2	89.2	83.7	80.4	77.9	76.5	74.9	122.5
NFA 9819. RPM	3150	94.7	95.2	96.4	96.1	97.0	95.9	93.4	88.7	86.4	83.9	81.5	80.2	126.1
(1028. RAD/SEC)	4000	105.9	106.6	108.6	107.5	105.1	103.6	100.6	96.1	93.4	91.6	88.2	88.9	135.5
NFK 9662. RPM	5000	102.1	103.3	102.8	100.7	99.1	98.5	95.8	90.8	87.3	84.8	82.9	82.9	129.9
(1012. RAD/SEC)	6300	98.2	99.4	100.3	99.1	99.3	99.5	96.8	91.3	88.1	85.7	84.0	82.6	129.3
NFD16100. RPM	8000	99.4	99.9	100.7	100.0	100.3	100.6	98.0	92.4	88.9	86.5	84.9	83.1	130.4
(1686. RAD/SEC)	10000	102.0	102.5	103.8	104.4	105.8	104.3	101.6	95.0	90.7	87.7	86.5	85.0	134.5
NO. OF BLADES 44	12500	99.9	100.2	100.5	99.8	100.2	99.3	97.0	90.0	85.2	82.8	82.0	80.5	130.0
	16000	98.3	99.1	99.5	97.7	98.2	98.0	94.2	86.1	81.9	79.7	79.2	79.4	128.5
Grid #1,	20000	96.4	97.1	97.5	96.7	96.7	96.1	92.3	83.9	78.3	75.8	74.0	74.1	127.2
60% Speed,	25000	94.7	94.8	95.6	93.6	94.5	93.4	90.4	81.0	75.4	70.9	70.7	69.2	125.5
Discharge Valve	31500	92.0	91.4	93.1	90.2	91.1	90.1	86.8	76.9	70.0	65.6	65.3	64.1	123.1
Setting = 1.45	40000	88.6	88.3	89.8	86.2	87.3	86.3	82.8	71.6	65.3	59.9	63.4	60.8	120.7
	50000	90.6	85.6	85.4	82.6	84.9	84.5	80.5	69.0	64.5	58.0	63.8	60.4	119.8
	63000	98.4	81.3	80.0	78.5	82.7	83.1	79.7	67.1	65.0	58.3	66.0	62.5	120.1
	80000	98.8	77.7	77.9	76.8	81.6	83.3	80.4	69.8	64.1	59.4	65.7	68.3	123.7
OVERALL MEASURED														
OVERALL CALCULATED		111.4	111.6	112.6	111.7	111.3	110.6	107.7	101.8	98.4	96.1	94.1	93.5	141.4

MODEL SOUND PRESSURE LEVELS (59. DEG. F, 70 PERCENT REL. HUM. DAY) - ANGLES FROM INLET

		0.	10.	20.	30.	40.	50.	60.	70.	80.	90.	100.	110.	PWL
	50													
	63													
RADIAL 17. FT.	80													
(5. M)	100	61.8	61.8	66.3	61.0	61.6	61.3	63.3	61.0	62.2	61.1	60.7	59.5	95.5
VEHICLE	125	67.3	66.8	68.8	64.0	65.8	66.3	66.5	68.0	71.2	69.3	68.7	72.3	102.7
	160	70.8	70.5	72.3	71.5	70.3	69.5	69.8	64.0	66.7	63.8	64.4	65.5	101.8
NASA Rotor 11	200	72.5	73.5	73.5	72.3	71.3	71.0	69.2	66.3	65.2	63.3	65.4	61.8	102.4
	250	76.5	75.8	75.0	74.0	72.8	71.0	72.2	68.5	67.4	66.3	65.9	63.3	104.1
	315	77.0	76.8	76.3	74.5	73.6	71.8	71.5	69.0	67.9	65.6	65.6	64.8	104.6
	400	76.3	76.5	79.0	74.7	74.1	72.5	71.2	68.3	67.4	65.3	64.6	63.0	105.1
BAR 29.7 HG	500	75.5	75.8	77.8	75.7	74.8	74.0	72.5	70.3	68.2	66.6	65.1	63.0	105.6
(00361. N/M2)	630	78.1	79.0	80.3	79.0	78.3	76.8	75.5	72.8	71.4	68.6	66.6	65.0	108.6
TAMB 77. DEG F	800	81.0	81.3	81.3	81.0	80.6	78.8	77.5	75.0	72.9	70.6	70.9	69.0	110.6
(298. DEG K)	1000	81.8	82.5	82.5	81.9	82.3	80.8	78.7	76.5	73.4	71.1	70.1	70.2	111.9
TWET 70. DEG F	1250	84.8	86.0	86.3	85.7	86.6	86.3	83.7	82.3	78.9	76.6	74.1	74.8	116.6
(294. DEG K)	1600	86.1	86.0	86.8	86.2	85.4	83.5	80.7	78.0	75.2	72.7	70.6	71.1	115.0
HACT16.33 GM/M3	2000	90.3	90.5	89.5	89.2	88.3	86.8	83.7	80.0	76.7	74.2	73.4	72.8	117.9
(.01633 KG/M3)	2500	90.5	91.3	92.2	91.4	90.6	89.2	86.5	82.7	79.2	76.9	75.9	74.9	120.3
NFA 8192. RPM	3150	96.8	98.7	101.7	100.1	100.3	100.0	96.7	93.2	89.4	86.7	86.4	84.6	130.0
(858. RAD/SEC)	4000	99.7	100.4	99.6	98.5	97.5	95.9	92.3	87.9	84.4	82.1	81.3	80.6	127.3
NFK 8053. RPM	5000	95.6	96.6	96.0	95.2	94.4	93.6	91.0	85.8	82.6	79.8	79.0	78.3	124.4
(843. RAD/SEC)	6300	96.5	97.4	97.8	96.6	96.2	96.5	93.1	88.0	84.6	82.0	81.4	80.0	126.4
NFD16100. RPM	8000	97.4	98.7	99.5	99.8	100.1	99.6	98.1	92.4	87.6	85.3	83.3	83.2	129.9
(1686. RAD/SEC)	10000	96.1	96.8	96.8	97.2	99.2	98.9	96.6	90.4	85.7	83.0	81.6	80.7	128.5
NO. OF BLADES 44	12500	96.7	97.3	97.7	96.1	96.5	95.6	93.0	85.2	80.2	78.3	78.4	77.9	126.4
	16000	94.1	94.1	95.0	93.2	93.8	92.5	89.0	82.1	76.9	75.2	74.6	75.6	123.7
Grid #1,	20000	91.7	92.4	93.6	92.0	92.6	91.1	86.8	79.2	73.3	71.3	70.1	70.5	122.6
50% Speed,	25000	89.2	90.4	90.6	88.9	89.3	88.2	84.9	75.8	69.4	66.2	66.6	65.1	120.4
Discharge Valve	31500	86.5	86.4	87.9	85.2	85.9	84.6	80.5	71.1	65.3	60.8	62.4	60.5	117.7
Setting = 1.45	40000	84.3	83.0	83.9	80.1	81.3	80.2	76.2	65.5	61.9	57.0	60.4	57.6	114.8
	50000	86.8	79.3	79.4	76.8	78.7	77.9	73.4	61.9	63.6	57.4	62.1	58.9	113.6
	63000	91.5	74.3	73.3	71.6	75.3	74.9	70.7	59.1	65.0	57.8	62.9	60.5	112.6
	80000	89.7	68.1	68.9	67.3	71.8	73.2	70.3	60.0	64.0	59.3	60.2	65.4	114.3
OVERALL MEASURED														
OVERALL CALCULATED		106.8	107.5	108.1	107.2	107.4	106.8	104.1	99.0	94.9	92.4	91.5	90.7	137.3

MODEL SOUND PRESSURE LEVELS (59. DEG. F, 70 PERCENT REL. HUM. DAY) - ANGLES FROM INLET

		0.	10.	20.	30.	40.	50.	60.	70.	80.	90.	100.	110.	
	50													PWL
	63													
RADIAL 17. FT.	80													
(5. M)	100	65.6	64.5	63.3	62.0	61.3	62.0	63.3	62.5	63.3	63.0	61.9	60.5	96.2
VEHICLE	125	68.8	70.0	68.0	63.5	66.1	66.8	66.8	69.5	71.3	70.2	68.4	72.0	103.0
	160	72.1	71.3	72.0	71.8	70.8	69.8	69.0	65.0	67.1	65.0	65.2	66.0	102.1
NASA Rotor 11	200	74.3	75.8	74.8	73.8	73.3	73.0	70.7	68.8	67.3	66.2	66.7	64.3	104.2
	250	80.3	79.3	78.5	77.3	76.1	75.0	73.7	71.8	71.1	70.5	69.4	66.5	107.3
	315	79.8	79.5	78.8	77.3	76.1	74.3	72.7	72.0	70.6	69.0	67.9	67.5	107.1
	400	78.3	78.3	78.3	77.2	75.8	75.0	72.7	70.8	70.1	68.5	67.1	65.3	106.7
BAR 29.7 HG	500	78.3	78.5	78.8	78.5	77.6	76.3	74.7	72.3	70.8	69.5	66.1	65.3	107.9
(00361. N/M2)	630	81.1	82.0	82.3	81.5	80.3	79.0	77.0	75.0	74.1	71.5	69.1	67.3	110.8
TAMB 77. DEG F	800	82.5	84.3	83.3	83.2	82.1	80.5	78.5	76.8	75.1	73.0	72.1	70.5	112.4
(298. DEG K)	1000	82.8	84.0	82.0	81.9	81.3	80.0	78.0	75.0	73.0	70.7	69.4	69.7	111.4
TWET 70. DEG F	1250	82.8	84.3	83.8	82.7	83.1	81.3	79.7	76.8	74.6	73.0	69.6	69.8	112.8
(294. DEG K)	1600	86.6	85.0	85.8	85.2	84.6	83.3	81.5	78.0	76.1	73.8	71.4	70.1	114.5
HACT16.33 GM/M3	2000	81.3	82.8	82.8	82.4	81.8	80.5	77.7	73.8	71.8	69.8	67.4	66.6	111.5
(.01633 KG/M3)	2500	82.8	83.8	83.2	83.1	82.6	81.5	78.5	74.2	71.8	69.8	67.9	66.1	112.2
NFA 8195. RPM	3150	83.0	84.2	83.9	83.4	83.1	82.5	79.4	75.2	73.1	71.1	68.1	66.9	112.9
(858. RAD/SEC)	4000	86.9	87.4	86.6	85.5	85.0	84.4	81.3	76.9	74.5	72.3	70.0	69.1	115.0
NFK 8056. RPM	5000	92.6	92.9	91.8	91.5	90.4	90.1	87.3	82.8	79.5	76.7	75.0	74.5	120.7
(844. RAD/SEC)	6300	95.0	95.7	95.5	95.1	94.2	94.3	91.6	86.5	83.5	81.4	80.2	78.8	124.5
NFD16100. RPM	8000	90.4	91.2	91.0	90.5	90.3	89.4	86.8	81.7	78.0	75.9	74.3	73.2	120.1
(1686. RAD/SEC)	10000	89.6	90.6	90.6	89.2	90.2	88.6	85.4	79.4	75.3	73.6	72.3	71.4	119.4
NO. OF BLADES 44	12500	92.2	94.0	92.5	91.1	91.0	89.6	87.5	81.0	75.9	73.9	72.6	74.2	121.2
	16000	87.3	87.8	88.3	86.5	86.8	85.5	82.5	75.6	70.8	69.1	68.8	69.6	117.0
Grid #1,	20000	85.9	86.4	87.3	86.5	86.6	85.1	82.5	73.7	68.7	66.9	65.9	65.0	116.9
50% Speed,	25000	83.5	84.1	84.4	82.9	83.1	82.2	79.4	70.8	65.1	61.8	62.8	60.3	114.4
Discharge Valve	31500	80.5	80.9	81.6	78.7	79.4	78.4	75.3	65.9	61.2	57.2	60.4	57.8	111.6
Setting = 0	40000	77.1	76.8	77.7	74.1	75.5	74.2	71.0	61.0	60.6	56.4	60.9	59.3	109.0
	50000	77.1	73.8	73.6	70.6	72.9	72.2	69.4	58.6	60.5	55.5	62.1	59.2	108.2
	63000	82.3	69.6	68.6	66.8	71.3	71.9	69.0	57.6	61.4	55.7	62.7	60.0	109.4
	80000	79.7	67.6	67.9	66.8	71.6	73.2	70.3	60.0	57.9	54.4	59.9	62.4	113.8
OVERALL MEASURED														
OVERALL CALCULATED		101.1	101.8	101.3	100.5	100.2	99.4	96.8	91.8	88.9	86.8	85.4	84.6	130.5

MODEL SOUND PRESSURE LEVELS (59. DEG. F, 70 PERCENT REL. HUM. DAY) - ANGLES FROM INLET

		0.	10.	20.	30.	40.	50.	60.	70.	80.	90.	100.	110.	PWL
	50													
	63													
RADIAL 17. FT.	80													
(5. M)	100	65.1	65.0	64.8	64.0	64.6	64.5	65.5	66.0	66.6	65.3	65.2	63.8	98.9
VEHICLE	125	70.1	70.0	69.3	67.0	67.8	67.5	68.5	69.8	70.6	68.8	68.7	68.3	102.6
	160	72.3	71.5	72.0	72.3	72.1	71.0	70.8	69.3	70.8	69.3	69.9	68.0	104.2
NASA Rotor 11	200	76.3	77.5	76.8	76.0	76.3	76.5	73.5	71.8	70.6	67.6	71.4	70.0	107.2
	250	81.5	81.3	80.0	78.8	78.1	76.5	75.7	73.5	72.8	71.6	70.9	68.3	109.0
	315	79.8	80.0	79.3	77.8	76.6	75.3	74.2	73.3	72.1	69.3	69.6	68.5	107.9
	400	77.5	78.0	77.3	76.2	75.1	74.3	72.0	70.0	68.8	66.8	66.1	65.3	105.9
BAR 29.6 HG	500	75.3	76.0	75.8	75.2	73.8	72.3	70.7	69.0	67.6	65.3	63.9	61.8	104.4
(00029. N/M2)	630	78.1	79.0	78.8	77.7	76.6	75.0	72.8	70.3	69.3	66.9	65.4	64.0	106.9
TAMB 74. DEG F	800	77.0	77.5	77.5	77.2	76.1	74.8	72.2	70.0	68.8	66.1	66.6	65.0	106.3
(296. DEG K)	1000	75.3	75.5	75.3	74.7	73.6	72.0	69.5	66.7	64.8	62.1	63.9	61.5	103.6
TWET 68. DEG F	1250	75.8	76.0	75.8	75.2	75.1	73.3	71.5	68.5	66.6	63.6	61.4	61.3	104.7
(293. DEG K)	1600	76.6	77.0	77.3	76.9	76.6	75.0	73.0	69.5	67.6	64.4	62.1	61.6	106.2
HACT15.48 GM/M3	2000	79.6	80.5	80.5	79.9	79.3	78.0	75.0	72.0	69.6	66.7	64.9	64.1	109.0
(.01548 KG/M3)	2500	84.3	84.5	84.5	83.4	82.6	81.5	79.2	75.2	72.3	69.7	67.6	66.9	112.6
NFA11435. RPM	3150	86.0	85.7	86.2	85.4	84.6	84.0	81.7	78.0	75.1	71.2	69.9	68.6	114.7
(1197. RAD/SEC)	4000	87.7	87.9	87.6	86.5	86.2	85.4	83.6	79.1	76.0	72.6	71.3	70.8	116.3
NFK11273. RPM	5000	89.6	89.6	89.0	88.2	87.4	86.6	84.3	79.8	77.0	73.6	73.0	72.3	117.5
(1180. RAD/SEC)	6300	90.0	90.9	91.3	90.9	90.4	89.3	86.6	82.3	78.8	76.0	74.7	74.3	120.1
NFD16100. RPM	8000	92.4	94.9	96.3	97.5	99.8	100.9	100.8	95.7	90.3	86.8	85.3	83.5	130.6
(1686. RAD/SEC)	10000	90.4	92.3	93.1	92.5	93.2	93.1	92.4	86.9	81.8	78.2	77.3	75.7	123.5
NO. OF BLADES 44	12500	92.5	93.3	93.7	93.1	93.0	92.1	90.7	84.7	79.6	76.5	75.4	75.2	123.2
	16000	97.3	95.6	95.5	95.2	96.3	95.7	93.5	87.1	81.5	78.7	78.1	78.1	126.4
Grid #2,	20000	90.9	91.6	93.3	92.7	92.8	91.3	89.3	82.7	76.5	72.8	71.9	71.3	123.2
70% Speed,	25000	91.0	91.9	94.1	92.4	93.8	92.4	89.6	82.8	76.3	70.9	70.6	69.6	124.4
Discharge Valve	31500	88.8	89.2	90.9	88.7	89.4	88.1	86.0	78.1	70.7	64.8	65.1	64.3	121.4
Setting = 0	40000	85.2	84.9	86.0	83.7	85.6	84.1	81.8	73.1	67.2	63.4	67.7	62.7	118.5
	50000	83.4	81.4	81.7	79.4	81.8	81.5	78.3	68.7	66.4	62.0	65.5	61.8	116.8
	63000	85.6	76.2	74.9	73.7	77.9	77.8	73.6	63.0	62.0	58.2	63.0	63.1	115.0
	80000	87.3	69.2	69.3	68.1	72.7	73.3	70.7	60.8	58.0	59.4	60.3	67.8	114.8
OVERALL MEASURED														
OVERALL CALCULATED		102.7	102.8	103.6	103.2	104.3	104.2	103.2	97.9	92.8	89.5	88.4	87.2	134.9

MODEL SOUND PRESSURE LEVELS (59. DEG. F, 70 PERCENT REL. HUM. DAY) - ANGLES FROM INLET

		0.	10.	20.	30.	40.	50.	60.	70.	80.	90.	100.	110.	
	50													PWL
	63													
RADIAL 17. FT.	80													
(5. M)	100	70.5	71.0	71.0	70.0	78.5	70.5	70.0	65.8	66.4	66.1	64.6	62.4	104.2
VEHICLE	125	72.0	73.7	72.0	71.5	77.7	72.2	72.2	70.0	70.7	69.3	68.6	68.6	105.6
	160	78.5	78.7	79.5	78.7	80.0	78.7	77.7	71.0	70.2	70.1	69.1	67.9	109.4
NASA Rotor 11	200	77.5	79.2	79.7	79.0	83.2	79.0	76.7	72.3	69.2	68.3	72.5	68.1	110.4
	250	80.7	80.2	79.5	78.2	80.2	76.5	75.2	72.5	71.2	70.8	69.5	66.8	108.9
	315	79.7	80.0	79.2	78.0	80.2	75.5	74.5	73.0	71.2	69.0	68.5	67.6	108.6
	400	78.2	79.0	78.5	77.2	76.5	75.5	73.7	70.3	68.7	67.0	65.3	63.8	106.9
BAR 29.6 HG	500	77.2	79.5	77.7	77.5	76.8	75.2	74.2	71.0	68.9	67.3	64.5	63.3	107.0
(00029. N/M2)	630	80.0	82.0	81.0	80.0	79.3	78.0	76.0	73.0	71.9	69.3	67.5	65.3	109.5
TAMB 74. DEG F	800	82.2	85.5	84.2	82.9	81.3	80.5	77.7	74.8	72.9	71.1	70.8	68.6	112.1
(296. DEG K)	1000	84.7	87.0	85.0	83.7	82.3	81.0	78.5	75.0	72.6	69.8	68.2	68.8	112.8
TWET 68. DEG F	1250	86.5	88.2	86.7	86.4	85.8	84.2	81.5	78.8	75.9	73.6	71.8	70.6	115.5
(293. DEG K)	1600	87.7	89.5	89.2	88.7	88.0	86.7	84.2	80.8	78.4	75.6	73.3	72.2	117.8
HACT15.48 GM/M3	2000	90.7	92.2	92.0	90.9	90.0	88.5	85.5	81.8	78.9	76.4	74.8	73.9	119.8
(.01548 KG/M3)	2500	95.7	95.7	94.7	93.9	92.7	91.5	87.9	84.5	81.2	78.4	77.0	75.9	122.6
NFA11433. RPM	3150	94.7	95.5	96.4	95.3	95.2	93.9	90.2	86.2	83.2	80.9	78.2	77.7	124.5
(1197. RAD/SEC)	4000	98.1	100.4	102.8	102.7	103.6	103.6	100.8	95.6	92.4	90.1	87.9	87.4	133.0
NFK11271. RPM	5000	102.6	109.1	110.3	105.9	104.1	102.5	98.0	93.3	90.6	88.0	87.1	87.1	135.2
(1180. RAD/SEC)	6300	98.9	101.4	102.3	101.3	101.3	99.7	96.6	91.5	88.4	85.9	85.0	84.1	130.6
NFD16100. RPM	8000	97.4	99.6	101.0	101.7	103.0	103.4	101.3	95.9	90.9	88.0	86.4	84.3	132.8
(1685. RAD/SEC)	10000	101.3	102.3	103.5	102.4	103.6	102.3	98.9	93.5	88.7	86.2	85.2	83.7	132.7
NO. OF BLADES 44	12500	101.2	102.2	105.0	106.8	107.5	106.1	105.2	98.5	92.7	89.7	88.5	87.5	136.9
	16000	98.5	100.3	101.7	100.7	101.2	101.0	98.0	90.1	85.4	82.7	82.2	82.9	131.4
Grid #2,	20000	96.6	98.6	101.0	101.2	102.2	101.8	99.0	90.9	84.3	82.0	79.5	78.9	132.4
70% Speed,	25000	95.2	96.8	99.3	98.6	100.0	98.6	95.4	87.3	80.4	76.1	75.2	73.7	130.3
Discharge Valve	31500	93.7	94.9	97.1	95.4	96.8	95.8	93.5	83.4	76.0	71.5	70.5	68.6	128.5
Setting = 1.45	40000	91.1	91.6	93.5	91.4	93.0	92.3	88.8	77.9	70.5	66.1	66.9	62.8	125.9
	50000	90.6	89.1	89.4	87.9	90.7	90.3	86.0	73.5	66.7	64.5	64.3	61.6	125.1
	63000	94.3	84.4	84.1	83.2	87.8	87.3	82.6	69.5	65.6	65.4	65.6	62.4	124.3
	80000	97.0	78.9	78.9	77.8	92.1	83.3	80.4	69.8	64.1	69.1	65.7	67.6	128.8
OVERALL MEASURED														
OVERALL CALCULATED		110.1	112.8	114.2	113.0	113.4	112.5	110.1	103.9	99.5	96.8	95.4	94.6	143.5

MODEL SOUND PRESSURE LEVELS (59. DEG. F, 70 PERCENT REL. HUM. DAY) - ANGLES FROM INLET

		0.	10.	20.	30.	40.	50.	60.	70.	80.	90.	100.	110	PWL
	50													
	63													
RADIAL 17. FT.	80													
(5. M)	100	64.8	68.5	64.3	63.3	63.3	63.3	64.8	64.3	65.1	64.5	63.4	62.3	97.9
VEHICLE	125	69.3	71.3	68.3	65.5	66.3	65.8	68.8	68.8	69.6	67.7	67.7	67.0	101.7
	160	72.6	74.0	73.8	73.8	71.8	72.0	69.8	71.3	74.1	71.0	75.2	74.3	106.7
NASA Rotor 11	200	75.0	76.5	75.0	74.0	73.3	73.3	70.5	69.0	67.8	67.0	67.4	65.5	104.5
	250	81.0	80.8	80.0	78.0	77.6	76.0	75.5	72.8	72.3	71.7	70.6	67.3	108.6
	315	79.0	79.0	78.3	77.0	75.6	74.3	73.2	72.0	71.3	69.0	68.1	67.8	107.0
	400	75.8	75.5	75.0	74.2	73.3	72.0	69.7	67.5	66.8	65.5	64.4	63.0	103.8
BAR 29.6 HG	500	73.5	74.0	74.0	73.2	72.3	70.5	69.0	66.8	65.1	63.2	61.4	59.8	102.5
(00029. N/M2)	630	76.1	76.3	76.5	75.0	74.1	72.3	70.0	67.3	66.8	64.2	62.9	61.0	104.3
TAMB 74. DEG F	800	73.8	74.8	74.8	74.7	75.3	72.0	69.7	67.3	65.3	64.0	63.9	62.3	104.0
(296. DEG K)	1000	73.3	73.7	73.0	72.4	74.6	69.8	67.7	65.0	62.5	60.0	58.9	58.7	102.3
TWET 68. DEG F	1250	74.3	74.3	74.0	73.9	75.6	72.0	70.0	67.3	64.6	62.8	60.4	59.8	103.8
(293. DEG K)	1600	75.3	76.0	76.5	75.7	76.1	74.3	71.7	68.3	65.8	64.3	61.1	60.3	105.3
HACT15.48 GM/M3	2000	78.1	79.3	79.8	78.9	78.1	76.5	74.2	70.5	68.3	65.8	63.6	63.1	107.9
(.01548 KG/M3)	2500	81.8	82.3	82.0	81.4	80.8	79.7	77.5	74.0	70.8	68.1	66.1	65.4	110.7
NFA 9801. RPM	3150	83.0	83.7	83.4	82.6	83.1	81.5	78.7	74.7	71.6	69.6	67.1	66.6	112.3
(1026. RAD/SEC)	4000	85.4	85.9	85.6	84.5	84.2	83.6	80.6	75.9	73.0	71.3	68.5	68.1	114.1
NFK 9662. RPM	5000	87.9	87.4	88.0	87.2	86.7	85.8	83.0	78.6	75.0	73.2	71.2	70.3	116.5
(1012. RAD/SEC)	6300	90.7	92.2	92.5	92.9	93.2	92.3	91.6	85.8	81.8	79.6	78.4	77.5	122.9
NFD16100. RPM	8000	91.7	93.9	94.3	94.8	95.6	95.4	94.3	88.7	84.8	82.7	80.5	80.5	125.6
(1685. RAD/SEC)	10000	88.4	90.6	91.1	90.7	91.2	90.4	88.1	82.4	78.3	75.9	73.8	73.2	120.8
NO. OF BLADES 44	12500	91.2	92.5	92.2	91.6	92.5	91.6	90.0	83.5	78.6	75.7	74.6	74.4	122.4
	16000	91.3	93.3	92.0	91.7	92.3	92.0	90.8	84.4	79.0	76.9	75.3	75.4	123.0
Grid #2,	20000	87.2	88.1	90.1	91.7	92.3	91.8	88.8	81.4	74.5	72.1	69.9	69.0	122.4
60% Speed,	25000	84.7	86.4	88.1	87.1	88.8	88.2	85.9	78.0	71.1	67.6	66.6	64.6	119.6
Discharge Valve	31500	82.8	83.9	85.4	84.0	86.2	85.1	83.0	74.4	67.2	62.7	63.4	60.5	117.7
Setting = 0	40000	80.2	80.4	82.3	79.7	81.1	80.8	77.8	68.6	67.2	60.8	67.0	58.4	114.6
	50000	80.9	77.9	78.0	75.7	78.0	77.8	74.0	63.2	61.9	56.4	62.2	59.3	113.0
	63000	87.9	73.4	72.2	70.9	74.4	74.5	71.3	60.2	62.0	55.8	63.0	61.1	112.1
	80000	89.6	68.0	68.2	67.1	71.9	73.3	70.4	60.8	58.5	54.5	60.3	65.5	114.2
OVERALL MEASURED														
OVERALL CALCULATED		100.3	101.0	101.2	101.1	101.8	101.2	99.6	93.7	89.6	87.4	86.1	85.5	132.1

MODEL SOUND PRESSURE LEVELS (59. DEG. F, 70 PERCENT REL. HUM. DAY) - ANGLES FROM INLET

RADIAL 17. FT.
(5. M)
VEHICLE
NASA Rotor 11
BAR 29.6 HG
(00029. N/M2)
TAMB 74. DEG F
(296. DEG K)
TWET 68. DEG F
(293. DEG K)
HACT15.48 GM/M3
(.01548 KG/M3)
NFA 9801. RPM
(1026. RAD/SEC)
NFK 9662. RPM
(1012. RAD/SEC)
NFD16100. RPM
(1686. RAD/SEC)
NO. OF BLADES 44
Grid #2,
60% Speed,
Discharge Valve
Setting = 1.45

	0.	10.	20.	30.	40.	50.	60.	70.	80.	90.	100.	110.	PWL
50													
63													
80													
100	69.5	69.2	70.0	70.0	72.5	72.7	67.8	64.5	64.4	63.3	63.1	60.4	101.7
125	70.5	70.2	70.2	70.7	72.0	73.2	69.3	68.3	68.2	67.3	67.3	67.4	103.3
160	77.5	77.7	78.5	78.7	79.7	79.2	72.0	72.5	72.9	70.3	74.8	73.4	109.5
200	76.0	76.2	77.0	76.7	76.7	77.7	72.7	68.5	65.7	63.8	66.8	63.3	106.6
250	78.2	77.5	77.5	76.0	76.7	76.7	72.7	69.8	68.2	67.8	66.8	63.6	106.6
315	76.2	77.0	76.2	75.5	75.7	73.2	74.0	69.3	67.7	65.6	65.3	63.8	105.6
400	75.2	75.2	75.0	74.0	81.5	73.2	71.0	67.0	64.9	63.1	64.5	60.3	106.7
500	74.2	74.2	74.7	74.5	81.3	76.5	70.2	67.5	65.4	64.1	61.8	59.6	107.0
630	77.2	78.0	77.7	77.5	81.5	84.0	72.5	69.3	67.9	65.6	64.0	62.3	110.4
800	80.2	80.7	81.0	80.4	82.3	84.5	75.2	72.3	69.7	67.6	67.5	66.1	111.7
1000	82.2	82.2	82.2	81.4	80.5	80.5	75.7	72.5	70.1	67.3	65.2	65.8	110.5
1250	84.0	84.5	84.7	84.4	83.5	82.2	79.7	76.5	73.9	71.4	68.8	68.6	113.3
1600	86.0	86.7	87.0	86.7	86.3	85.5	83.0	79.0	75.9	74.2	71.3	70.4	116.0
2000	89.7	90.7	90.5	89.6	89.0	87.2	84.2	80.8	77.7	75.7	73.5	71.9	118.5
2500	94.0	94.0	93.4	91.9	91.5	90.0	86.5	82.7	79.4	77.7	75.5	74.4	121.1
3150	94.0	94.7	95.7	96.3	96.7	96.4	94.2	90.2	86.9	84.2	81.7	80.7	126.3
4000	105.1	107.1	109.3	108.7	105.9	104.1	102.1	97.1	94.6	92.1	90.2	90.4	136.4
5000	101.1	103.1	102.8	101.7	99.3	98.3	95.3	90.3	87.1	84.8	82.9	83.4	130.0
6300	96.7	97.9	99.0	98.6	98.1	97.7	95.1	90.3	86.4	84.0	82.5	81.1	128.0
8000	96.1	98.4	99.5	99.7	99.8	98.9	96.8	90.4	87.1	84.5	82.9	82.1	129.3
10000	98.3	100.5	102.8	105.2	106.8	105.8	102.9	96.2	91.7	89.2	87.2	86.5	135.4
12500	97.7	99.0	100.5	99.5	100.7	100.6	98.5	90.7	86.2	83.5	81.8	81.8	130.6
16000	95.5	98.1	99.2	98.0	98.7	98.7	96.3	88.4	83.1	81.2	79.9	80.4	129.1
20000	93.9	96.1	97.0	97.4	98.0	97.6	94.5	85.7	79.6	77.5	75.5	74.6	128.2
25000	91.7	93.6	95.6	94.4	95.3	95.1	93.4	83.3	76.9	73.2	72.2	70.2	126.6
31500	89.5	90.9	92.6	91.4	92.8	92.3	89.5	78.9	71.8	68.6	67.3	65.1	124.5
40000	86.9	87.6	89.5	87.2	88.5	87.8	84.8	73.1	66.8	61.4	62.9	60.0	121.6
50000	88.6	85.6	85.7	83.6	85.9	86.0	81.3	69.0	65.0	58.8	63.8	60.4	120.7
63000	97.8	81.2	80.4	79.4	83.6	83.8	76.1	67.5	64.9	58.7	65.9	61.9	120.3
80000	97.3	77.7	77.9	76.8	81.6	83.3	70.9	69.8	64.1	59.6	65.7	64.6	122.7
OVERALL MEASURED													
OVERALL CALCULATED	109.8	111.0	112.5	112.4	111.8	110.9	108.4	102.2	98.7	96.2	94.4	94.1	141.8

MODEL SOUND PRESSURE LEVELS (59. DEG. F, 70 PERCENT REL. HUM. DAY) - ANGLES FROM INLET

		0.	10.	20.	30.	40.	50.	60.	70.	80.	90.	100.	110.	PWL
	50													
	63													
RADIAL 17. FT.	80													
(5. M)	100	62.5	62.3	61.8	60.7	61.6	60.9	62.2	63.9	64.1	63.7	62.7	61.0	96.3
VEHICLE	125	67.7	66.3	67.6	64.7	64.8	66.6	68.4	69.4	72.1	70.2	66.4	71.0	102.8
	160	68.7	67.8	69.1	68.7	68.1	65.9	64.9	64.9	66.6	65.0	63.9	65.3	99.9
NASA Rotor 11	200	72.5	73.3	72.6	71.4	71.0	70.6	67.7	67.1	65.3	64.2	64.9	62.8	102.0
	250	78.7	79.8	77.3	76.2	75.5	74.4	72.6	71.6	70.3	69.7	68.6	65.5	106.5
	315	76.0	76.3	75.3	74.2	73.0	71.1	69.9	70.1	67.8	66.0	64.9	64.3	104.1
	400	72.0	72.3	71.6	70.2	69.1	69.4	65.4	64.4	63.3	61.5	60.9	60.0	100.2
BAR 29.6 HG	500	70.0	70.3	69.8	69.2	67.8	67.4	64.7	63.9	61.6	60.0	57.6	56.8	98.7
(00029. N/M2)	630	73.0	73.3	73.1	71.7	70.3	68.4	65.9	64.1	62.8	60.0	58.6	58.0	100.7
TAMB 73. DEG F	800	70.2	71.0	71.3	70.6	70.1	67.9	65.4	63.6	61.6	59.5	59.9	58.3	99.8
(296. DEG K)	1000	70.7	70.7	70.6	69.6	70.8	67.6	65.1	63.1	60.3	57.7	56.4	56.5	99.4
TWET 68. DEG F	1250	73.0	73.0	73.1	72.4	73.3	70.4	67.6	65.9	62.8	61.3	58.9	57.8	102.0
(293. DEG K)	1600	73.5	74.3	75.1	74.1	73.8	72.4	69.9	67.9	64.6	62.8	60.4	58.8	103.6
HACT15.78 GM/M3	2000	76.0	77.0	77.3	76.9	76.6	75.3	72.6	69.9	66.3	64.1	62.4	61.3	106.2
(.01578 KG/M3)	2500	78.7	79.8	79.0	79.1	78.6	77.6	74.4	71.4	68.1	66.1	63.1	62.4	108.2
NFA 8163. RPM	3150	80.2	80.7	81.2	80.3	80.5	79.1	76.1	72.8	69.1	66.8	64.9	63.6	109.8
(855. RAD/SEC)	4000	84.1	84.2	83.7	83.0	82.2	81.7	78.8	74.8	71.5	68.8	67.0	65.8	112.3
NFK 8055. RPM	5000	86.8	87.9	88.3	87.4	85.9	85.2	82.4	78.4	75.0	72.5	70.7	70.0	116.2
(843. RAD/SEC)	6300	91.9	93.7	94.3	94.8	92.7	91.6	89.7	85.4	82.3	79.1	77.7	77.3	123.0
NFD16100. RPM	8000	86.6	87.4	88.1	87.4	87.6	86.7	83.2	79.0	75.0	73.2	71.3	70.0	117.1
(1686. RAD/SEC)	10000	87.3	88.8	88.9	88.4	89.1	88.2	85.8	79.6	75.1	72.4	71.1	69.9	118.6
NO. OF BLADES 44	12500	91.7	95.3	91.8	90.8	91.5	90.4	88.4	82.1	77.4	74.2	73.4	73.9	121.6
	16000	85.0	86.8	87.6	86.4	87.0	85.8	84.7	76.5	71.5	69.1	69.3	69.1	117.2
Grid #2,	20000	83.1	84.9	86.4	85.9	87.8	86.4	85.2	76.3	70.0	67.9	65.9	65.3	117.7
50% Speed,	25000	81.2	82.8	84.2	83.6	84.3	84.2	82.0	73.1	66.8	64.1	63.3	61.3	115.6
Discharge Valve	31500	78.1	79.3	81.6	79.5	80.8	80.1	77.1	69.2	64.3	65.9	62.5	58.4	112.8
Setting = 0	40000	75.5	75.7	77.7	74.5	75.5	75.5	71.9	62.1	60.1	55.7	60.4	56.6	109.3
	50000	76.0	73.3	72.9	71.0	73.2	72.8	68.6	58.3	61.0	55.5	61.6	59.2	108.2
	63000	78.5	68.6	67.4	66.0	69.8	69.3	64.9	56.0	61.9	55.7	62.7	59.7	107.5
	80000	76.2	61.9	61.2	59.7	64.1	64.4	61.3	54.4	58.2	54.7	60.0	61.2	107.2
OVERALL MEASURED														
OVERALL CALCULATED		97.9	99.8	99.3	98.9	98.6	97.5	95.4	90.0	86.5	83.9	82.6	82.1	128.8

MODEL SOUND PRESSURE LEVELS (59. DEG. F, 70 PERCENT REL. HUM. DAY) - ANGLES FROM INLET

RADIAL 17. FT.
(5. M)
VEHICLE
NASA Rotor 11
BAR 29.6 HG
(00029. N/M2)
TAMB 73. DEG F
(296. DEG K)
TWET 68. DEG F
(293. DEG K)
HACT15.78 GM/M3
(.01578 KG/M3)
NFA 8148. RPM
(853. RAD/SEC)
NFK 8040. RPM
(842. RAD/SEC)
NFD16100. RPM
(1686. RAD/SEC)
NO. OF BLADES 44
Grid #2,
50% Speed,
Discharge Valve
Setting = 1.45

	0.	10.	20.	30.	40.	50.	60.	70.	80.	90.	100.	110.	PWL
50													
63													
80													
100	67.1	61.3	62.0	61.5	61.1	61.3	63.0	61.3	62.2	61.1	60.9	59.8	95.2
125	68.8	65.5	67.0	64.3	63.1	67.3	67.3	68.8	72.4	70.1	66.2	71.0	102.7
160	70.6	69.3	70.3	70.3	69.6	69.5	68.8	63.8	66.4	64.3	62.4	64.5	101.0
200	71.5	71.0	71.0	70.0	69.3	69.0	67.5	63.3	63.4	60.8	63.2	59.0	100.2
250	74.8	73.3	72.5	71.3	70.1	68.8	68.5	65.5	64.7	63.6	63.1	60.3	101.3
315	72.5	72.3	71.5	70.5	69.1	67.5	66.5	65.3	63.9	61.6	61.6	60.3	100.2
400	71.3	70.8	70.5	69.2	68.6	67.5	65.5	62.8	62.7	60.1	59.6	58.0	99.1
500	69.8	69.5	69.5	69.5	68.6	67.0	66.0	64.0	62.2	60.1	58.6	56.5	99.0
630	75.1	75.0	75.5	73.7	72.8	71.0	69.0	66.3	64.9	62.1	61.4	59.3	103.0
800	77.0	77.3	77.5	77.0	75.6	73.8	71.7	69.3	67.2	65.1	65.4	63.8	105.8
1000	81.0	79.0	79.0	77.7	77.1	75.5	73.0	70.2	67.9	64.8	63.6	63.5	107.0
1250	83.0	81.8	81.8	81.4	81.4	79.8	77.5	75.0	71.9	69.9	67.4	67.3	110.9
1600	85.6	84.3	84.8	84.9	84.9	83.5	80.7	77.0	74.7	72.7	70.4	69.6	114.2
2000	88.8	89.0	88.8	87.7	86.8	85.3	82.0	78.5	75.7	73.7	71.6	71.1	116.6
2500	89.6	90.5	90.7	90.1	89.1	88.2	85.2	81.7	77.9	75.7	74.1	73.4	119.0
3150	95.5	98.0	101.9	99.4	99.8	99.5	96.4	92.7	89.2	86.7	85.4	83.6	129.6
4000	99.2	100.9	99.1	98.5	96.2	95.4	91.8	86.9	83.9	80.9	80.5	80.1	126.8
5000	94.1	95.4	95.3	94.2	93.7	92.6	90.0	85.1	81.6	78.8	78.2	77.3	123.5
6300	94.0	95.4	96.8	96.4	95.4	94.5	91.8	87.0	83.1	81.5	80.7	79.3	125.3
8000	95.4	97.2	98.8	99.5	100.6	99.4	98.3	92.4	87.6	85.0	84.0	83.0	129.8
10000	93.1	95.3	96.6	96.7	98.4	98.4	96.9	91.9	85.7	82.7	81.3	80.7	128.1
12500	94.7	97.0	97.7	96.6	97.0	96.3	93.5	86.2	81.2	78.8	79.1	78.4	126.8
16000	92.1	93.6	95.0	93.0	94.0	93.5	90.5	82.1	78.4	76.0	75.8	76.4	124.1
20000	88.9	91.1	93.3	92.5	93.3	92.1	88.8	80.2	74.8	72.5	71.1	70.8	123.2
25000	86.7	88.6	90.6	89.1	90.3	89.2	86.6	77.0	71.4	67.9	67.8	65.8	121.0
31500	84.2	86.1	87.5	85.6	86.6	85.5	82.7	72.3	65.4	62.2	62.8	60.9	118.4
40000	81.8	82.0	83.9	81.8	82.3	81.5	78.2	66.3	62.4	57.3	60.4	57.6	115.5
50000	82.1	79.8	79.4	76.8	79.7	78.7	74.7	61.6	63.6	57.7	62.1	58.7	114.2
63000	84.3	74.6	73.3	72.1	75.8	75.7	71.2	59.4	64.8	57.8	62.4	60.2	113.0
80000	81.5	68.9	68.4	67.1	71.9	73.0	70.1	60.3	63.8	59.1	59.5	63.5	114.2
OVERALL MEASURED													
OVERALL CALCULATED	105.0	106.7	107.8	106.8	107.1	106.4	104.1	98.6	94.5	92.0	91.0	90.0	137.0

MODEL SOUND PRESSURE LEVELS (59. DEG. F, 70 PERCENT REL. HUM. DAY) - ANGLES FROM INLET

		0.	10.	20.	30.	40.	50.	60.	70.	80.	90.	100.	110.	PWL
	50													
	63													
RADIAL 17. FT.	80													
(5. M)	100	69.5	69.5	65.5	63.8	65.8	64.0	65.5	67.0	66.4	66.1	66.2	64.4	99.6
VEHICLE	125	73.2	73.2	69.0	66.8	66.1	67.5	68.0	70.0	69.4	68.3	70.7	68.6	102.8
	160	78.0	77.7	71.8	72.3	72.8	71.0	70.5	71.3	70.4	69.6	70.7	68.6	104.9
NASA Rotor 11	200	78.5	79.2	77.5	75.8	76.6	76.8	74.0	72.8	70.2	68.1	73.4	69.6	107.9
	250	82.2	81.7	80.8	79.5	78.8	77.0	76.0	74.3	72.4	71.8	71.6	67.8	109.6
	315	81.0	81.0	79.5	78.5	77.6	76.0	74.7	74.0	72.7	70.1	69.6	68.8	108.6
	400	79.5	79.7	79.0	77.7	76.6	75.3	73.2	71.0	69.7	68.1	67.4	65.8	107.3
BAR 29.7 HG	500	78.0	78.7	78.5	77.2	76.8	74.5	73.2	71.3	68.9	67.1	65.9	63.8	106.8
(00361. N/M2)	630	81.7	82.2	82.3	81.2	80.3	78.8	76.5	74.3	72.9	70.4	68.9	66.3	110.5
TAMB 82. DEG F	800	83.5	84.0	84.3	83.7	82.8	81.5	79.2	77.0	74.9	72.8	72.6	71.1	113.0
(301. DEG K)	1000	84.5	85.0	85.0	83.9	83.8	82.0	79.5	76.5	73.9	71.6	70.9	70.8	113.4
TWET 70. DEG F	1250	86.0	86.0	85.8	85.2	84.9	83.8	81.7	78.8	76.4	73.6	72.1	70.4	114.8
(294. DEG K)	1600	86.0	85.7	86.8	85.7	86.6	83.8	81.5	78.0	75.4	73.7	71.9	69.9	115.3
HACT14.85 GM/M3	2000	86.5	87.7	87.8	87.7	86.6	84.3	81.0	77.5	74.7	72.4	71.1	70.2	115.9
(.01485 KG/M3)	2500	89.0	89.7	89.2	88.1	87.1	85.5	82.7	79.0	75.7	73.7	72.4	70.7	117.0
NFA11510. RPM	3150	89.7	89.5	89.4	88.4	87.3	86.2	84.2	79.5	76.4	73.9	72.4	70.4	117.5
(1205. RAD/SEC)	4000	109.9	105.9	101.9	102.3	99.2	100.6	97.3	88.6	87.1	85.6	82.5	80.6	130.9
NFK11263. RPM	5000	108.6	105.1	101.0	101.7	98.7	99.6	96.8	90.3	88.6	85.8	83.0	80.6	130.3
(1179. RAD/SEC)	6300	93.7	94.1	94.8	94.9	94.7	93.8	91.3	86.8	82.9	80.2	78.9	77.1	124.3
NFD16100. RPM	8000	97.2	98.5	99.1	100.1	103.4	100.7	99.9	95.5	90.0	86.6	85.4	83.9	131.5
(1686. RAD/SEC)	10000	96.0	97.3	97.8	97.5	98.9	98.1	96.1	91.2	86.2	82.7	81.3	79.5	128.4
NO. OF BLADES 44	12500	94.8	95.1	95.6	94.7	95.4	94.7	92.6	86.3	81.1	78.4	77.7	76.6	125.3
	16000	95.4	96.4	96.9	95.1	95.6	95.3	92.9	85.5	80.2	77.1	77.2	77.3	126.1
Grid #3,	20000	92.2	92.7	93.7	92.6	92.4	91.7	88.9	82.5	75.7	72.9	71.5	70.7	123.2
70% Speed,	25000	91.9	92.3	93.6	91.3	91.8	90.6	88.1	80.5	73.6	69.1	69.3	66.9	123.0
Discharge Valve	31500	88.7	88.8	90.1	86.9	87.9	86.1	84.0	76.1	68.2	63.3	63.8	61.6	120.0
Setting = 0	40000	84.9	85.4	85.6	82.7	83.7	82.1	79.6	71.4	64.6	60.7	64.5	62.8	117.1
	50000	83.4	82.6	82.0	78.7	80.8	80.3	76.3	69.2	66.7	64.3	72.0	73.1	116.5
	63000	82.3	80.4	75.9	73.1	77.9	77.0	72.5	67.2	65.6	58.6	64.2	63.6	115.3
	80000	83.0	78.9	71.2	68.6	74.2	74.3	71.4	70.8	65.1	60.4	61.3	68.1	117.1
OVERALL MEASURED														
OVERALL CALCULATED		113.0	110.1	108.1	108.1	108.0	107.2	105.1	99.5	95.5	92.7	91.1	89.5	138.1

MODEL SOUND PRESSURE LEVELS (59. DEG. F, 70 PERCENT REL. HUM. DAY) - ANGLES FROM INLET

		0.	10.	20.	30.	40.	50.	60.	70.	80.	90.	100.	PWL
	50												
	63												
RADIAL 17. FT.	80												
(5. M)	100	70.0	69.2	70.0	70.0	69.7	70.5	70.2	65.5	55.4	64.6	63.8	62.1	101.4
VEHICLE	125	73.2	72.0	72.7	71.2	71.2	72.0	70.7	69.5	70.2	69.3	69.8	68.9	104.2
	160	78.5	78.0	79.2	79.2	78.7	78.7	77.7	71.3	70.4	68.3	69.1	67.9	109.1
NASA Rotor 11	200	78.5	80.0	80.5	80.2	79.2	79.7	78.0	72.8	69.4	67.6	75.0	67.6	110.2
	250	80.7	80.5	80.2	78.7	77.7	77.0	76.2	73.0	71.7	71.1	69.8	67.3	108.9
	315	80.0	79.7	79.5	78.2	77.2	76.0	75.5	73.3	71.4	69.1	68.3	67.8	108.2
	400	79.7	80.5	79.7	78.7	77.7	76.7	75.0	70.5	69.4	67.3	66.3	65.3	108.1
BAR 29.7 HG	500	78.2	78.2	79.0	78.5	77.5	76.5	75.0	72.0	69.7	68.1	65.5	64.1	107.8
(00361. N/M2)	630	81.2	81.5	82.5	82.0	80.8	79.5	77.5	74.5	73.7	71.1	68.5	66.6	111.0
TAMB 82. DEG F	800	83.7	84.2	84.7	84.4	83.5	82.2	79.7	77.3	74.7	73.3	72.5	70.8	113.5
(301. DEG K)	1000	85.5	85.5	85.7	84.9	84.0	82.2	80.5	76.8	74.1	71.8	70.5	70.6	113.9
TWET 70. DEG F	1250	86.2	87.0	87.5	86.7	86.5	84.7	82.5	79.3	76.9	74.4	72.0	71.4	116.0
(294. DEG K)	1600	88.2	88.7	89.0	88.2	87.3	85.5	83.2	79.5	77.4	75.2	72.8	71.7	117.1
HACT14.85 GM/M3	2000	90.0	91.5	92.0	90.9	89.5	87.7	84.2	80.3	78.2	75.9	73.5	72.9	119.3
(.01485 KG/M3)	2500	95.5	95.2	94.7	93.4	92.7	91.2	87.7	84.0	80.9	78.4	76.8	75.2	122.4
NFA11513. RPM	3150	94.7	95.5	96.4	95.3	94.7	93.4	91.2	86.5	83.7	81.2	78.7	77.4	124.5
(1205. RAD/SEC)	4000	99.6	102.4	103.3	103.0	103.6	103.3	101.3	96.6	92.9	90.6	88.2	88.1	133.3
NFK11266. RPM	5000	101.8	107.6	111.5	105.9	104.3	103.3	98.5	94.1	90.8	88.6	87.1	87.6	135.7
(1180. RAD/SEC)	6300	100.4	101.1	103.0	102.8	101.6	100.5	96.8	92.0	88.9	86.5	85.3	84.1	131.3
NFD16100. RPM	8000	99.0	100.7	102.3	103.1	104.1	103.5	100.9	95.8	91.5	88.6	86.8	85.7	133.3
(1686. RAD/SEC)	10000	101.3	102.8	104.0	103.4	103.6	102.6	99.9	93.7	89.4	86.7	85.5	84.2	133.2
NO. OF BLADES 44	12500	103.3	103.6	105.6	107.1	107.1	105.7	104.6	97.3	91.8	89.6	88.1	87.9	136.6
	16000	99.6	100.4	101.8	99.8	100.8	99.8	96.8	88.7	84.5	82.3	81.3	82.0	130.7
Grid #3,	20000	98.5	100.0	101.1	100.5	100.6	99.7	96.9	88.8	82.4	80.1	78.1	78.0	131.1
70% Speed,	25000	97.1	97.8	99.0	97.6	97.7	96.6	94.3	85.7	79.4	74.6	74.1	72.9	128.9
Discharge Valve	31500	94.9	95.3	96.5	94.4	95.3	94.5	91.5	81.6	74.2	69.3	69.0	67.6	127.3
Setting = 1.45	40000	92.2	91.6	93.8	90.7	91.3	90.1	87.1	76.9	69.6	64.4	65.9	67.1	124.8
	50000	90.4	89.6	90.4	87.1	89.4	88.5	84.8	73.5	66.7	60.3	64.3	62.1	124.2
	63000	87.5	85.4	86.1	82.9	86.5	86.5	81.8	69.4	65.3	59.1	65.3	63.1	123.8
	80000	83.0	80.2	81.9	78.6	82.6	84.3	81.4	70.8	65.1	60.4	66.7	70.6	125.0
OVERALL MEASURED														
OVERALL CALCULATED		110.6	112.7	115.0	113.3	113.2	112.2	109.7	103.7	99.5	97.1	95.5	95.0	143.4

MODEL SOUND PRESSURE LEVELS (59. DEG. F, 70 PERCENT REL. HUM. DAY) - ANGLES FROM INLET

		0.	10.	20.	30.	40.	50.	60.	70.	80.	90.	100.	110.	PWL
	50													
	63													
RADIAL 17. FT.	80													
(5. M)	100	64.8	64.5	64.5	62.8	63.1	63.3	64.3	64.8	65.1	64.3	64.4	62.5	97.8
VEHICLE	125	69.3	69.5	68.8	66.5	66.1	66.0	67.3	69.0	69.8	68.6	70.4	68.8	102.3
	160	72.8	72.3	74.3	74.5	73.1	73.3	71.0	69.0	71.8	72.6	72.4	75.3	106.6
NASA Rotor 11	200	75.3	76.5	75.8	74.8	74.1	74.0	70.7	69.5	68.1	67.1	66.9	66.3	105.1
	250	81.3	80.8	80.3	78.8	77.8	76.5	76.0	73.0	72.6	71.8	70.9	67.5	109.0
	315	79.3	79.5	79.0	78.0	76.6	74.8	73.5	73.3	71.8	68.8	68.4	68.3	107.7
	400	77.0	77.3	77.0	75.7	74.6	73.3	71.2	69.0	68.1	66.1	65.4	64.8	105.3
BAR 29.7 HG	500	76.3	76.5	76.5	76.0	74.6	73.3	71.7	69.8	67.8	65.3	64.1	62.3	105.2
(00361. N/M2)	630	79.3	80.5	80.0	79.2	78.3	76.8	74.8	71.8	71.3	68.4	66.4	65.0	108.5
TAMB 83. DEG F	800	81.0	81.5	82.0	81.7	80.6	79.5	76.7	75.3	73.1	70.6	70.6	69.5	110.9
(301. DEG K)	1000	81.5	82.0	81.5	81.2	80.5	79.0	77.0	73.7	71.8	68.3	68.1	68.2	110.4
TWET 71. DEG F	1250	83.0	83.8	83.0	82.4	81.3	80.8	78.7	76.3	73.6	70.9	69.4	68.5	112.0
(295. DEG K)	1600	82.3	82.3	83.0	82.4	81.9	80.3	78.0	74.5	72.3	69.7	68.4	66.8	111.5
HACT15.45 GM/M3	2000	82.3	83.3	84.5	84.2	82.8	80.3	77.5	73.8	71.8	69.2	67.9	66.8	112.3
(.01545 KG/M3)	2500	84.8	85.0	85.5	85.1	83.8	82.5	78.7	75.7	72.8	70.4	68.6	67.6	113.6
NFA 9881. RPM	3150	89.5	90.5	86.4	87.9	85.1	84.7	82.2	78.7	74.3	73.4	69.9	69.6	116.1
(1035. RAD/SEC)	4000	108.9	108.7	99.4	105.0	94.5	97.1	98.1	95.6	80.3	90.4	76.8	84.1	131.9
NFK 9660. RPM	5000	94.6	95.4	93.0	92.5	91.2	90.1	88.0	84.6	80.0	78.3	75.5	75.0	121.7
(1011. RAD/SEC)	6300	93.2	94.7	95.8	94.9	95.2	94.8	91.8	86.8	83.3	80.5	79.4	78.5	124.9
NFD16100. RPM	8000	95.0	96.5	97.6	96.9	97.7	98.0	94.9	89.3	85.6	82.4	81.1	80.8	127.5
(1686. RAD/SEC)	10000	91.6	92.8	93.1	92.5	93.2	92.6	90.1	84.2	80.3	76.5	76.1	74.9	122.9
NO. OF BLADES 44	12500	92.3	92.9	93.3	91.7	93.1	92.2	89.8	84.1	79.2	75.4	75.2	74.5	122.8
	16000	92.9	93.4	92.6	91.3	92.4	92.6	90.9	84.2	79.1	75.6	74.7	75.2	123.1
Grid #3,	20000	88.5	89.0	90.4	89.6	91.9	88.9	86.1	78.8	72.8	69.4	68.5	68.4	120.8
60% Speed,	25000	86.6	87.2	87.5	86.2	87.4	86.3	84.2	75.6	69.9	65.5	65.4	64.4	118.4
Discharge Valve	31500	83.7	84.4	85.3	83.2	84.1	82.8	79.7	71.3	64.9	60.3	62.1	61.7	115.9
Setting = 0	40000	80.6	80.8	82.0	78.1	79.8	78.8	75.3	66.6	62.9	60.8	64.7	66.6	113.3
	50000	80.8	78.3	77.6	74.8	77.2	76.4	72.4	62.6	62.0	58.7	64.1	65.2	112.2
	63000	82.2	74.0	72.3	70.5	74.3	74.6	71.2	60.3	62.6	58.5	63.9	61.4	112.1
	80000	81.4	70.5	69.3	67.9	72.5	74.1	71.2	60.9	59.0	60.2	60.6	64.3	115.0
OVERALL MEASURED														
OVERALL CALCULATED		109.8	110.6	104.9	107.0	103.7	103.7	102.1	98.1	91.2	92.4	87.4	88.5	135.6

MODEL SOUND PRESSURE LEVELS (59. DEG. F, 70 PERCENT REL. HUM. DAY) - ANGLES FROM INLET

RADIAL 17. FT. (5. M)
VEHICLE
NASA Rotor 11

BAR 29.7 HG (00361. N/M2)
TAMB 83. DEG F (301. DEG K)
TWET 71. DEG F (295. DEG K)
HACT15.45 GM/M3 (.01545 KG/M3)
NFA 9881. RPM (1035. RAD/SEC)
NFK 9660. RPM (1011. RAD/SEC)
NFD16100. RPM (1685. RAD/SEC)
NO. OF BLADES 44

Grid #3,
60% Speed,
Discharge Valve
Setting = 1.45

	0.	10.	20.	30.	40.	50.	60.	70.	80.	90.	100.	110.	PWL
50													
63													
80													
100	69.7	69.2	70.0	70.0	70.0	70.5	69.7	64.3	63.2	62.8	62.6	60.9	100.9
125	70.2	71.5	72.0	71.0	69.7	71.5	71.2	68.0	67.9	67.8	69.6	67.4	103.4
160	78.0	78.0	79.0	79.0	78.5	79.2	77.7	70.8	70.7	72.3	70.6	73.9	109.6
200	76.2	76.7	77.2	77.0	75.7	76.5	75.5	68.8	66.2	64.6	65.8	64.8	106.7
250	78.7	78.0	78.2	76.5	75.7	74.7	74.2	70.5	69.2	68.6	67.0	65.1	106.7
315	77.5	77.5	77.0	75.7	75.0	73.7	72.7	70.3	68.7	66.6	66.0	65.3	105.7
400	76.2	76.5	76.5	75.7	74.7	74.2	72.5	68.0	66.2	64.8	63.8	62.3	105.2
500	75.7	76.8	76.2	75.7	74.8	74.0	72.7	70.0	67.2	65.1	63.5	61.8	105.3
630	79.0	79.5	79.5	79.0	78.3	77.5	75.5	72.0	70.7	68.4	66.0	64.3	108.5
800	81.5	82.2	82.5	82.4	81.3	80.0	77.7	74.8	72.2	70.1	69.5	67.8	111.3
1000	82.7	83.5	83.0	82.4	81.5	80.0	78.0	74.3	71.6	69.3	68.0	67.6	111.4
1250	84.2	84.7	84.7	84.7	84.0	82.0	79.7	76.8	74.2	72.1	69.8	68.9	113.5
1600	85.5	85.7	86.7	86.2	85.5	84.0	81.5	77.5	75.2	73.4	71.0	69.9	115.1
2000	89.0	90.7	90.5	89.4	88.3	86.5	83.0	79.0	77.4	74.7	72.5	71.7	118.1
2500	93.7	93.7	93.4	91.9	91.5	90.0	86.7	82.7	79.7	77.7	75.5	74.2	121.1
3150	93.5	94.2	95.9	95.8	97.5	96.7	94.4	90.5	87.4	83.9	82.5	81.4	126.6
4000	106.1	106.9	109.3	108.5	106.1	104.6	101.8	97.4	93.9	92.6	89.9	90.6	136.4
5000	101.6	103.1	103.8	101.2	99.8	98.8	95.5	90.3	86.8	85.1	82.9	83.1	130.3
6300	97.4	98.6	100.3	99.3	99.3	98.5	95.6	90.0	86.6	84.5	83.0	82.1	128.9
8000	97.0	99.5	100.8	99.8	100.4	99.5	96.4	91.3	87.5	85.1	83.8	82.4	129.8
10000	100.3	100.8	103.5	104.9	107.3	106.1	102.4	95.5	90.9	88.7	86.7	85.7	135.6
12500	97.8	99.1	100.3	99.1	101.1	101.2	98.1	91.3	86.3	84.1	82.1	81.9	130.7
16000	96.4	97.7	98.8	98.1	98.5	98.1	95.6	87.2	82.5	80.6	79.8	79.5	128.7
20000	94.5	95.7	96.6	96.5	97.1	96.4	92.9	84.5	78.7	76.4	74.4	74.0	127.2
25000	93.3	93.7	94.7	93.7	94.1	94.2	91.0	81.9	76.0	71.3	70.8	69.3	125.5
31500	90.4	91.1	92.3	90.1	91.5	90.5	87.5	77.4	70.7	66.3	66.2	65.6	123.2
40000	87.1	87.8	89.0	85.9	87.7	87.0	83.0	72.1	65.2	61.1	63.6	67.7	120.9
50000	85.5	85.0	84.8	83.3	85.3	85.2	80.4	68.6	64.4	58.4	63.7	64.0	120.1
63000	84.4	82.0	80.2	78.8	83.2	83.6	78.9	66.6	64.5	58.0	65.7	70.7	120.5
80000	82.8	78.7	78.7	77.6	82.4	84.1	81.2	70.6	64.9	60.2	66.5	70.1	124.5
OVERALL MEASURED													
OVERALL CALCULATED	110.0	111.1	112.8	112.1	112.1	111.1	108.0	102.2	98.3	96.4	94.3	94.2	141.8

MODEL SOUND PRESSURE LEVELS (59. DEG. F, 70 PERCENT REL. HUM. DAY) - ANGLES FROM INLET

RADIAL 17. FT.
(5. M)
VEHICLE
NASA Rotor 11

BAR 29.7 HG
(00361. N/M2)
TAMB 83. DEG F
(301. DEG K)
TWET 71. DEG F
(295. DEG K)
HACT15.45 GM/M3
(.01545 KG/M3)
NFA 8237. RPM
(862. RAD/SEC)
NFK 8053. RPM
(843. RAD/SEC)
NFD16100. RPM
(1686. RAD/SEC)
NO. OF BLADES 44

Grid #3,
50% Speed,
Discharge Valve
Setting = 1.45

	0.	10.	20.	30.	40.	50.	60.	70.	80.	90.	100.	110.	PWL
50													
63													
80													
100	61.6	61.3	62.0	60.5	60.8	61.0	61.8	60.5	61.4	61.1	61.2	59.8	94.8
125	67.3	68.0	67.0	64.5	65.6	66.5	65.0	68.0	71.4	71.1	69.4	73.3	103.3
160	69.8	69.8	70.8	70.3	69.6	69.5	68.5	63.5	66.9	64.8	63.4	66.8	101.3
200	70.0	71.3	71.0	70.3	69.8	69.3	68.0	64.0	64.2	61.3	62.7	59.3	100.6
250	74.0	73.8	72.5	71.8	71.3	69.5	68.7	66.3	65.7	64.6	63.9	61.3	102.0
315	73.3	73.5	72.8	71.5	70.6	68.8	67.5	66.3	64.9	62.6	62.6	61.5	101.4
400	73.8	73.5	73.0	71.7	70.8	69.0	67.5	65.0	63.9	62.1	62.1	60.3	101.3
500	72.0	72.8	72.8	72.5	71.6	70.3	69.0	66.5	65.2	62.8	61.4	59.5	102.0
630	75.8	76.3	77.0	76.0	75.3	73.5	72.3	69.3	67.9	65.4	64.1	61.8	105.4
800	78.3	78.8	79.3	78.7	78.3	76.3	74.0	71.8	69.9	68.1	68.4	66.0	108.0
1000	79.8	80.2	79.8	79.4	78.3	76.8	74.7	72.0	69.6	66.1	66.9	65.2	108.4
1250	81.3	81.8	82.5	81.9	81.6	79.5	77.2	74.5	71.7	69.6	69.6	67.0	111.1
1600	84.3	83.8	84.3	84.2	83.4	81.8	79.0	76.0	75.7	71.4	72.1	68.8	113.1
2000	87.8	88.5	88.3	87.7	86.6	84.5	81.5	77.8	76.2	73.2	72.6	70.8	116.3
2500	89.8	90.0	90.7	90.4	89.6	88.7	85.7	82.0	78.9	76.4	75.1	74.1	119.4
3150	96.8	98.5	102.2	100.1	100.6	101.0	96.9	94.0	90.9	86.2	86.4	84.9	130.5
4000	99.9	101.2	100.4	98.8	98.0	96.1	92.3	87.4	84.6	81.9	81.5	80.6	127.7
5000	94.6	96.4	96.0	94.5	94.4	93.6	90.3	85.8	82.1	79.1	78.7	78.3	124.2
6300	94.7	96.2	97.8	96.9	96.4	95.3	92.8	87.5	84.4	82.0	81.2	80.0	126.1
8000	95.8	97.8	99.1	99.9	100.2	99.5	97.2	92.0	87.7	85.1	84.4	83.1	129.6
10000	93.6	95.3	96.6	97.0	99.4	98.9	96.9	91.4	86.7	83.7	82.6	81.4	128.7
12500	94.3	96.6	97.8	96.9	96.9	96.2	93.8	85.3	81.1	78.6	79.2	78.3	126.8
16000	91.7	93.7	94.4	93.1	94.1	93.1	89.9	81.7	76.7	74.8	75.4	75.5	123.9
20000	90.0	91.2	92.4	91.3	92.9	91.9	87.1	79.0	73.2	71.4	70.2	70.1	122.6
25000	87.3	88.2	89.2	88.2	89.4	88.0	84.7	75.4	69.5	65.8	66.4	65.4	119.9
31500	84.5	85.6	86.8	84.7	85.9	84.3	81.2	70.8	64.7	61.0	62.6	61.2	117.4
40000	81.4	82.1	83.2	79.9	81.3	80.3	76.3	65.1	62.5	57.3	60.7	59.6	114.6
50000	80.1	79.6	79.6	76.8	78.9	77.9	73.7	61.6	63.6	57.7	62.4	61.4	113.7
63000	79.2	75.0	74.0	72.0	76.3	75.6	71.2	59.1	65.0	58.3	63.6	62.2	113.3
80000	76.4	69.5	69.8	67.9	73.0	74.1	71.2	60.9	64.9	60.2	60.6	67.8	115.4
OVERALL MEASURED													
OVERALL CALCULATED	105.5	107.0	108.1	107.2	107.6	106.9	104.0	99.0	95.4	92.1	91.7	90.6	137.3

MODEL SOUND PRESSURE LEVELS (59. DEG. F, 70 PERCENT REL. HUM. DAY) - ANGLES FROM INLET

		0.	10.	20.	30.	40.	50.	60.	70.	80.	90.	100.	110.	
	50													PWL
	63													
RADIAL 17. FT.	80													
(5. M)	100	63.8	63.3	63.0	62.3	59.1	59.4	62.9	62.9	63.6	63.5	62.7	61.5	96.2
VEHICLE	125	68.6	69.3	68.3	64.3	65.1	66.6	66.7	69.4	71.3	71.5	69.4	73.3	103.6
	160	70.8	70.0	70.8	70.8	67.3	66.1	63.9	65.1	67.1	66.0	65.2	67.3	100.8
NASA Rotor 11	200	73.0	74.3	73.8	73.0	71.5	71.1	69.4	67.6	65.6	64.7	64.4	62.8	102.8
	250	79.5	78.8	77.8	76.8	76.3	74.6	72.9	71.9	70.8	70.2	68.6	66.3	107.0
	315	76.5	77.0	75.8	75.5	73.8	72.6	71.4	71.4	68.8	67.0	65.9	65.0	105.2
	400	74.5	74.5	74.3	73.0	72.1	70.4	68.4	66.9	65.6	64.0	63.1	61.3	102.6
BAR 29.7 HG	500	73.8	74.0	73.8	73.5	72.3	70.9	71.2	67.6	65.8	64.0	61.4	59.8	103.1
(00361. N/M2)	630	76.8	77.3	77.8	76.7	76.1	74.9	75.2	71.1	69.3	67.0	64.4	62.5	106.7
TAMB 84. DEG F	800	78.3	78.5	79.0	78.7	77.6	76.4	76.2	72.9	70.6	68.5	67.6	65.8	108.3
(302. DEG K)	1000	78.8	78.7	78.8	78.2	77.8	76.6	74.1	72.1	69.0	66.2	65.4	65.5	107.7
TWET 71. DEG F	1250	80.0	80.5	80.0	78.9	78.6	77.6	75.9	72.6	69.8	67.8	65.6	65.3	108.8
(295. DEG K)	1600	77.6	78.3	79.5	78.4	77.6	76.4	73.9	71.1	68.6	66.8	64.4	63.3	107.6
HACT15.15 GM/M3	2000	78.3	79.8	79.8	79.4	78.3	76.3	73.1	70.4	67.8	65.6	64.1	63.1	107.9
(.01515 KG/M3)	2500	79.5	80.8	80.7	80.6	80.3	79.1	75.9	72.9	69.3	67.8	65.6	64.4	109.8
NFA 8240. RPM	3150	82.3	82.5	82.4	81.4	82.0	81.1	78.1	74.8	71.6	69.6	67.4	65.6	111.5
(863. RAD/SEC)	4000	95.7	92.9	90.6	86.3	88.0	86.7	83.3	79.0	75.5	73.5	72.0	71.8	117.9
NFK 8048. RPM	5000	90.4	90.9	91.5	90.0	88.6	88.2	85.7	81.2	77.7	75.0	73.0	73.0	119.2
(843. RAD/SEC)	6300	93.5	94.4	96.8	95.1	93.7	93.9	91.2	86.4	83.5	79.9	79.4	77.8	124.5
NFD16100. RPM	8000	88.8	89.8	90.4	89.4	89.4	88.3	85.3	80.6	77.1	74.5	72.9	72.3	119.0
(1686. RAD/SEC)	10000	87.6	88.3	88.8	88.2	89.6	88.2	84.8	79.3	75.1	72.9	71.3	69.9	118.6
NO. OF BLADES 44	12500	93.1	93.6	91.6	90.7	91.9	90.3	87.5	83.9	76.5	73.8	73.2	73.0	121.3
	16000	85.2	86.2	86.1	85.8	86.6	85.7	82.8	75.9	70.6	68.7	67.9	68.2	116.5
Grid #3,	20000	83.5	84.5	85.7	85.1	87.1	85.8	82.8	75.4	68.6	67.0	66.2	65.6	116.8
50% Speed,	25000	81.2	82.1	83.3	81.8	83.0	82.9	79.2	71.3	65.3	62.0	62.5	60.0	114.1
Discharge Valve	31500	78.5	79.4	80.3	77.9	79.1	78.2	74.4	66.5	61.6	58.7	61.3	60.2	111.1
Setting = 0	40000	75.5	75.4	76.6	73.7	75.1	74.2	70.3	61.5	61.0	59.6	63.3	62.7	108.6
	50000	74.9	73.2	73.5	70.9	72.3	71.9	67.2	58.1	61.6	56.6	62.2	59.3	107.8
	63000	77.9	69.7	69.0	67.5	69.2	69.2	64.1	56.2	62.3	56.4	63.8	60.9	107.8
	80000	75.6	68.7	69.0	67.9	64.4	64.9	62.1	55.4	58.7	55.3	60.8	66.0	110.2
OVERALL MEASURED														
OVERALL CALCULATED		100.9	100.7	101.1	99.6	99.5	98.8	96.0	91.0	87.8	85.2	84.1	83.5	129.8

APPENDIX 2

List of Commonly Used Notations

A, A'	$A = \dfrac{C_L \sigma W_r M_a M_t}{4(1 - M_a^2)}$, $A' = 2A$
B, B'	$B = \dfrac{C_L \sigma W_r \sqrt{1 - M_r^2}}{4(1 - M_a^2)}$, $B' = 2B$
B	sometimes also used to denote the number of rotor blades
C, C'	$C = \sigma C_L W/4$, $C' = 2C$
C_L	lift coefficient of isolated rotor
C_i	Fourier coefficient of inlet distortion as in [6]
c_o	static speed of sound
d	rotor blade row pitch
i	integer
M_a, M_t	axial and wheel tip Mach numbers
n	harmonic of blade passing frequency noise of interest
S	number of lobes in inlet distortion as in [6]
u'_{ip}	i^{th} component of perturbation velocity associated with rotor potential flow field
u'_{is}	i^{th} component of perturbation velocity associated with inlet turbulence
W_r	relative velocity through rotor
x, x_i	Cartesian coordinates
y	Cartesian coordinate
∇^2	Laplacian
α_n	$\dfrac{2\pi \lvert n \rvert \sqrt{1 - M_r^2}}{d(1 - M_a^2)}$: $(M_r^2 = M_a^2 + M_t^2)$
β_n	$2\pi n/d$

δ_n	$2\pi n\ M_a\ M_t/d(1 - M_a^2)$
σ	rotor solidity

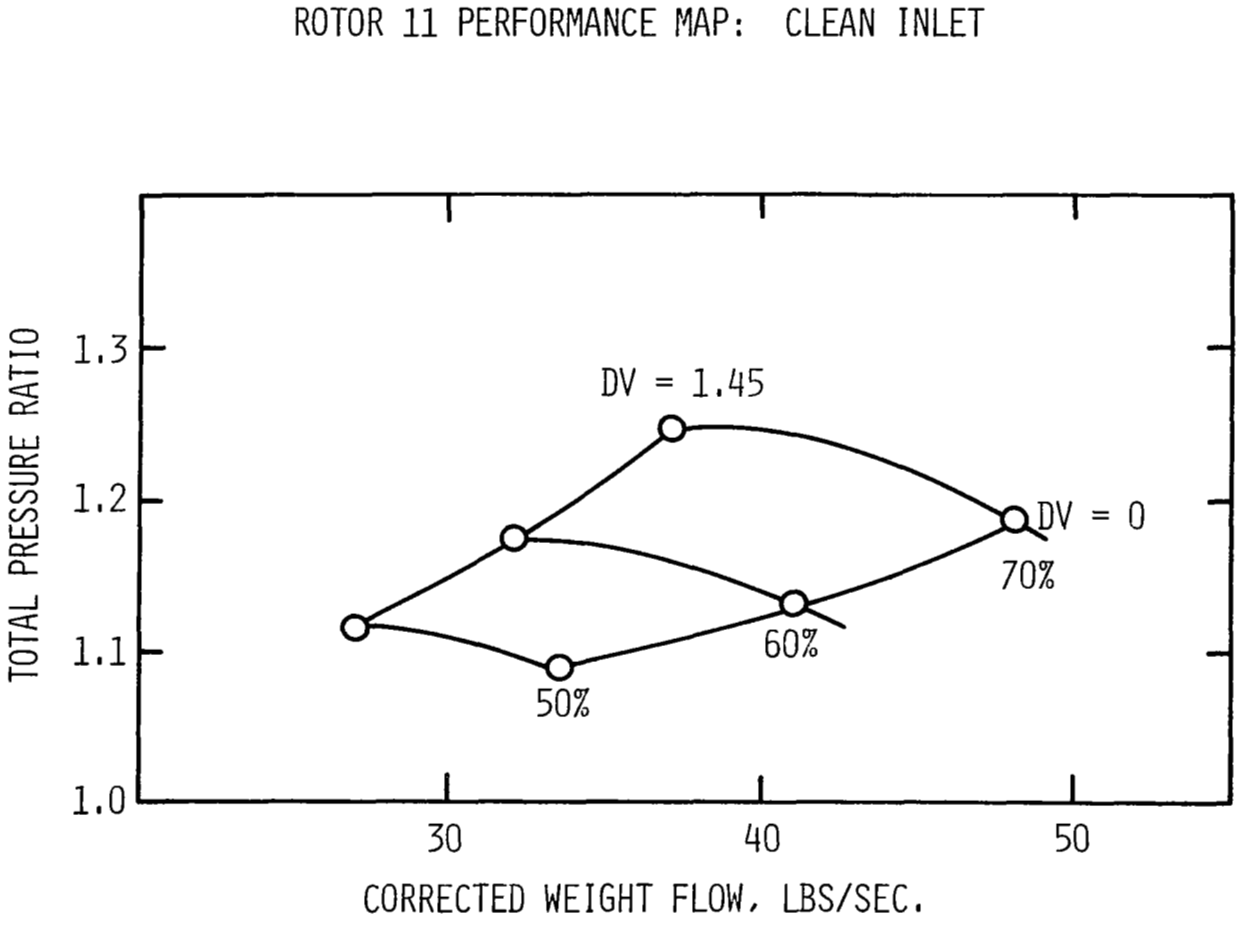

FIGURE 1. Aerodynamic Map of Fan Used in Present Studies: DV = 0 Denotes Low System Resistance While DV = 1.45 Denotes High System Resistance.

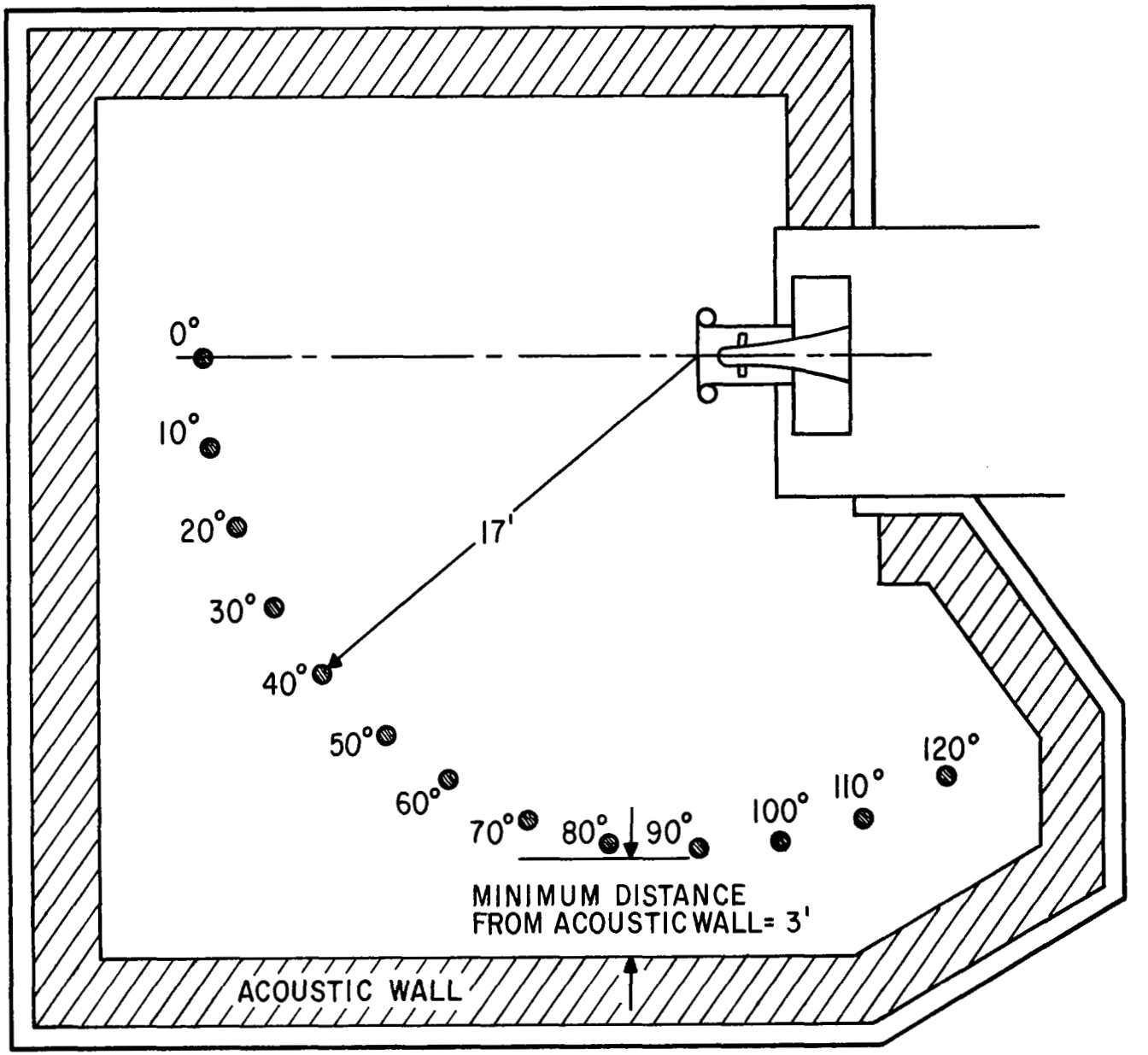

FIGURE 2. Schematic of the GE Aero-Acoustic Facility at Schenectady, N. Y.

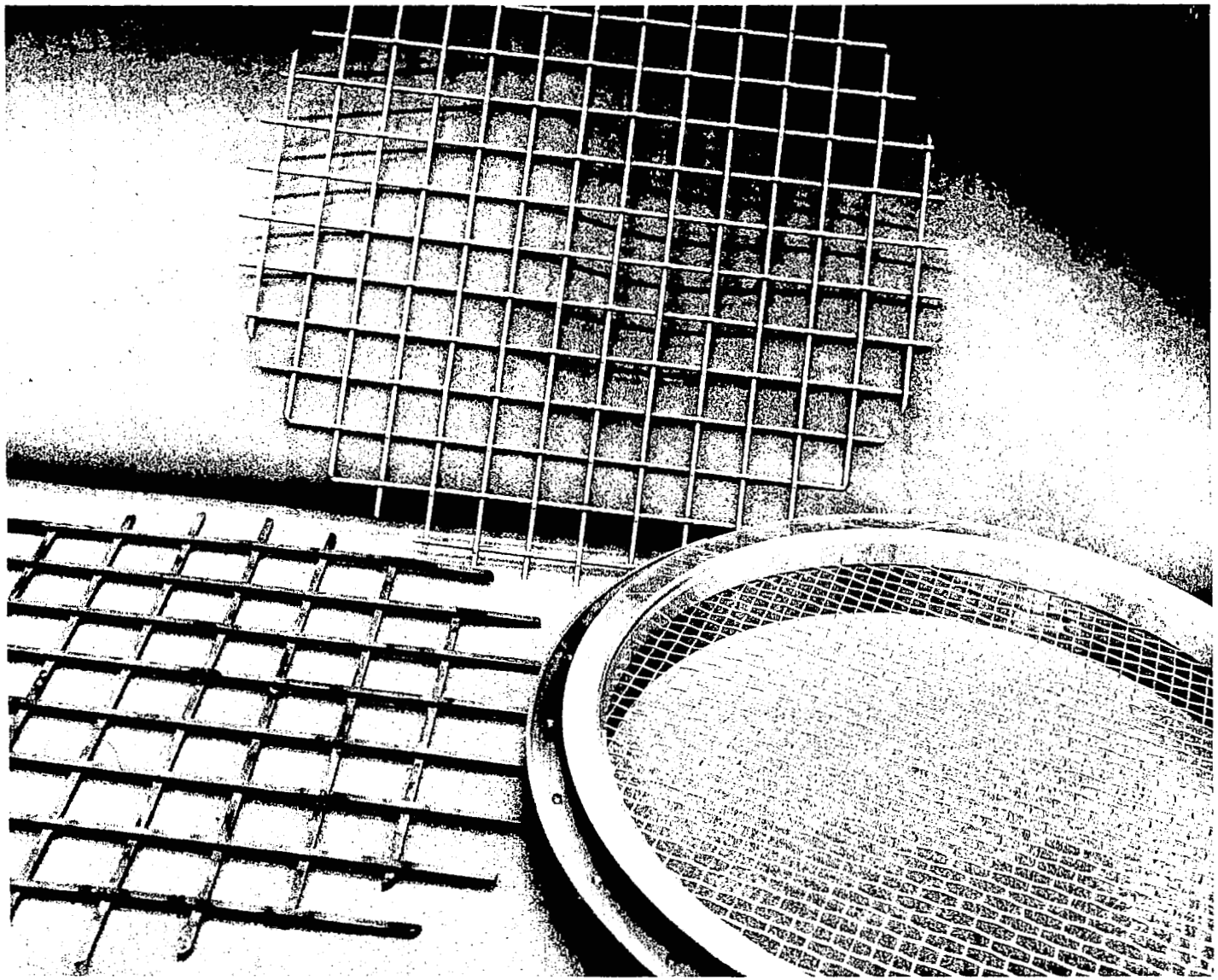

FIGURE 3. Photograph Showing Three Grids Employed in Current Study.

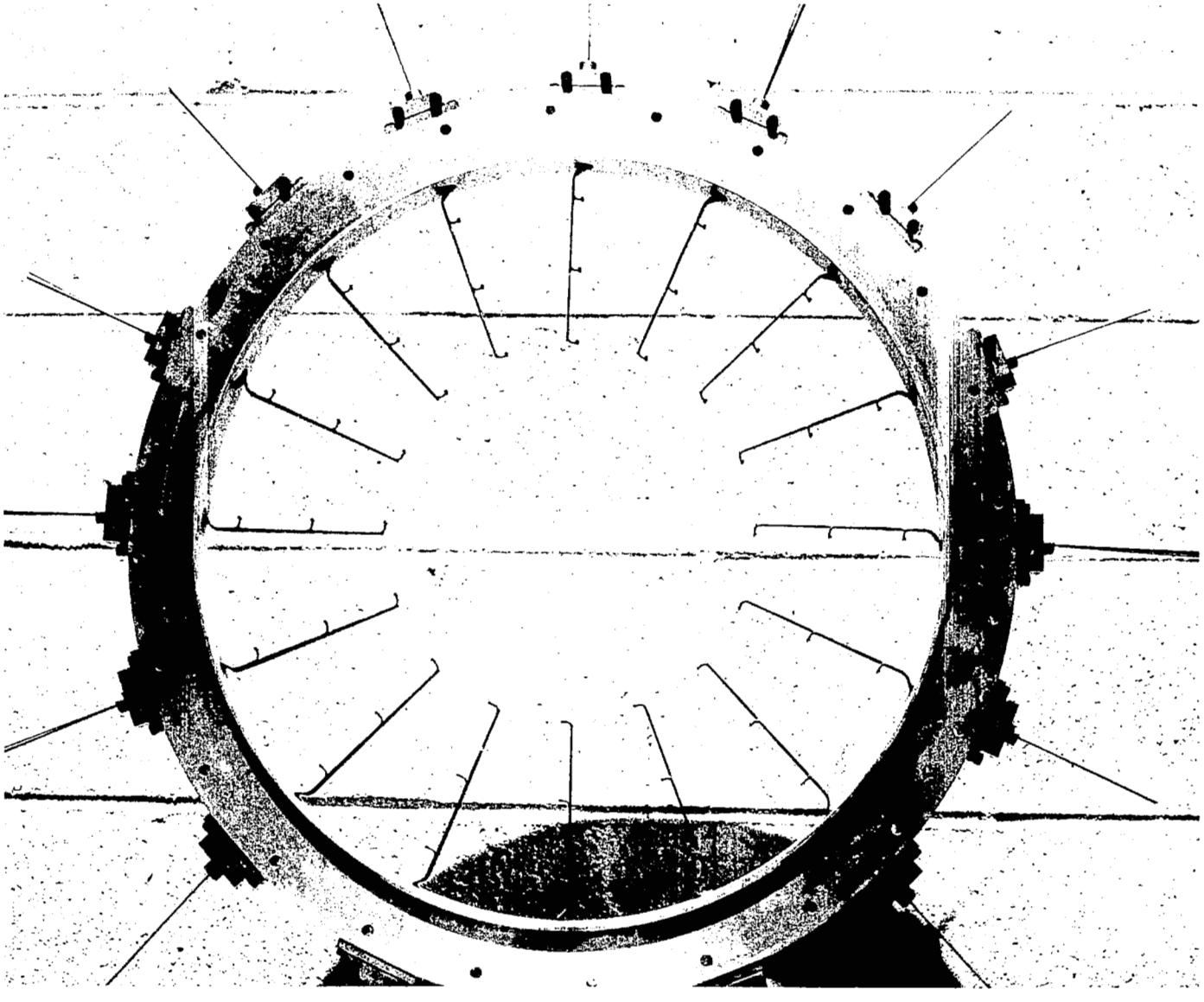

FIGURE 4. Photograph Showing Specially Designed Kiel Probe Array for Mapping Inlet Distortion.

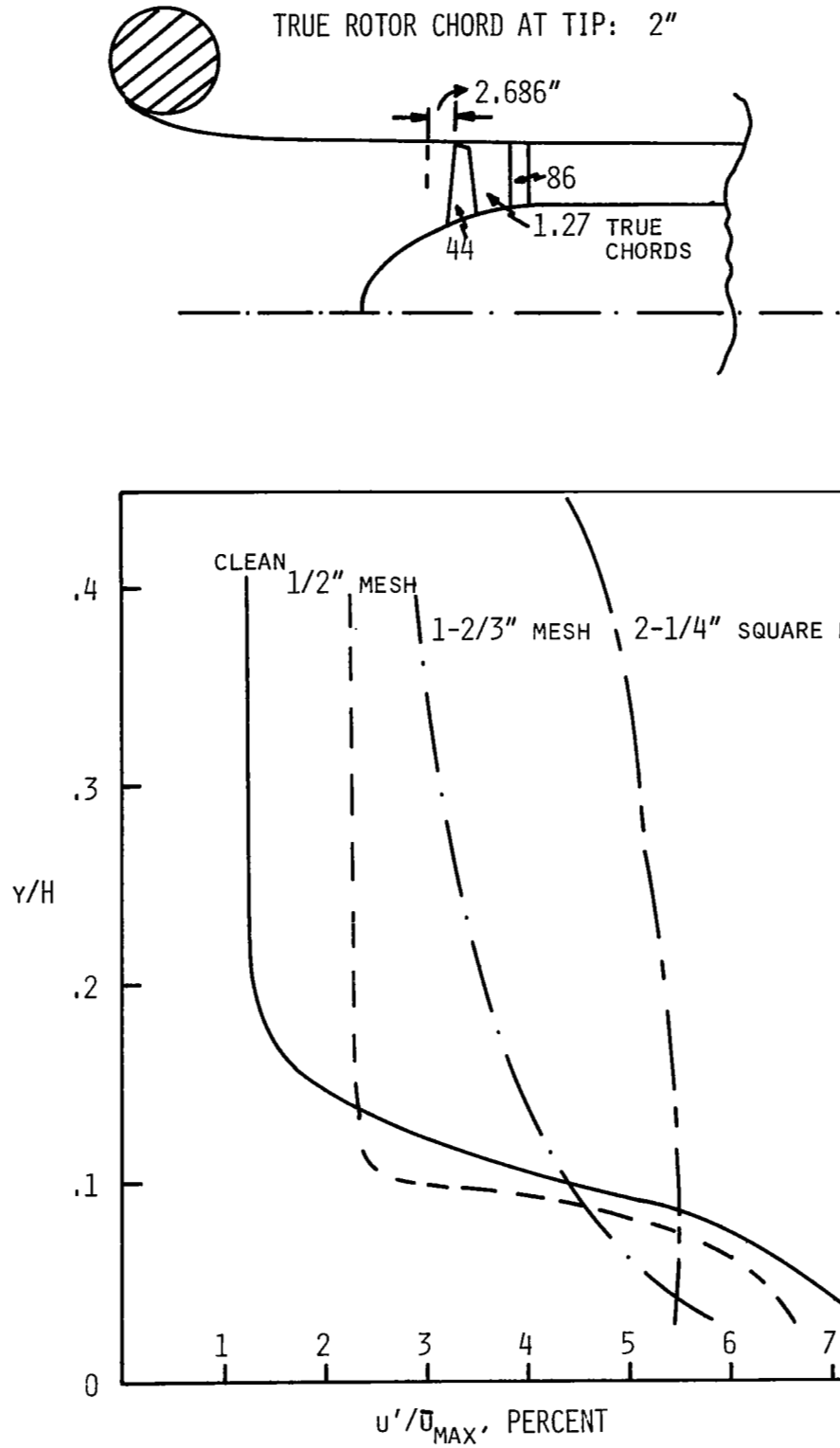

FIGURE 5. Turbulence Intensity as Function of Distance from Outer Wall.

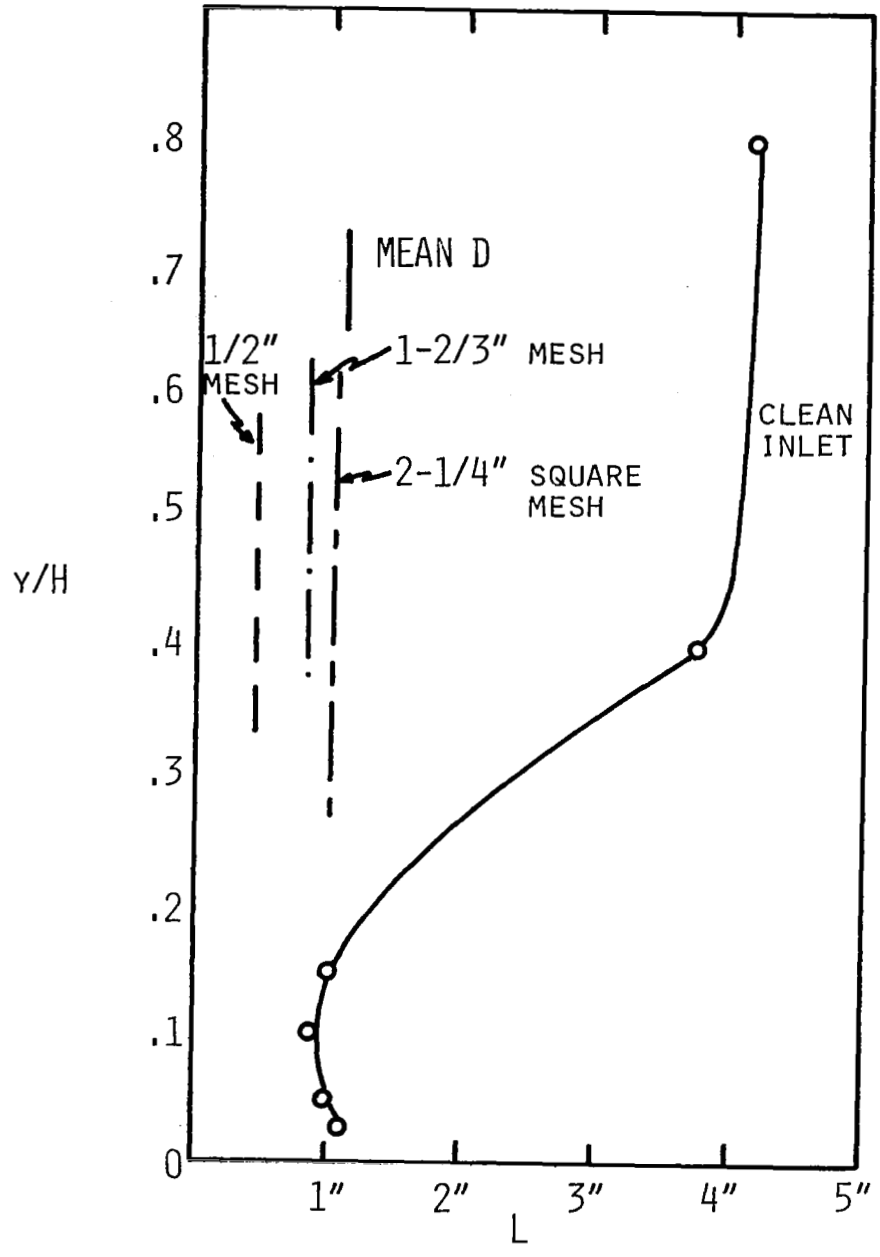

FIGURE 6. Integral Length Scales as Function of Distance from the Wall.

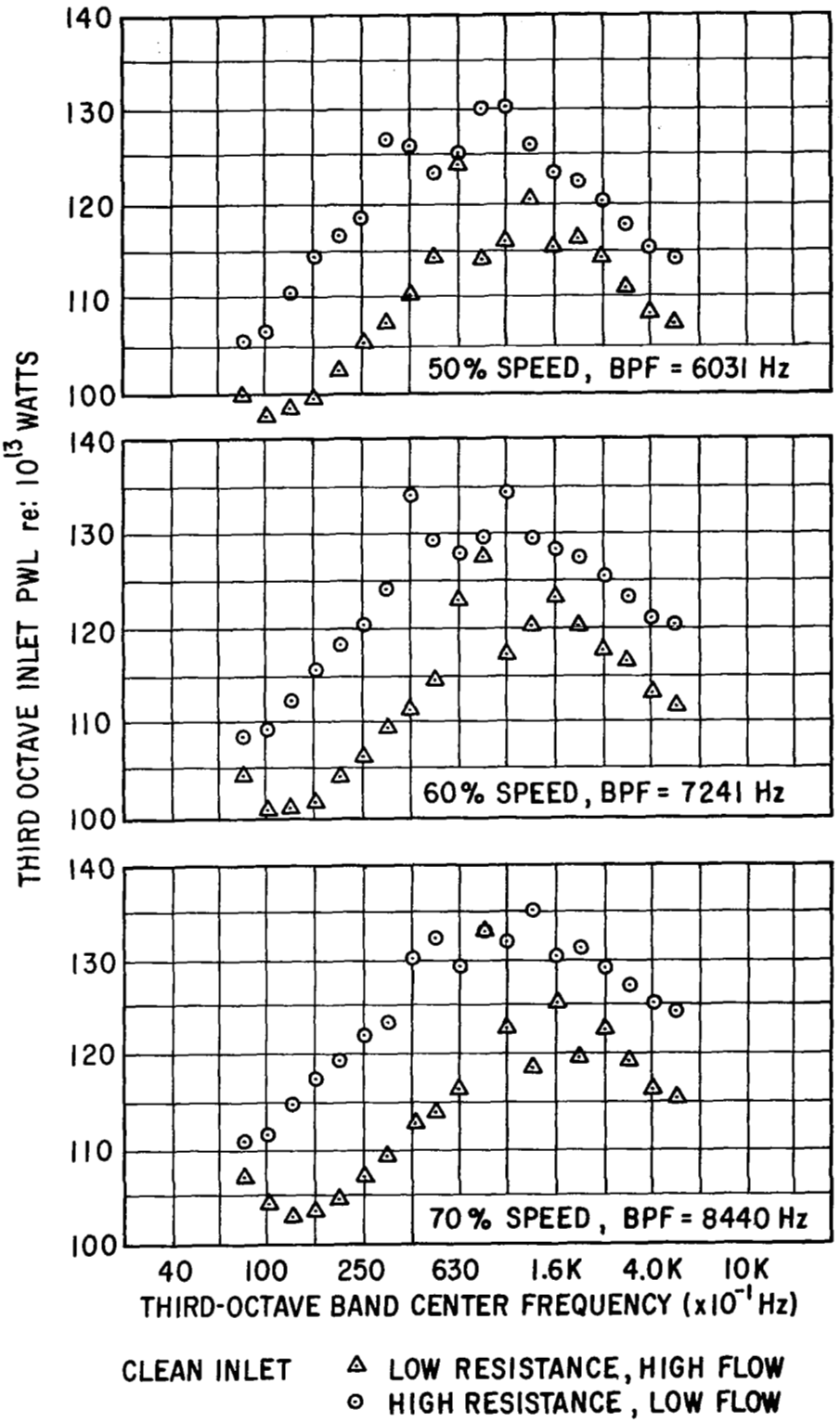

FIGURE 7. Acoustic Data - Clean Inlet.

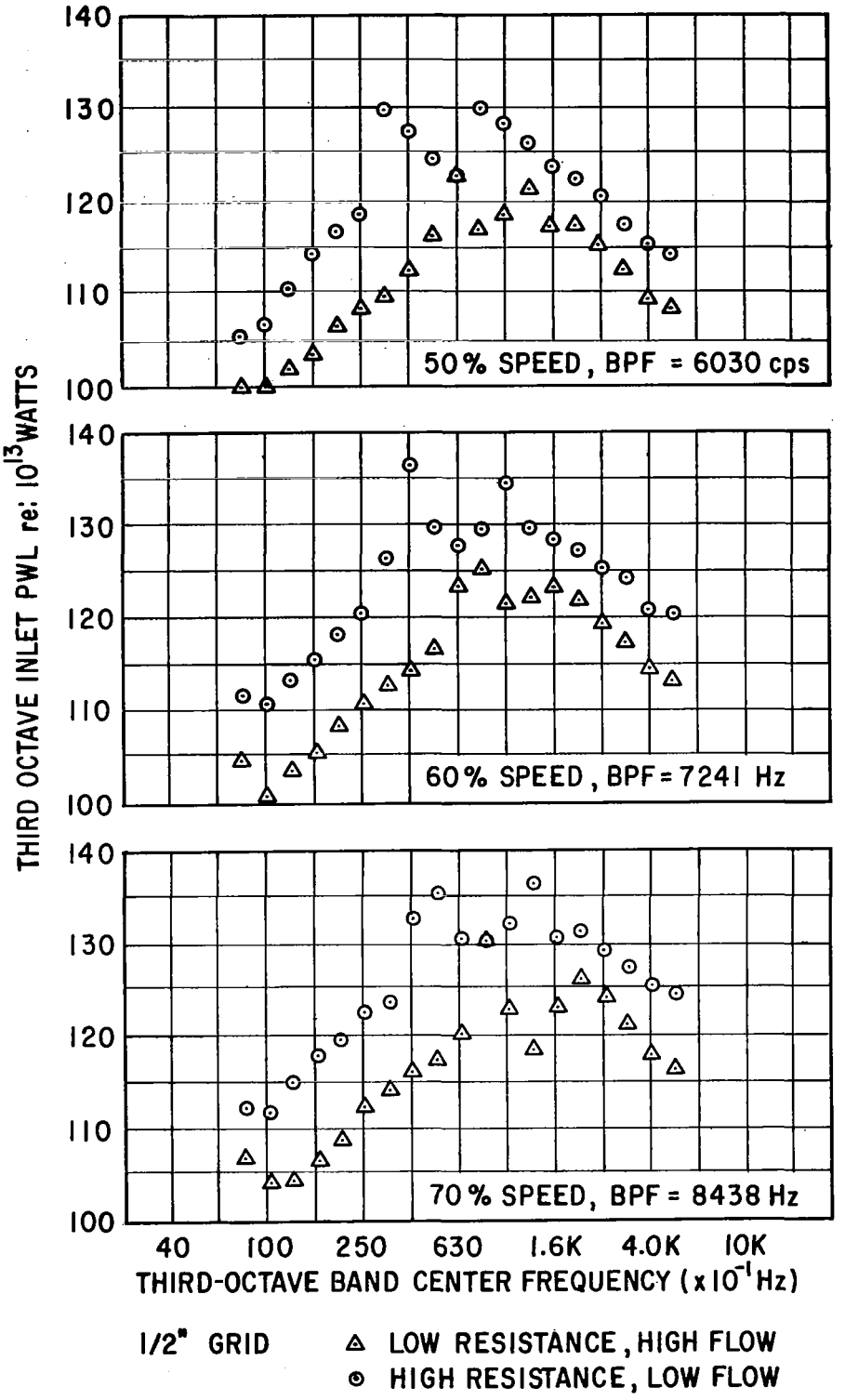

FIGURE 8. Acoustic Data - ½" Grid.

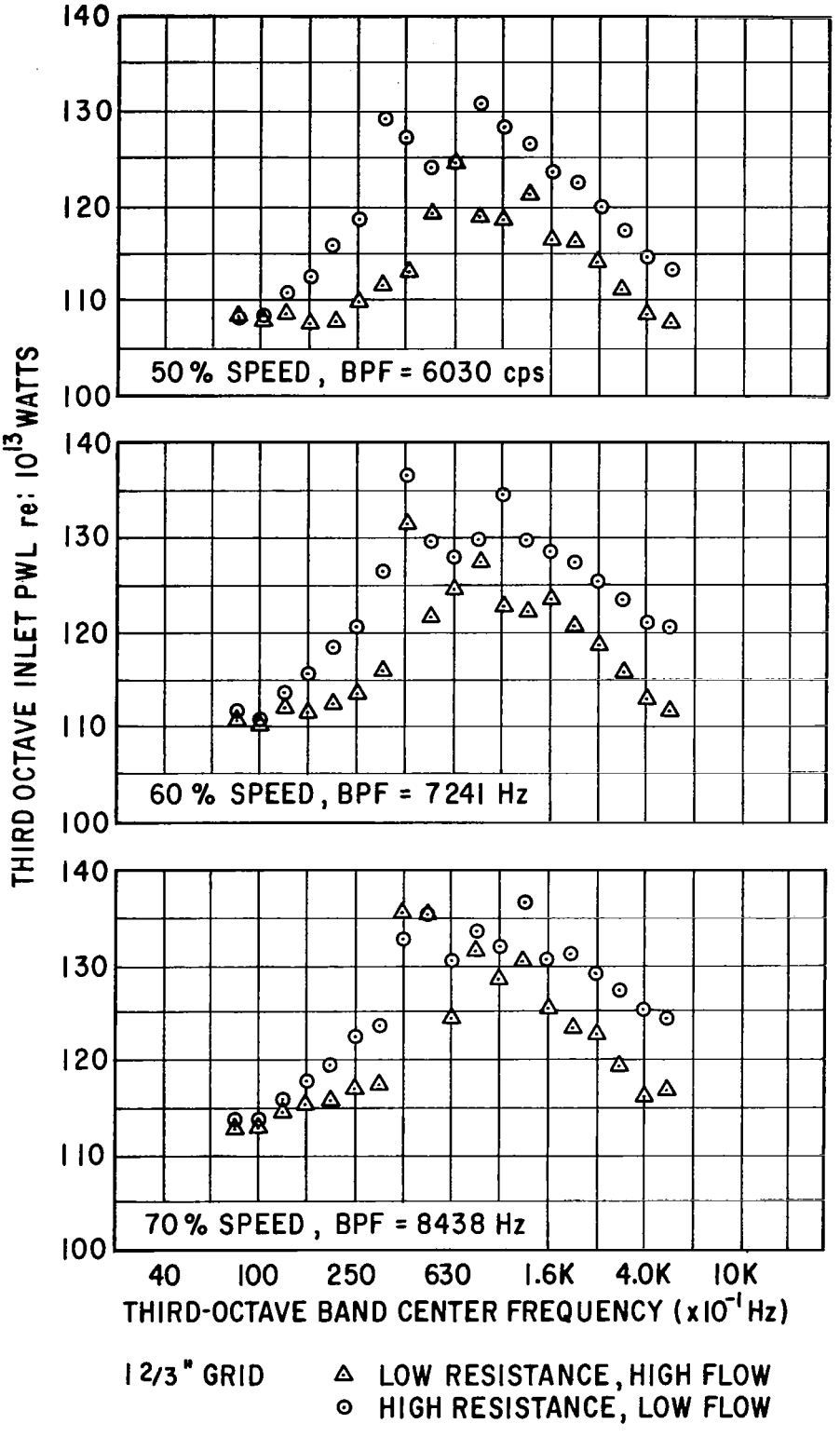

FIGURE 9. Acoustic Data - 1-2/3" Grid.

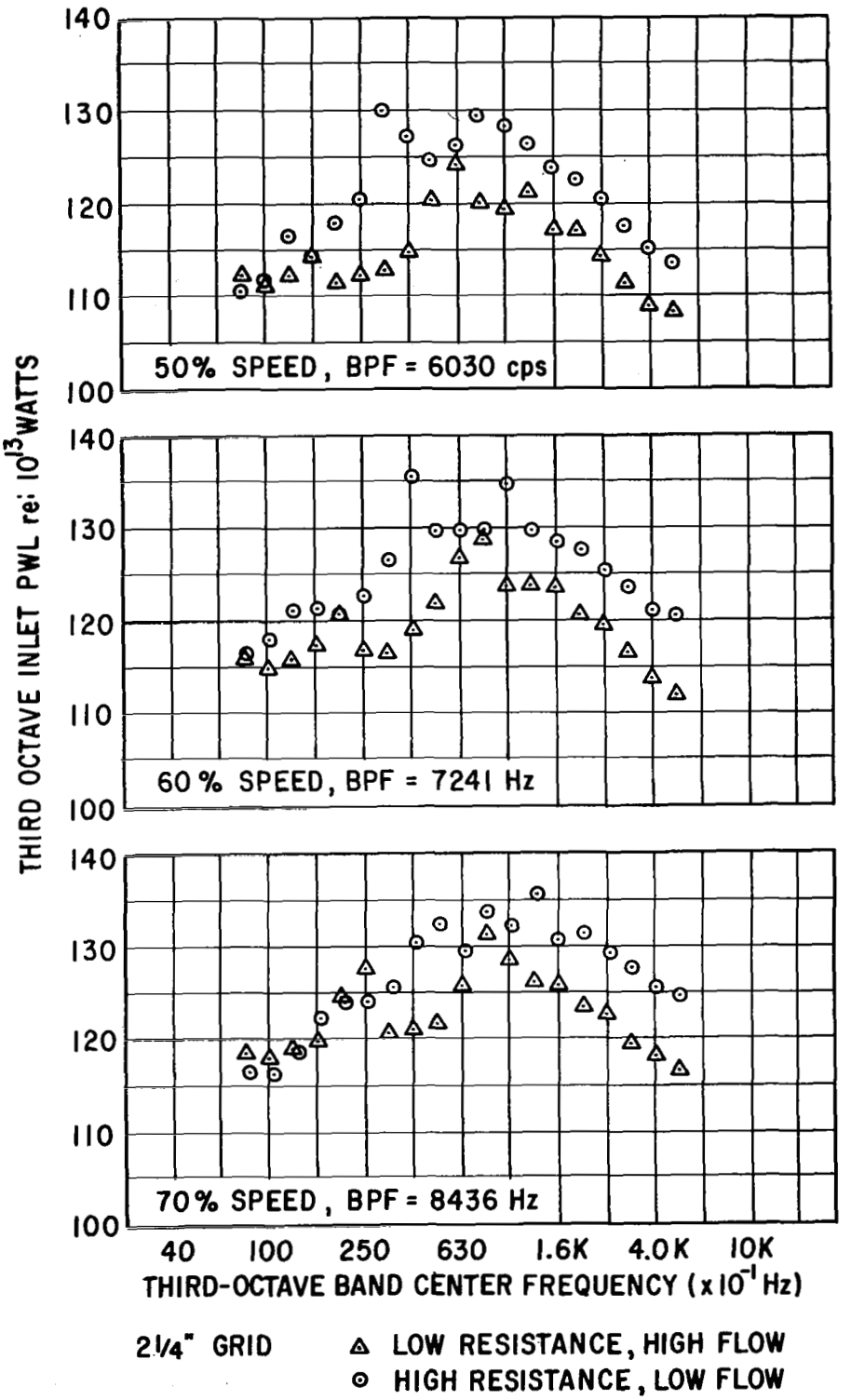

FIGURE 10. Acoustic Data - 2¼" Grid.

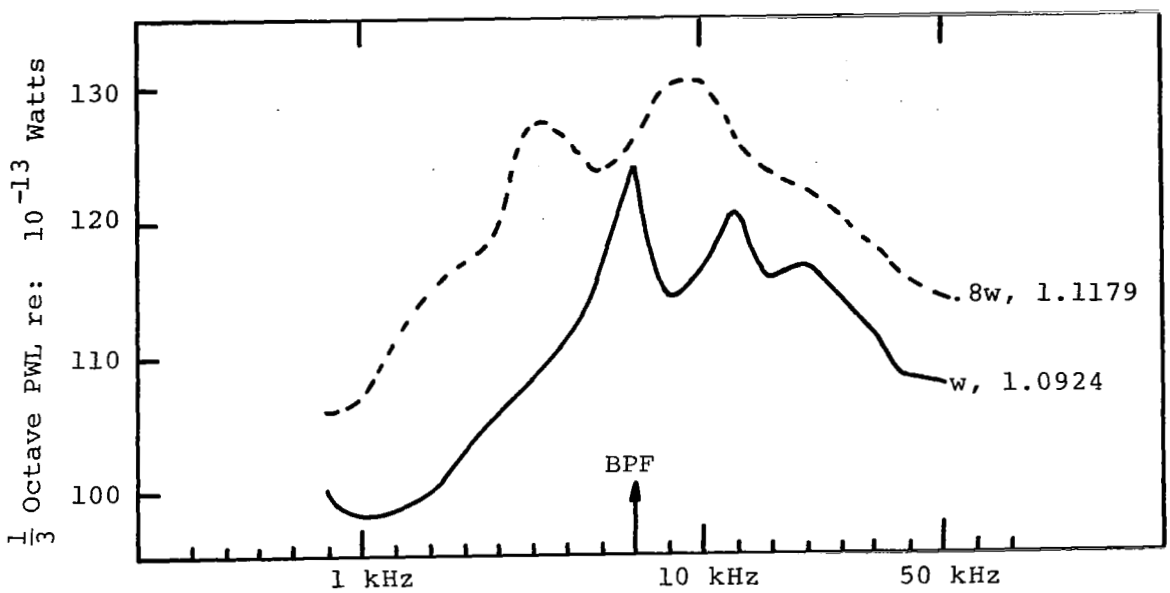

50% SPEED: CLEAN INLET: M_t = .575

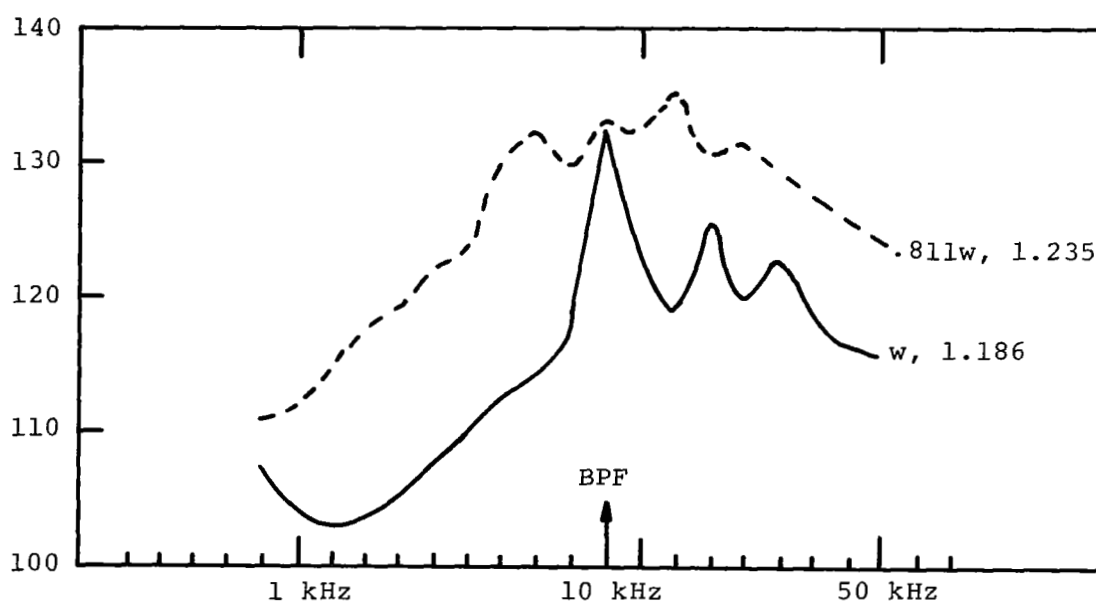

70% SPEED: CLEAN INLET: M_t = .805

FIGURE 11. Effect of Pressure Ratio on the PWL Spectrum.

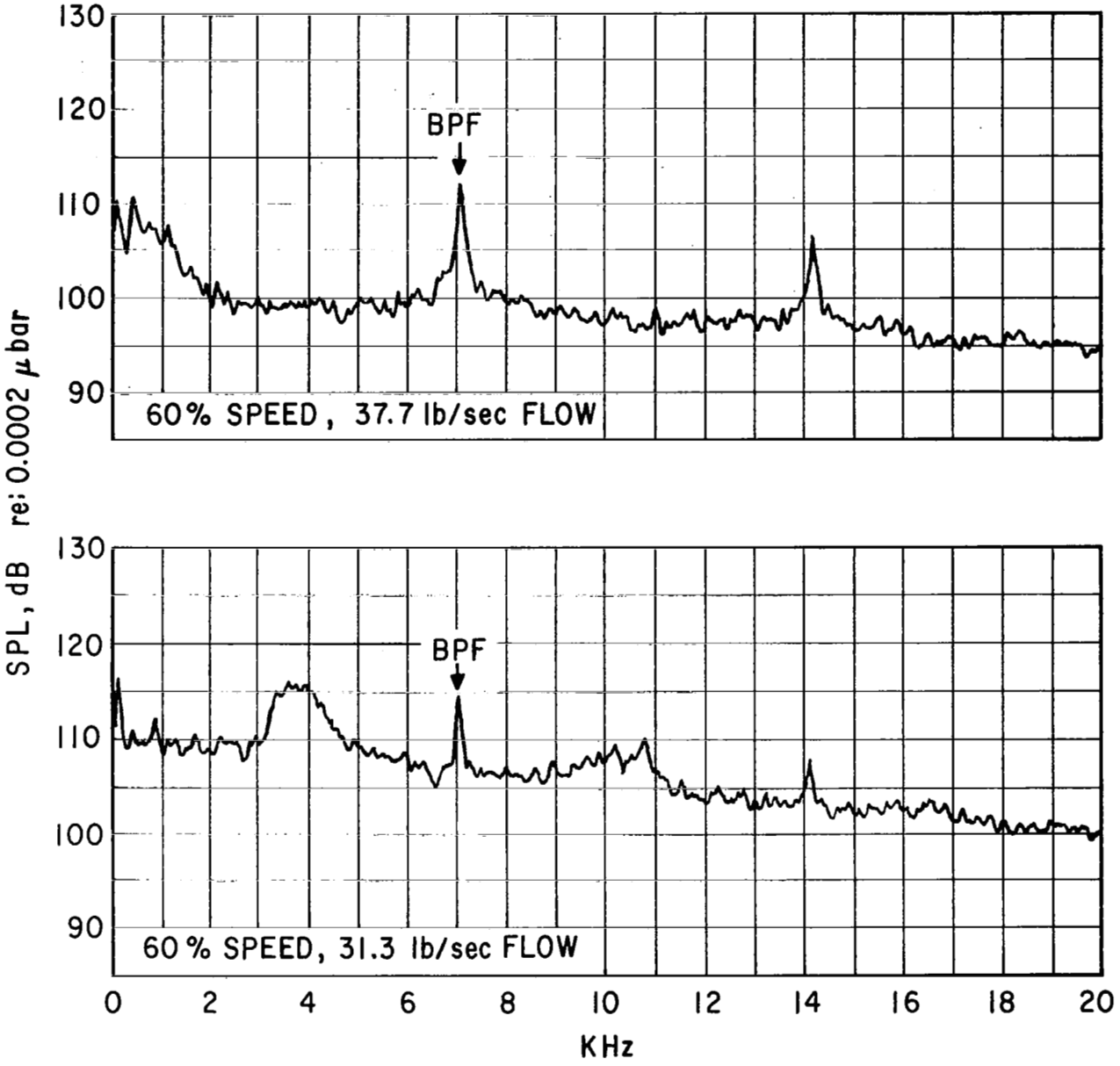

FIGURE 12. Inlet Plenum Reverberant SPL Data from [5].

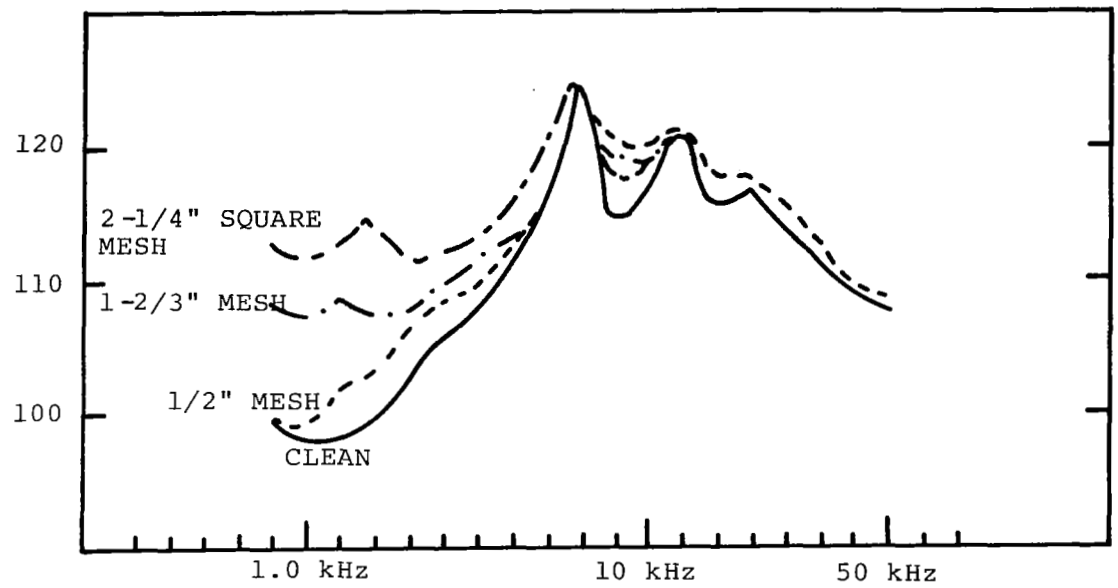

50% SPEED - DISCHARGE VALVE SETTING = 0.0

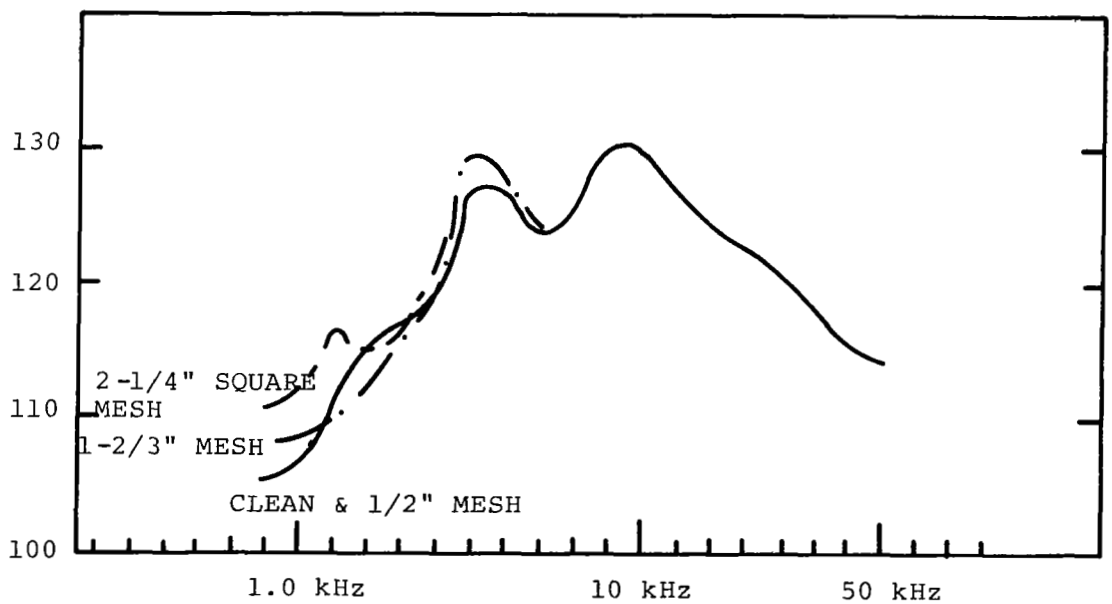

50% SPEED - DISCHARGE VALVE SETTING = 1.45

FIGURE 13. Effect of Grids on Fan Noise.

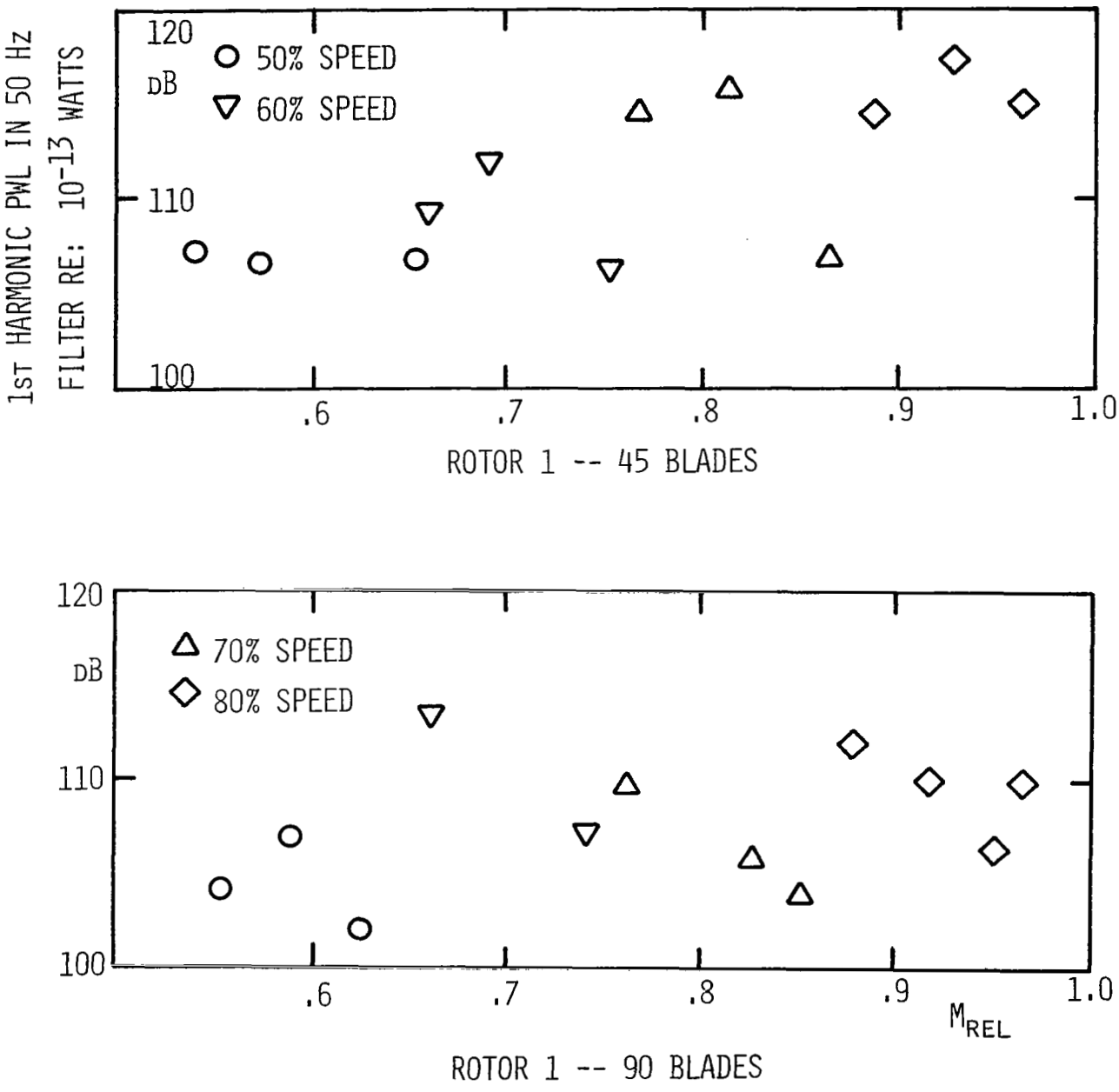

FIGURE 14. Effect of Pressure Ratio and Tip Speed on Isolated Subsonic Rotor Noise ([7]).

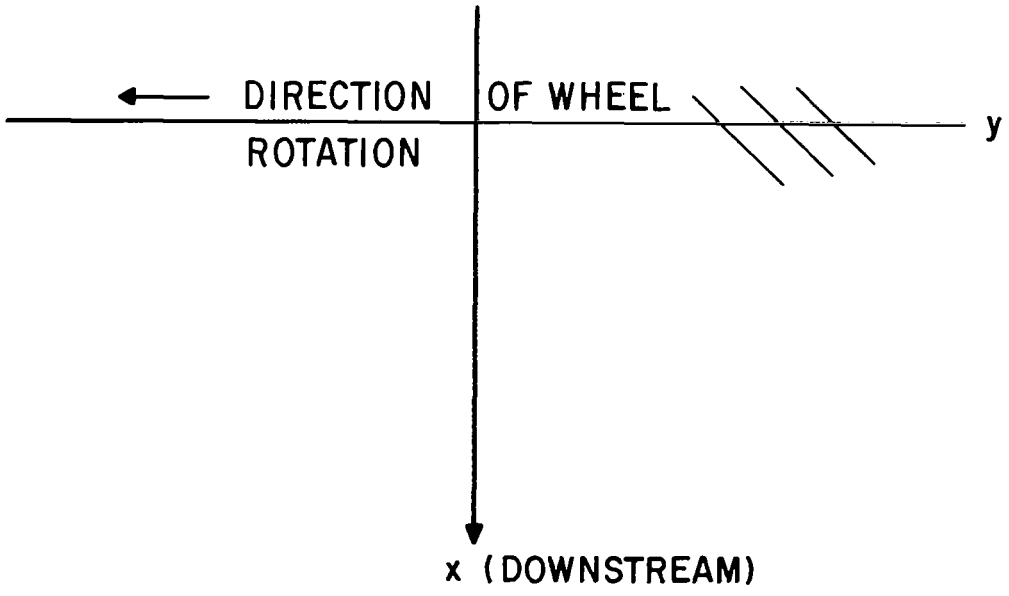

FIGURE 15. Cascade Plane Representation of Blade Row.

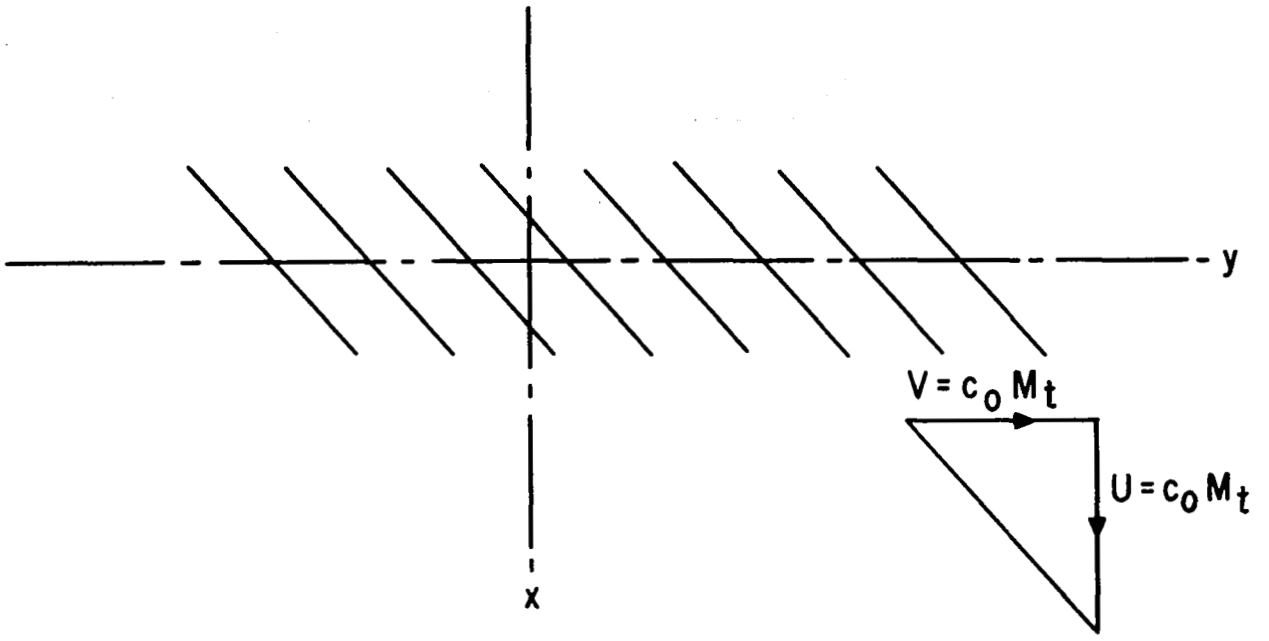

FIGURE 16. Rotor Fixed Frame of Reference.

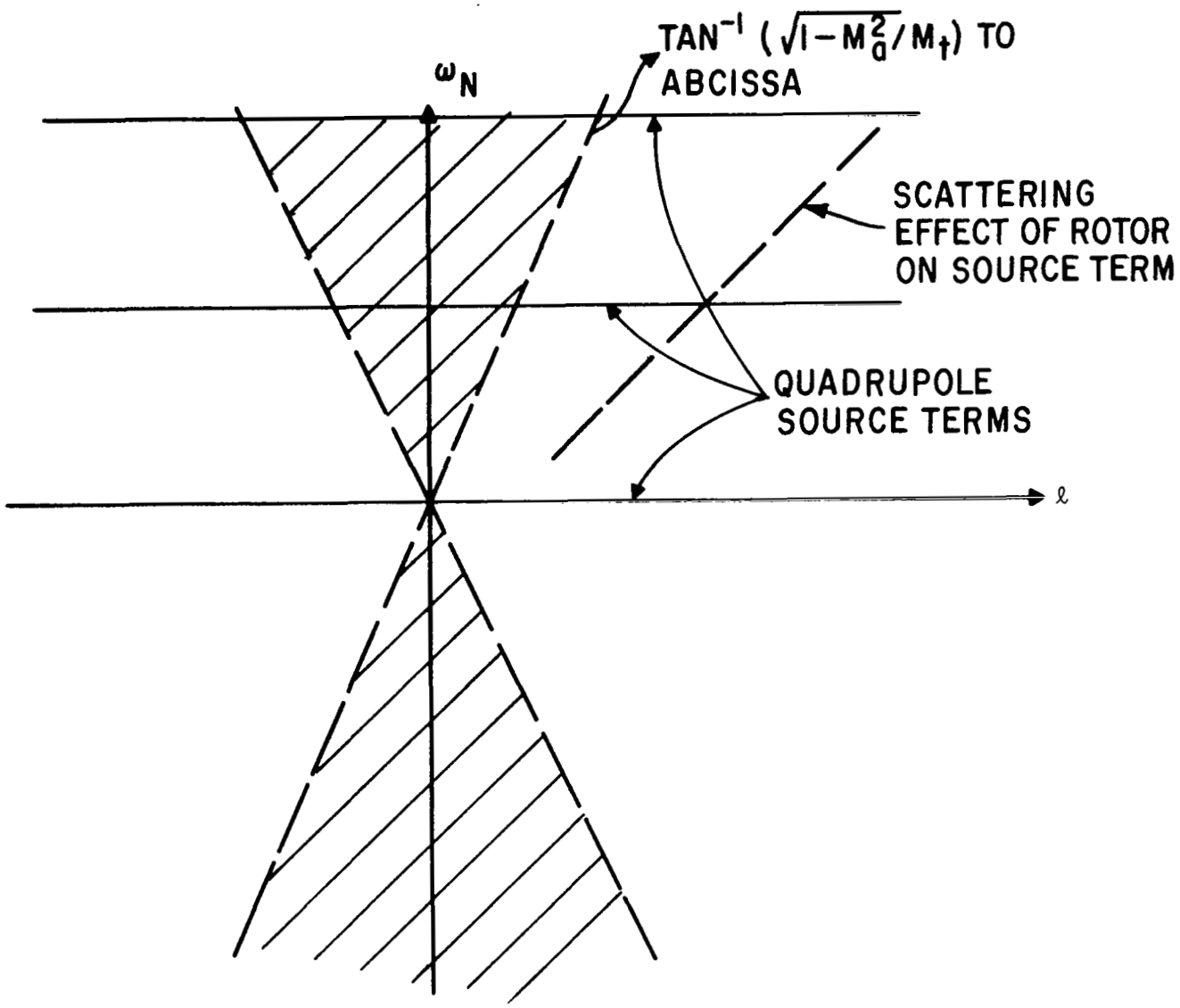

FIGURE 17(a). Lobe Number - Frequency Diagram.

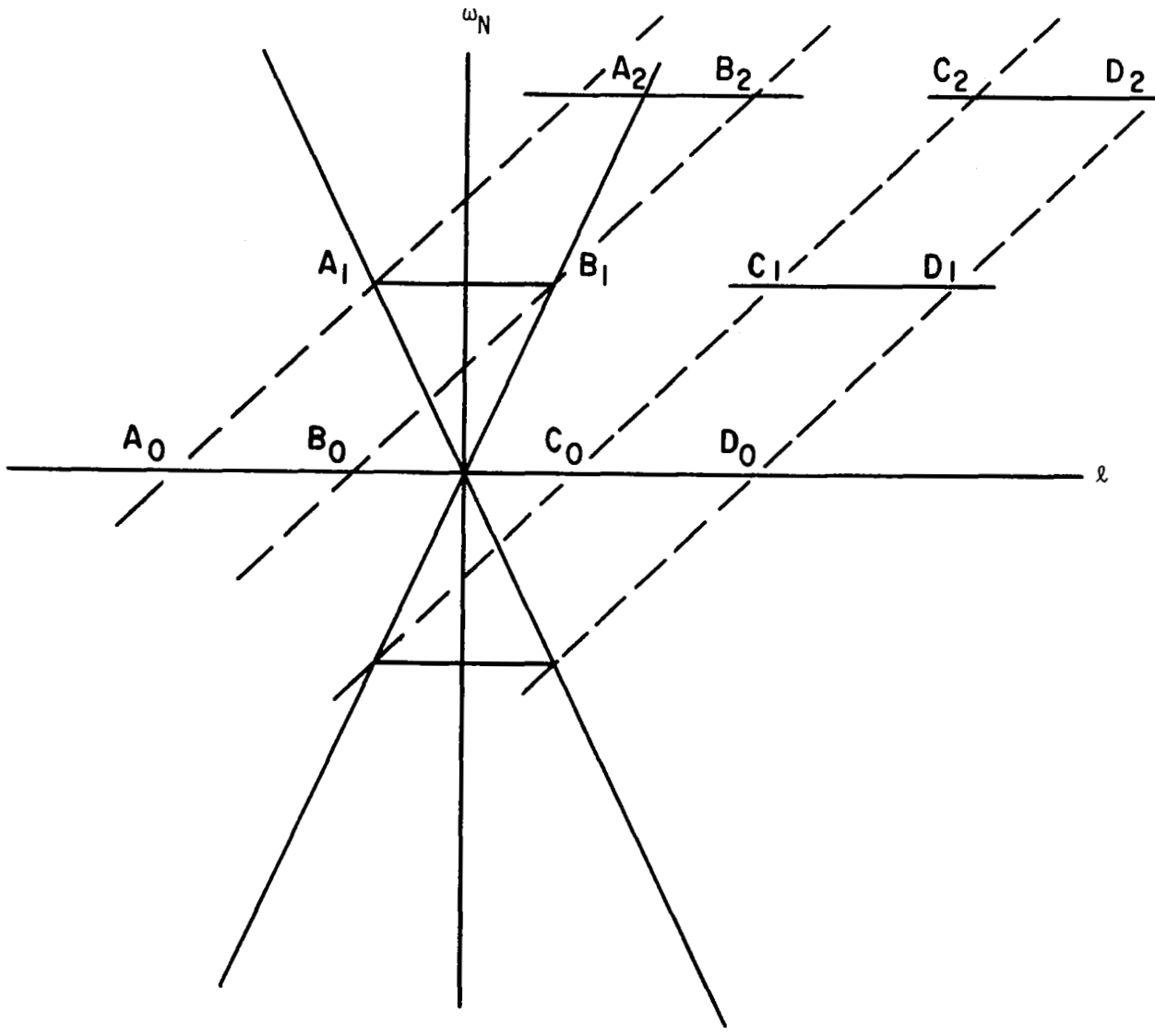

FIGURE 17(b). **Kinematics of Scattering of Quadrupole Source Terms.**

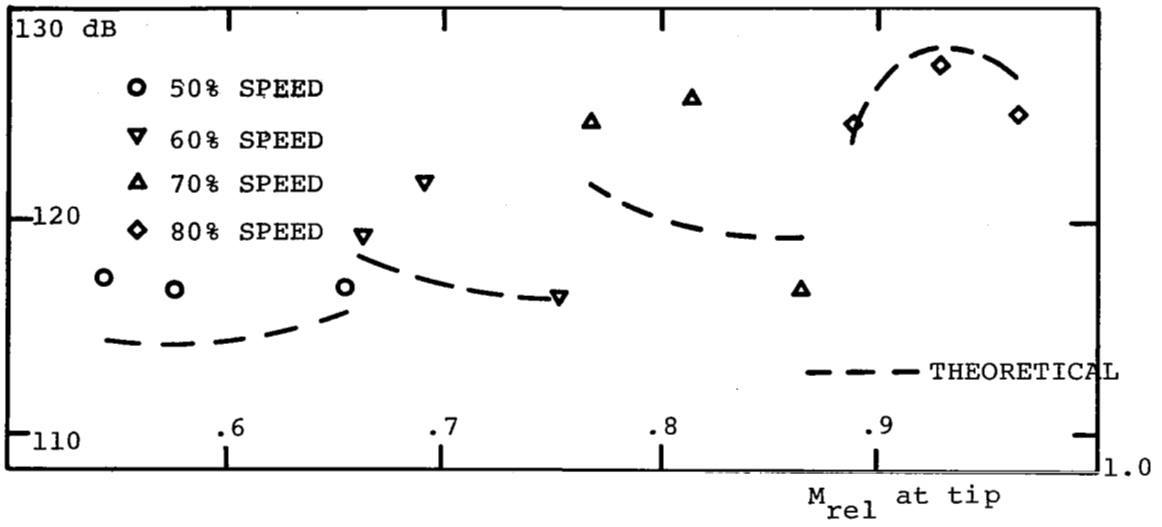

ROTOR 15 DATA - 45 BLADES - f_b = FUNDAMENTAL BLADE PASSING FREQUENCY
(NASA)

INLET DISTORTION ANALYSIS

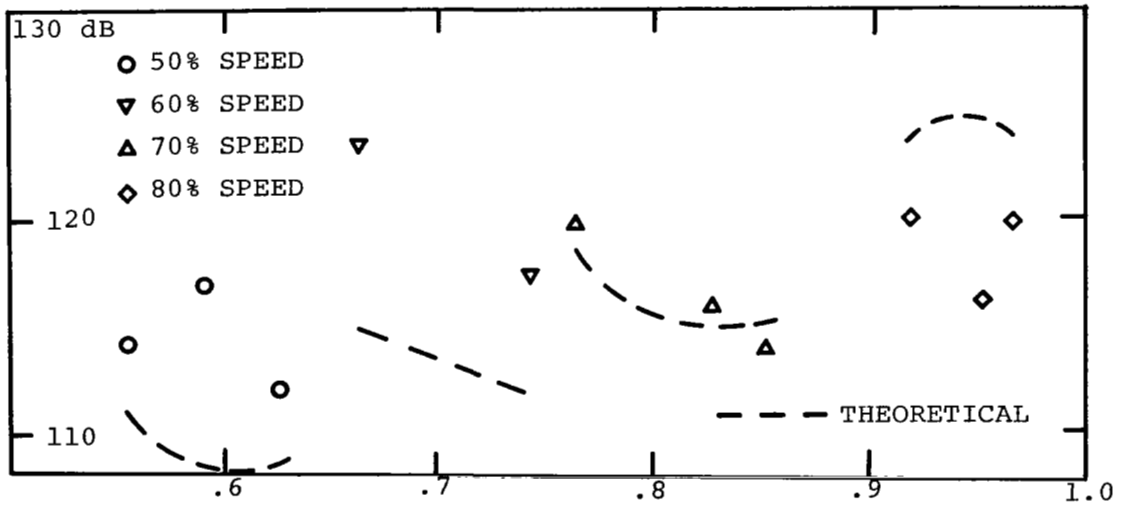

ROTOR 15 DATA - 90 BLADES (NASA)

INLET TURBULENCE ANALYSIS

FIGURE 18. Comparison with Results from [7].

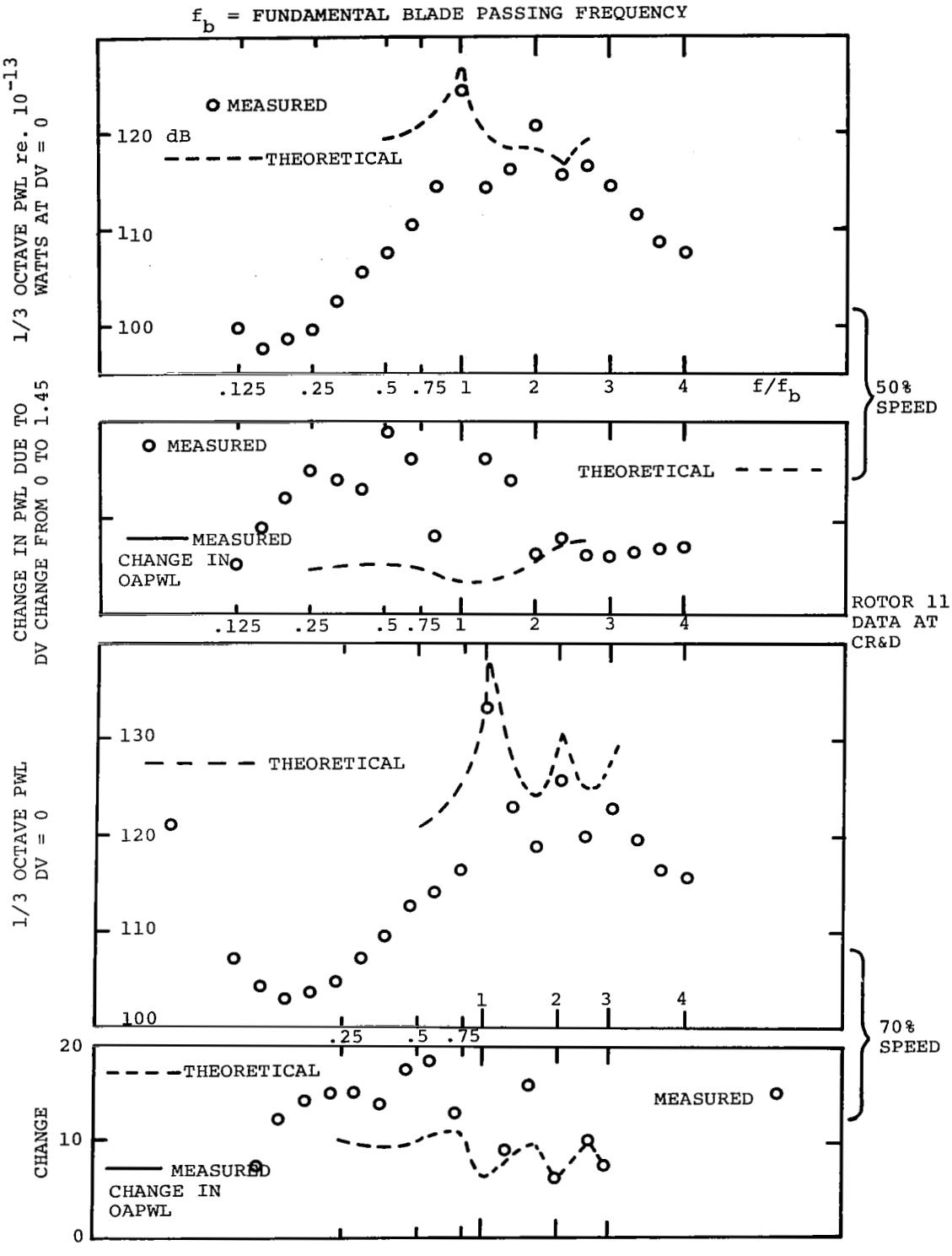

FIGURE 19. Comparison with Clean Inlet Results of Part I. Isotropic Turbulence - Rotor Interaction.

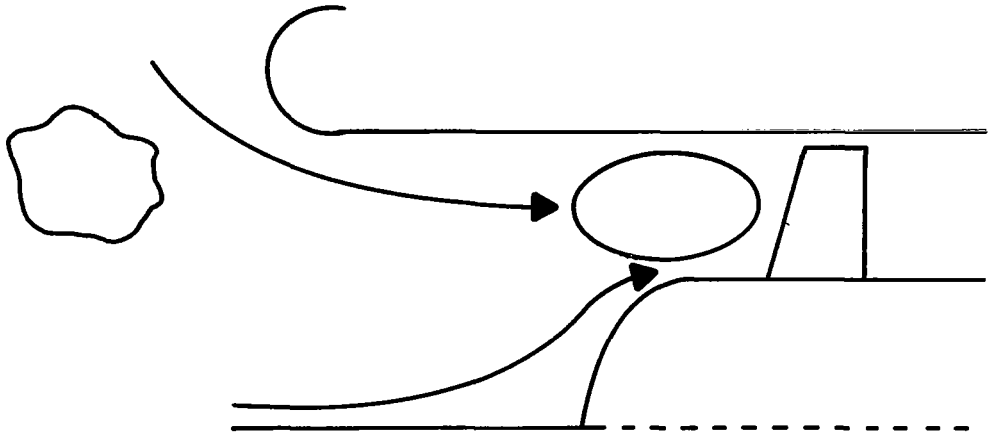

- BATCHELOR-RIBNER/TUCKER THEORY FOR EFFECT OF SUDDEN CONTRACTIONS ON SPECTRUM OF ISOTROPIC TURBULENCE.

- $\frac{u'}{U} << \frac{\ell}{D}$

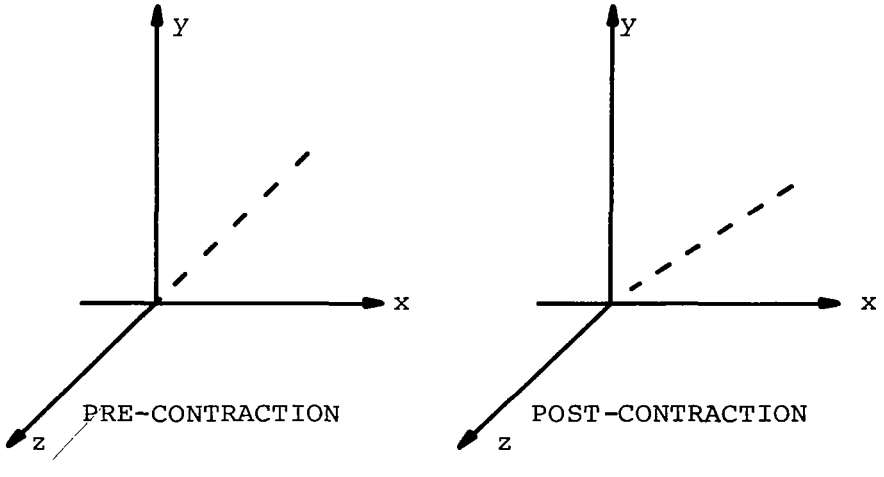

FIGURE 20. Distortion of Isotropic Eddies Due to Inlet Contraction.

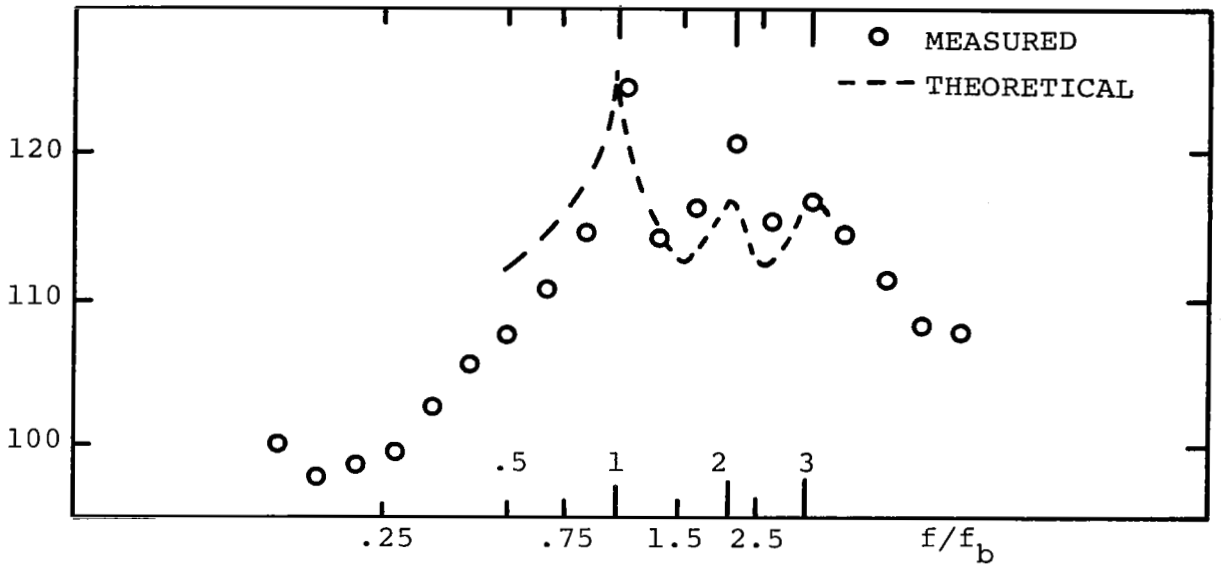

ROTOR 11, 50% SPEED DV = 0

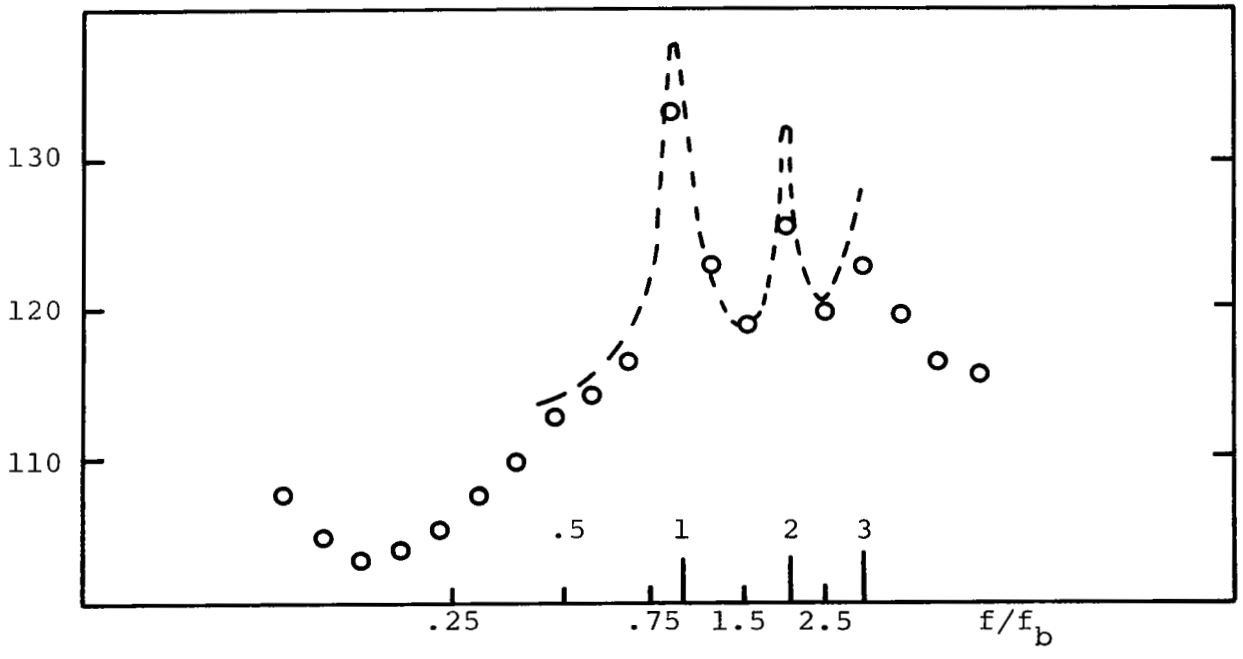

ROTOR 11, 70% SPEED DV = 0

FIGURE 21. Anisotropic Turbulence - Rotor Interaction (Contraction Ratio: 2).

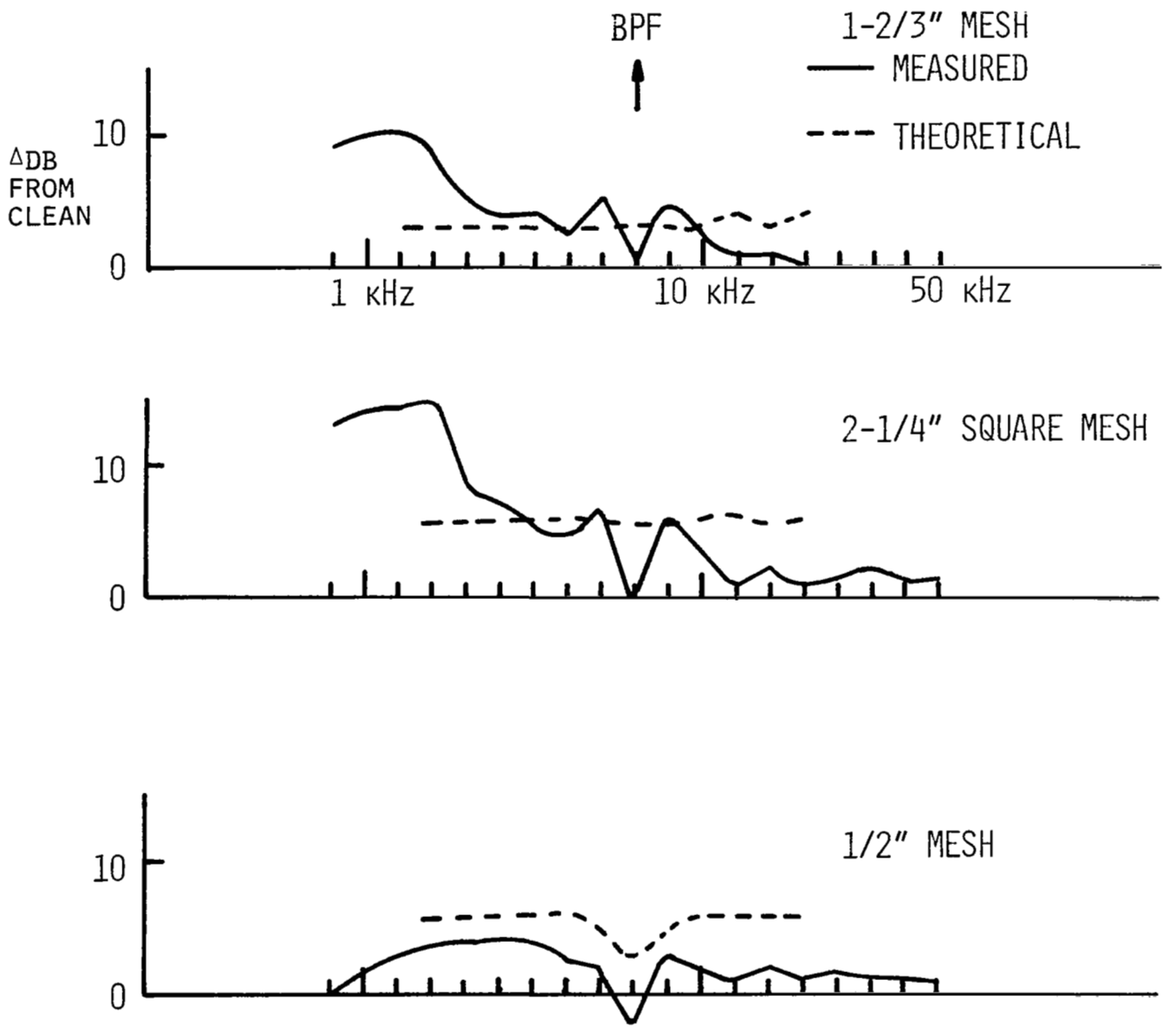

FIGURE 22. Effect of Grids. 50% Speed - Discharge Valve = 0.0.

NASA-Langley, 1976 E-8616